UNIVERSITY OF CALIFORNIA — BERKELEY

UCRL-5101

UNCLASSIFIED

cy 2.

TWO-WEEK LOAN COPY

This is a Library Circulating Copy which may be borrowed for two weeks. For a personal retention copy, call Tech. Info. Division, Ext. 5545

RADIATION LABORATORY

DISCLAIMER

This document was prepared as an account of work sponsored by the United States Government. While this document is believed to contain correct information, neither the United States Government nor any agency thereof, nor the Regents of the University of California, nor any of their employees, makes any warranty, express or implied, or assumes any legal responsibility for the accuracy, completeness, or usefulness of any information, apparatus, product, or process disclosed, or represents that its use would not infringe privately owned rights. Reference herein to any specific commercial product, process, or service by its trade name, trademark, manufacturer, or otherwise, does not necessarily constitute or imply its endorsement, recommendation, or favoring by the United States Government or any agency thereof, or the Regents of the University of California. The views and opinions of authors expressed herein do not necessarily state or reflect those of the United States Government or any agency thereof or the Regents of the University of California.

UCRL-2191

UNIVERSITY OF CALIFORNIA
Radiation Laboratory
Contract No. W-7405-eng-48

MESON PRODUCTION BY HIGH-ENERGY NEUTRONS

Leland Kuns Neher

(Thesis)

April 23, 1953

Berkeley, California

TABLE OF CONTENTS

		Page
I.	ABSTRACT	4
II.	INTRODUCTION	5
III.	APPARATUS	7
	A. General Arrangement	7
	B. Counter and Coincidence Methods	12
	C. Circuits for Time-of-Flight Counter	18
IV.	PROCEDURE FOR MESON IDENTIFICATION	28
	A. Equipment Calibration	28
	B. Tests for Mesons	33
V.	EXPERIMENTAL RESULTS	40
	A. Negative to Positive Ratio	40
	B. Qualitative Angular Distribution Results	46
VI.	CORRECTION OF ANGULAR DATA	47
	A. Energy Spectra Computations	47
	B. Relative Spectrum Efficiency of Detector - Target System	66
	C. Beam Intensity Measurement	71
	D. Differential Cross Sections at 90°	77
VII.	CORRECTED ANGULAR DATA	85
	A. Laboratory System	85
	B. Average Center-of-Mass System	95
	C. Fitting of Data in C. M. System	105
	D. Fitting of Data in Laboratory System	107
VIII.	DISCUSSION OF RESULTS	110
	A. Uncorrected Data	110
	B. Corrected Data	110

TABLE OF CONTENTS

		Page
IX.	ACKNOWLEDGMENTS	112
X.	APPENDIX	113
	A. Kinematics of Meson Production	113
	B. Angle and Solid Angle Transformations	118
XI.	REFERENCES	119

MESON PRODUCTION BY HIGH-ENERGY NEUTRONS

Leland Kuns Neher

Radiation Laboratory, Department of Physics
University of California, Berkeley, California

April 23, 1953

I. ABSTRACT

The angular distribution of charged π mesons produced by 300 ± 30 Mev neutrons on C^{12} and Be^9 have been studied. An analysis of the kinematics for meson production in a nucleon-nucleon collision indicates a fairly well defined center-of-mass system. The $(n + n \rightarrow \pi^-)$ process is observed by a Be^9 - 2/3 C^{12} target subtraction and the data are consistent with the process $(p + p \rightarrow \pi^+)$. The total cross section of the $(n + p \rightarrow \pi^+)$ process is about 1/40 the $(n + n \rightarrow \pi^-)$, and the π^+ angular distribution is probably more uniform than the π^-. These data support the hypotheses of charge symmetry and charge independence of nuclear forces.

MESON PRODUCTION BY HIGH-ENERGY NEUTRONS

Leland Kuns Neher

Radiation Laboratory, Department of Physics
University of California, Berkeley, California

April 23, 1953

II. INTRODUCTION

The qualitative prediction by the Yukawa theory of nuclear forces, that mesons should be produced in the collisions of fast nucleons, was verified by E. Gardner and C. M. G. Lattes in 1948.[1] They bombarded various targets with the internal 380 Mev α-particle beam of the Berkeley 184-inch synchro-cyclotron, and observed the charged π mesons in nuclear emulsion detectors.

Conditions for further study of meson production in a nucleon-nucleon collision were greatly improved when the cyclotron was converted to provide a monoenergetic external beam of 340 Mev protons. A high energy neutron beam was also produced when the internal proton beam struck a beryllium target mounted on a probe. However, the neutron beam was less favorable for meson studies because the intensity was about 0.1 percent compared to the external proton beam. In addition, the neutron energy[2] was lower and spread over a wide range (300 ± 30 Mev). As a result, most of the meson production experiments have been performed with 340 Mev protons. The energy spectrum and angular distribution of charged π mesons have been experimentally studied for hydrogen,[3] carbon,[4] and lead.[4] One experiment has been reported for the charged meson ratio from carbon bombarded by neutrons.[5]

It was pointed out by Breuckner and Watson[6] that the hypothesis of charge symmetry in nuclear phenomena (n - n forces = p - p forces, except for Coulomb effects) and the role of the meson in nuclear forces could be tested by comparing the process, $n + n \rightarrow \pi^-$ with

$p + p \rightarrow \pi^+$, since the matrix element for each of the processes is the same. Similarly, the processes $n + p \rightarrow \pi^-$ and $n + p \rightarrow \pi^+$ should be equal. Proton bombardment of deuterium[7] showed a large positive to negative meson ratio in the forward direction, indicating that the $p + n \rightarrow \pi^-$ matrix element is suppressed relative to the $p + p \rightarrow \pi^+$. From charge symmetry it is expected that $n + p \rightarrow \pi^+$ is also suppressed relative to $n + n \rightarrow \pi^-$. The large ratio is interpreted as a consequence of the charge independence of nuclear forces ($n - n = p - p = n - p$) with its concomittant notion that elementary nuclear processes proceed strongly through virtual states of isotopic spin 3/2. The angular dependence ($1/3 + \cos^2 \theta$) of the π^+ mesons produced in p - p collisions, or of the π^- mesons produced in n - n collisions, is predicted from similar considerations.[8]

The purpose of the experiment described in this paper is to test the ideas outlined above by measuring the angular distribution of charged mesons from Be^9 and C^{12} bombarded by 300 ± 30 Mev neutrons. The n - n interaction is studied by the Be^9 - 2/3 C^{12} target difference. The validity of the subtraction is based upon the alpha particle model of the nucleus.[9] However, because of the forbiddance of the $n + p \rightarrow \pi^+$ processes, nearly all the π^- mesons may be assumed to originate in a n - n collision in carbon or beryllium. The interpretation of the angular distribution data is made difficult, but not impossible, by the momentum distribution[10] of the target nucleons and the energy spread of the neutron beam.

III. APPARATUS

The equipment used to study charged pion production by high energy neutrons consists essentially of four parts:

(1) Source of 300 Mev neutrons, the 184-inch synchro-cyclotron.
(2) Magnet and time-of-flight detectors for pion identification.
(3) Coincidence and pulse registering apparatus.
(4) Monitors for neutron beam intensity.

A. General Arrangement

A general plan of the experimental arrangement is shown in Figure 1. The 350 Mev internal proton beam of the 184-inch synchro-cyclotron strikes a two-inch beryllium target mounted on a probe at 80.5 inch radius. The beam strikes the target in a series of short bursts which each last 150 microseconds and repeat 59 times per second. Some of the protons are converted into a distribution of high energy neutrons by means of direct collision and charge exchange processes with the neutrons in the beryllium.[11] The neutrons emerge into a forward angular distribution of about $\pm 30^{\circ}$ half width. Reduction of the neutron beam to an approximate diameter of five inches at 50 feet from the Be target is achieved by two stages of lead and concrete collimation.

There is considerable intensity of secondary charged particles from the exit region of the second collimator, which was recorded by a coincidence monitor (No. 1) as a relative measure of the neutron intensity. A second monitor (No. 2) was placed about 30 feet down the beam, in order to measure the absolute intensity of the neutron beam. Protons from a CH_2 - C target difference were scattered into a threshold detector similar to the n - p scattering experiment performed by Segrè, et al.[12]

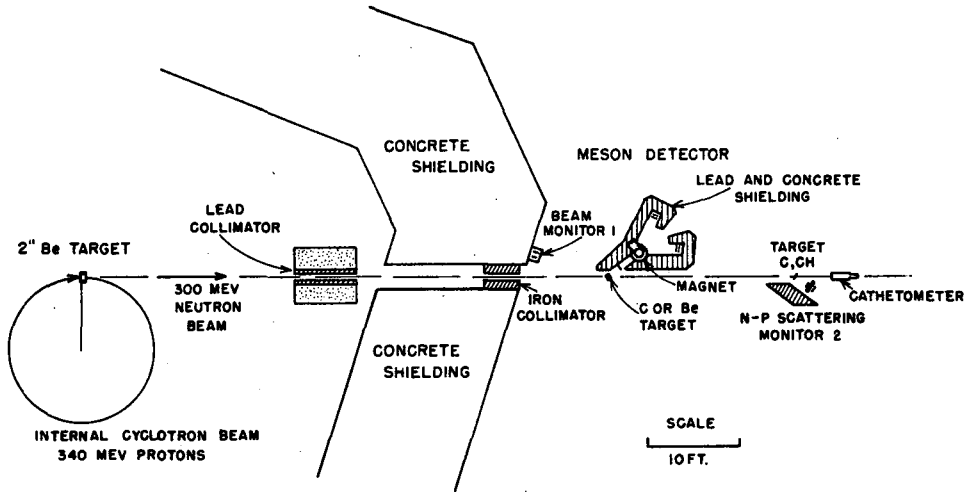

GENERAL VIEW OF EXPERIMENTAL ARRANGEMENT
NEUTRON BEAM, COLLIMATION, MESON DETECTOR, MONITORS

FIG. 1

MU-5406

Targets from which mesons were recorded were placed about five to ten feet from the collimator. The target volume was completely exposed to the neutron beam. Alignment of the two-inch Be target, the collimating system, meson target, and n-p scattering target, was checked by a cathetometer. The geometry of the meson detector is shown in Figure 2. A magnetic field generated by a small water-cooled magnet is arranged symmetrically between two time-of-flight counter systems. The flight path is 205 cm. In this way, positive and negative mesons may be counted concurrently. The relative efficiency of the two systems can be compared by reversing the magnetic field. The magnet-counter system is placed on a movable platform, which pivots under the meson target. The geometry of the system was kept constant as the angle ϕ to the beam was varied. Figure 3 is a photograph of the detector system, and illustrates, by means of stretched white tapes, the trajectories of the neutron beam from the second collimator, and the flight path of the meson through the front counter, into the magnetic field, and finally into one of the rear counter sets (A or B). The observation angle is $\phi = 125^{o}$. Monitor No. 1 is mounted on the concrete wall, near the collimator. Monitor No. 2 is not shown. The fast coincidence circuits and counter power supplies are mounted in the cabinets shown in the lower half of the picture.

Photomultiplier scintillation counters are used. A photomultiplier tube (RCA-1P21) is used to view the fluorescent light pulse from an ionizing particle which passes through a crystal of trans-stilbene.

The rise time of the current pulse from the phototube is sufficiently short ($\approx 10^{-9}$ seconds) compared to the meson's flight time ($\approx 10^{-8}$ seconds), to afford a rough measurement of the meson's velocity.

The magnet time-of-flight counter system has a large discrimination against medium to high energy protons which are knocked out of the target. The probability of a knock on proton to a single meson creation is estimated as 10^3 to 10^4. If the meson and proton have the same velocity, the larger radius of curvature of the proton in the magnetic field causes it to miss the rear counter set. If the proton and meson have the same momentum the proton is rejected because of its

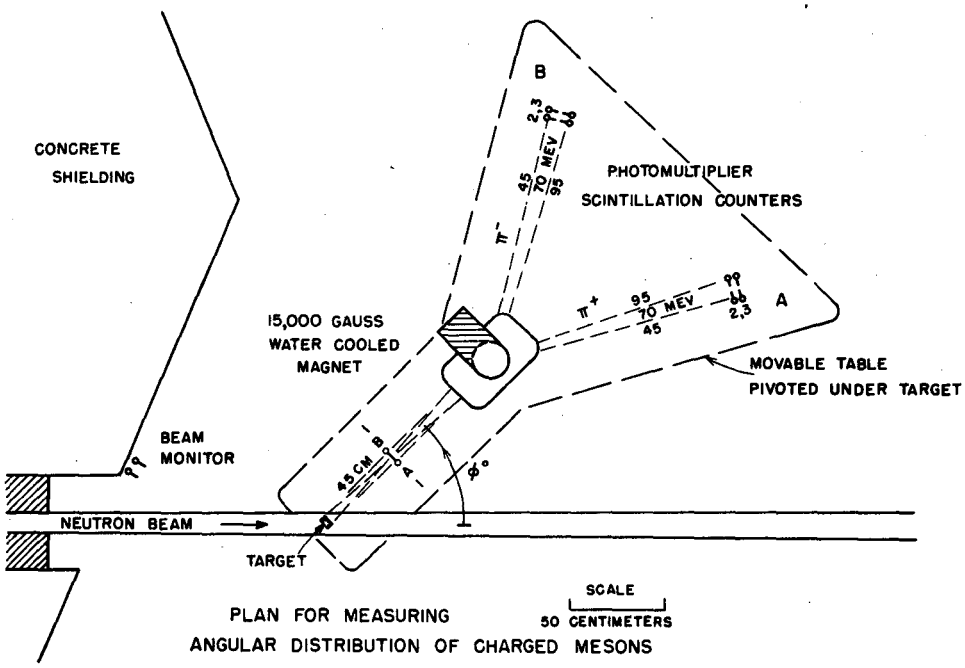

PLAN FOR MEASURING
ANGULAR DISTRIBUTION OF CHARGED MESONS
BY MOMENTUM AND TIME OF FLIGHT

FIG. 2

MU-5407

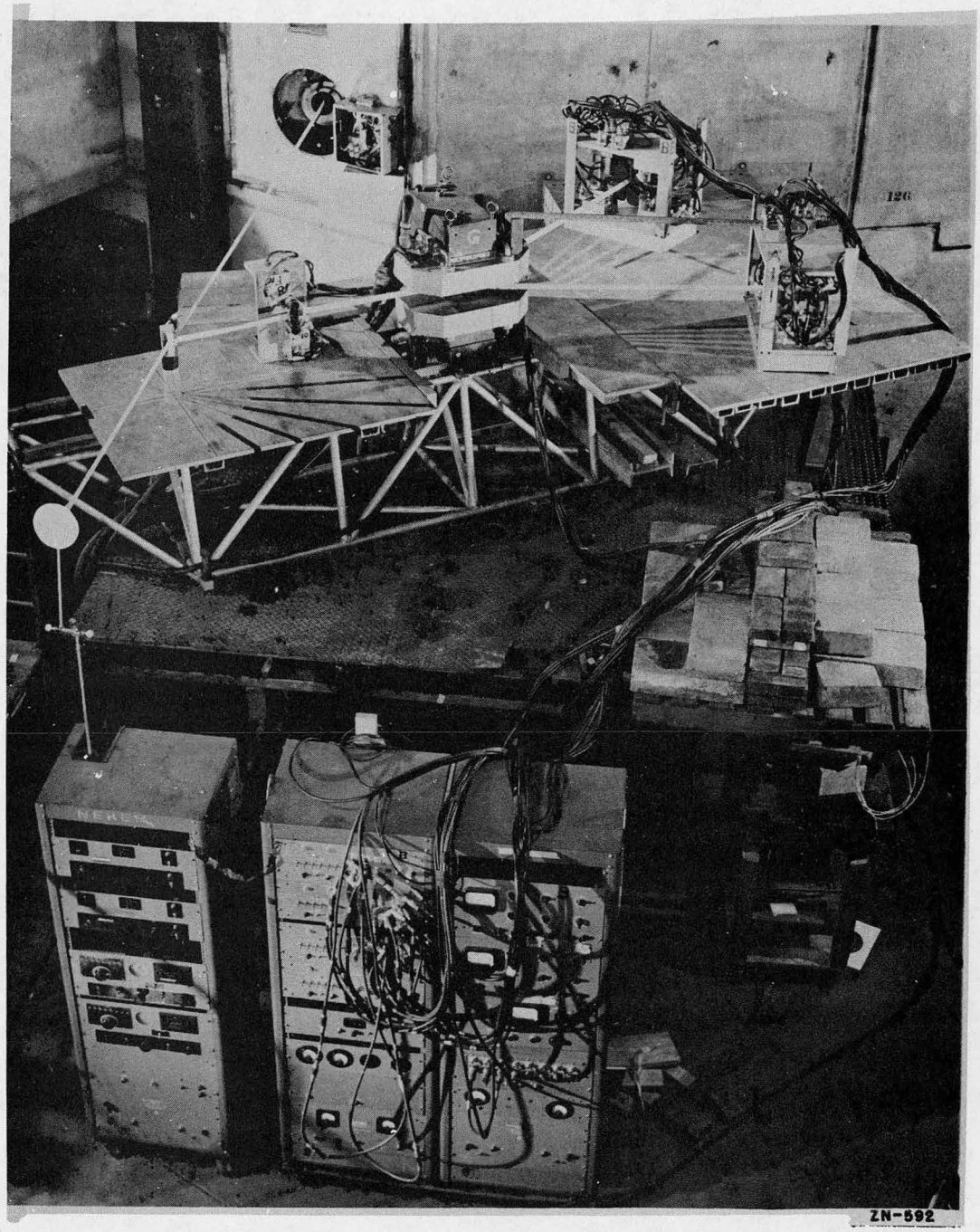

Fig. 3 Photograph of meson detector on the pivotable platform. The white tapes show the trajectory of the neutron beam and the meson through the magnet, G. The white disk at the left, is the diameter of the neutron beam.

longer flight time. However, because of the large ratio of knock on protons to mesons, the probability that a proton is scattered by the magnet pole faces is important. Fortunately, the number of high energy protons scattered 30° into A or B is not large and can be easily measured by counting with the magnetic field off.

Shielding of all the counters, except the relative monitor, from the charge particle spray originating from the neutron collimator and the meson target was necessary to reduce the number of accidental coincidences. The shielding was especially required for the forward observation angles. The counters were covered, insofar as practical, with 10 cm. of lead and 30 cm. of concrete. The shielding was removed for the photographs; however, it is indicated in Figure 1. Approximately three tons of shielding material was used.

B. Counter and Coincidence Methods

The positive pion counting rate was found to be in the order of one to three per hour from a 470 gram carbon target. During one hour, approximately 10^7 to 10^8 charge particles are registered by the front counter. It is obvious that particular care must be taken to prevent accidental coincidences between the real events in the front counter and the random noise counts in the rear counters of the time-of-flight system. The final arrangement which proved to be quite satisfactory is a quadruple coincidence system for counter set A and an identical separate system for set B.

It was desirable to keep the time error, due to the dimensions of the scintillator, less than 10^{-9} seconds. Dimensions of 5 x 8 x 1^{cm} is about the maximum size for the scintillator, when the light pulse is viewed from the 1^{cm} edge. A number of these counters were used in A and B to provide a larger solid angle for counting. The scheme of connecting the nine phototubes in each system to a diode bridge coincidence unit is shown in Figure 4. The front counter, labeled "1", has two phototubes observing a single crystal of dimensions 7 x 7 x 1 cm. The rear counters consist of two layers (labeled "2" and "3") of four counters each. (B_2, B_3, A_2, and

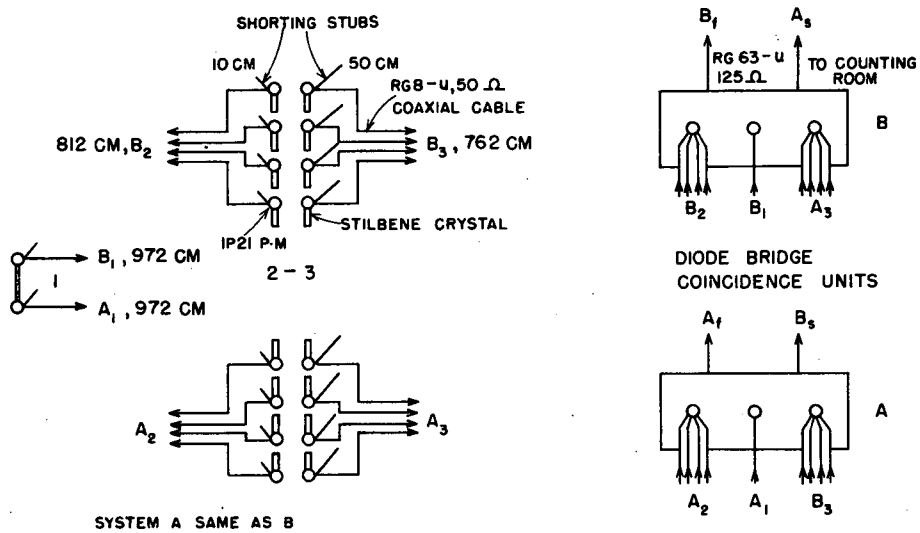

CONNECTION OF DIODE BRIDGES TO PHOTOMULTIPLIER SCINTILLATORS IN SYSTEM B AND A

FIG. 4

MU-5408

A_3). The combined area of layer two is 180 cm^2. The area of layer three is slightly greater. Figures 5 and 6 are photographs of these units. The signals from the four counters in each layer are fed by 25-foot coaxial cables to a common terminal at the diode bridge, so that each layer acts as a single counter. The coincidences for counter set A are made as follows: A 1.2×10^{-9} second coincidence is formed between A_1 (delayed) and row A_2 by one section of the diode bridge coincidence unit A; a 2.5×10^{-9} second coincidence is made between B_1 (delayed) and row A_3 by one section of bridge unit B. Similarly for counter set B, a fast coincidence is formed between B_1 and B_2 and a slower coincidence between A_1 and B_3 in the remaining sections of bridge unit B and A. The outputs from the four sets of double coincidence are labeled B_f, B_s, A_f, A_s. A meson which is to be counted passes through counters one, two, and three, and produces simultaneous signals at B_f and B_s or A_f and A_s, which are recorded by standard 10^{-6} second coincidence apparatus in the counting room of the cyclotron building about 100 feet from the diode bridge units. The lengths of RG8-U, 50 ohm coaxial cable, used to connect the system are also indicated in Figure 4.

A block diagram of the counting room apparatus is given in Figure 7. The signals B_f, B_s, A_f, A_s are amplified (x 500) by a linear amplifier (L.A.). A variable gate discriminator unit (V.G.) forms a one-microsecond square pulse at a given pulse height from the L.A. The performance of these units is recorded by the scalers (S.C.), $1 \rightarrow 6$. Coincidences are formed between two different bias settings on B_f (labeled high and low) and one bias setting for B_s. This was done partly to demonstrate that the data does not depend upon bias setting and partly to insure against equipment failure. The final coincidence representing a triple event 1-2-3, is registered on scalers eight and nine for system B, and ten and eleven for A.

The scalers were turned on during the beam pulse from the cyclotron by a synchronized gate signal. If the instantaneous rates in counters 1, 2, 3 are 10^7, 10^4 and 10^4 sec^{-1} respectively, and if these are independent events, the expected accidental counting rate is one every three hours.

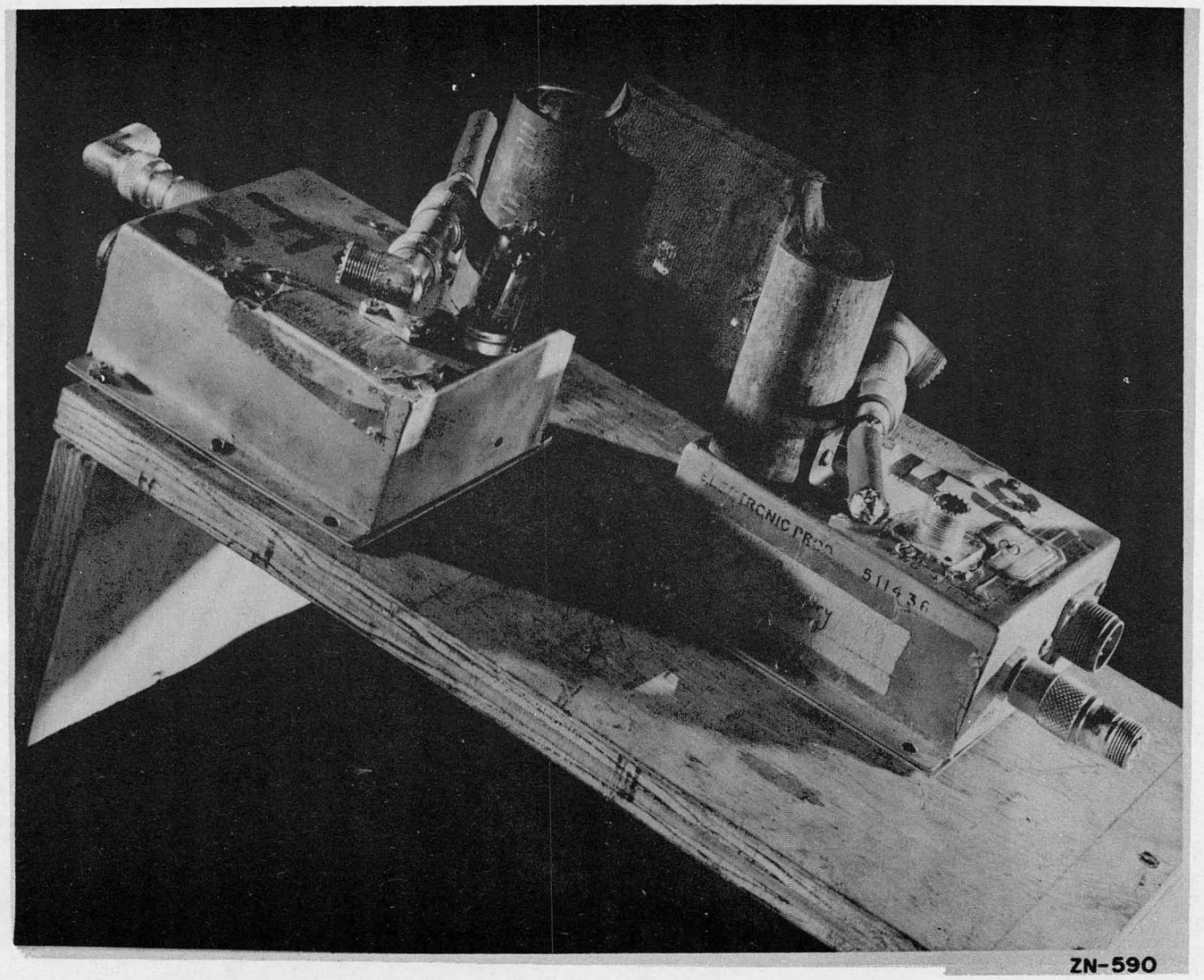

Fig. 5 Photograph of front counter. Phototubes are partially enclosed in a cylindrical magnetic shield. Pulse limiter tube, 6AH6, and 15 cm shorted 50 ohm line for pulse clipping are also shown.

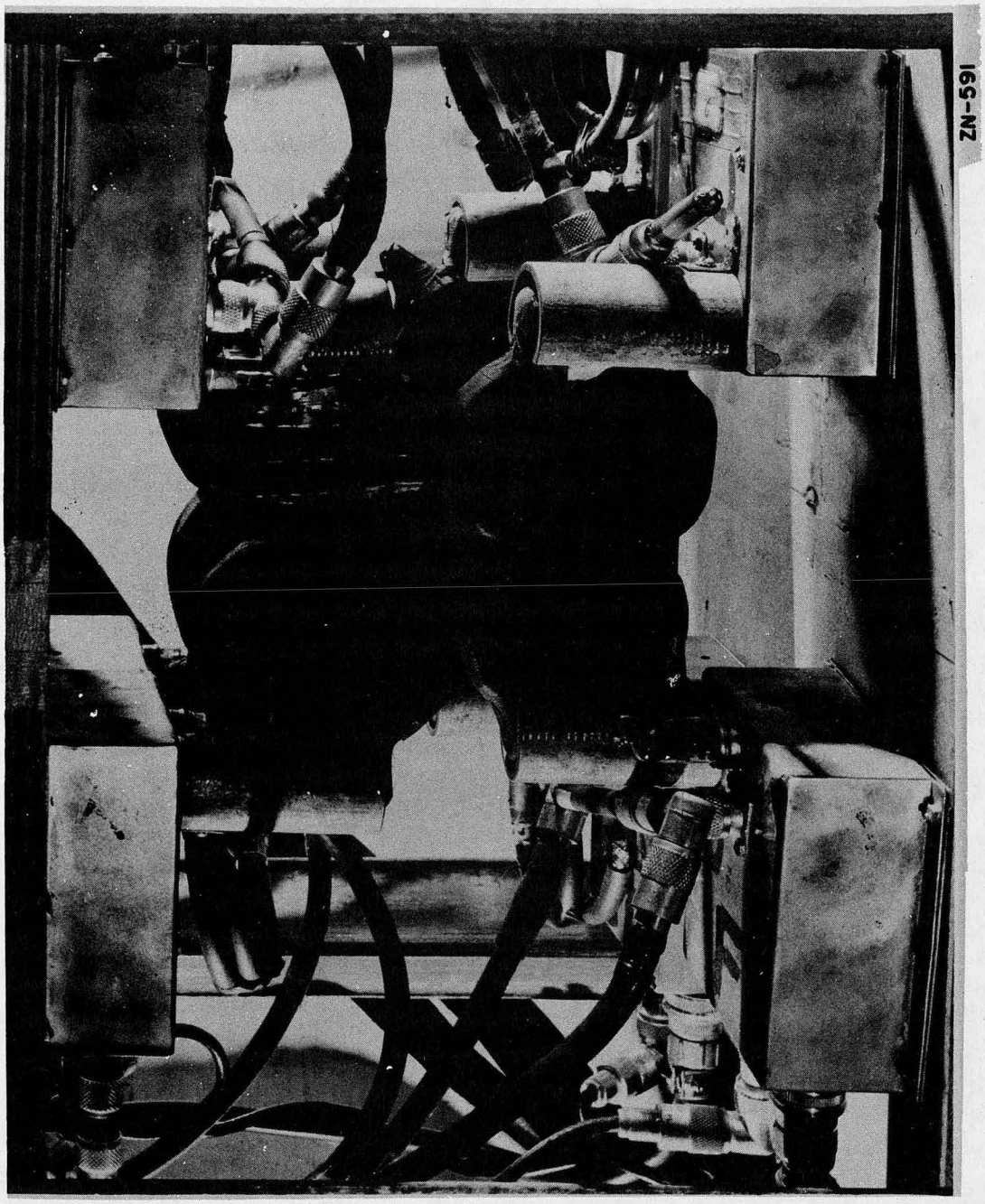

Fig. 6 Rear Counter Set A

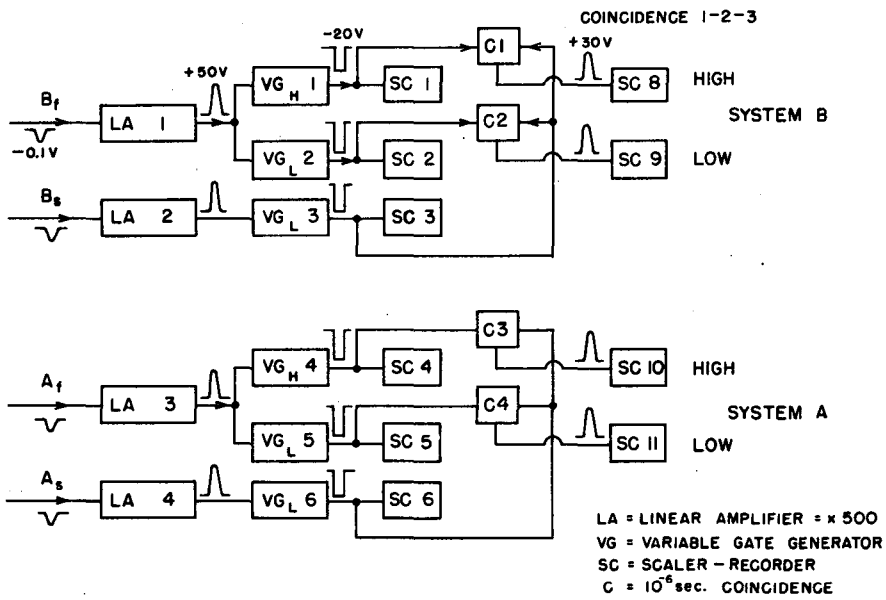

10^{-6} sec. COINCIDENCE AND MONITORING OF COUNTER SETS 1-2-3 IN SYSTEM B AND A

FIG. 7

MU-5409

C. Circuits for Time-of-Flight Counter

Considerable time was spent in developing and testing the time-of-flight detector used in this experiment. The circuits used find wide application in high energy nuclear particle counting experiments where photomultiplier detectors are used. The purpose of the following account is to present circuitry which is relatively simple and reliable and which works with good efficiency at 10^{-9} second resolving time with the unamplified pulses from a 1P21 photomultiplier tube.

1. History of Fast Circuits for P.M.

Z. Bay[13] was probably the first to point out the advantages of an electron multiplier as a fast (10^{-8} second) detector of single electrons. In 1947, H. Kallman[24] described the method of counting ionization radiation by the photoelectric measurement of the fluorescent light pulses emitted by certain organic substances, such as napthalene and anthracene. The efficiency of the photomultiplier scintillation counter was demonstrated as comparable and in some respects superior to the widely used geiger counter.

Coincidence circuits for the photomultiplier counter were approaching 10^{-9} second resolving time by 1949 and 1950,[15] and their application to nuclear physics counting problems were being reported in the literature. The circuit which interested us the most, out of the many reported in the journals, was the crystal diode bridge circuit. The idea of a diode bridge which stores the coincidence charge on condensers was first proposed by Z. Bay[16] and later a circuit[17] was published by him. The advantage of Bay's circuit over other diode mixing circuits is its sensitivity to small voltage pulses ($\approx$ 0.1 to 0.5 volt) of short duration (10^{-9} seconds and less). This sensitivity means that the small current pulses from the presently available phototubes (RCA, 1P21) can be fed directly into a low impedance (50 ohm) transmission line of good propagation characteristics, and with no intermediate amplification, will efficiently operate the coincidence circuit. A disadvantage of the bridge circuit, in some applications, is the discharge time of condensers ($\approx 10^{-7}$ seconds). A useful diode mixing circuit which has less sensitivity but perhaps a faster recovery time is described by Benedetti and Richings.[18]

At present, the principal source of timing error is in the photomultiplier. The bridge coincidence circuit has a timing error probably less than 10^{-10} seconds because of the high frequency response of the crystal diode. Two RCA 1P21 phototubes viewing a single small (1 cm^3) trans-stilbene crystal will count high energy protons (100 to 300 Mev) with 50 percent efficiency with 1/e resolving time in the order of $\pm 5 \times 10^{-10}$ seconds. The resolution curve is approximately gaussian. Resolving time less than this may be obtained but with a decrease in counting efficiency. The measured resolving time compares favorably with the "educated guess" made by R. F. Post.[19]

2. Diode Bridge and Different Amplifier

The diode bridge circuit used in this experiment is an adaptation of Bay's circuit. The parameters of the circuit were adjusted experimentally to provide the optimum sensitivity to 10^{-9} second pulses of amplitude 0.1 to 1.0 volts.

The need for a multiple coincidence between the photomultiplier scintillation counters led to the design of a triple coincidence bridge circuit shown in Figure 8. The idea can be extended, within limits, to higher orders of coincidence. The basic operation of the circuit is as follows:

A positive pulse, S_1, charges condenser C. After S_1 has been absorbed in the cable terminating impedance, Z_o, a net charge remains on C, due to the unidirectional current flow allowed by the series diode D. The charge decays essentially through R in about 2×10^{-7} seconds. The voltage V_1 on the condenser, during the decay time, may be observed by an amplifier and oscilloscope. Diodes which produced about the same maximum charge on C were selected for the circuit. The type IN56 diode, made by the Sylvania Electrical Company, was, in general, the best. The decay constant and the amplitude of the negative voltages V_2, V_3, are made equal to V_1 by adjustment of R_2C_2 and R_3C_3. V_1 is considered as a reference voltage. Two difference-voltage amplifiers, shown in Figure 9, are connected to V_1, V_2 and V_1, V_3, and will

DIODE BRIDGE
TRIPLE COINCIDENCE CIRCUIT
FOR 10^{-8} SEC., ¼ VOLT, POSITIVE PULSES

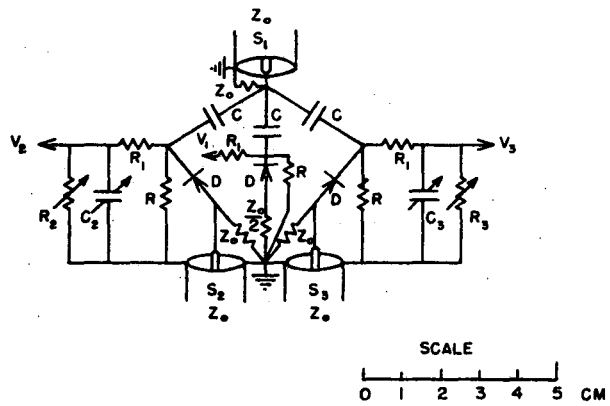

$R_2, R_3 = 10^5 \rightarrow 10^6$ OHMS
$R, R_1 = 10^4$
$C_2, C_3 = 2 \rightarrow 10 \times 10^{-12}$ FARADS
$C = 20 \times 10^{-12}$
Z_o = CABLE IMPEDANCE = 50 OHMS
D = TYPE IN56 DIODE

FIG. 8

MU-5475

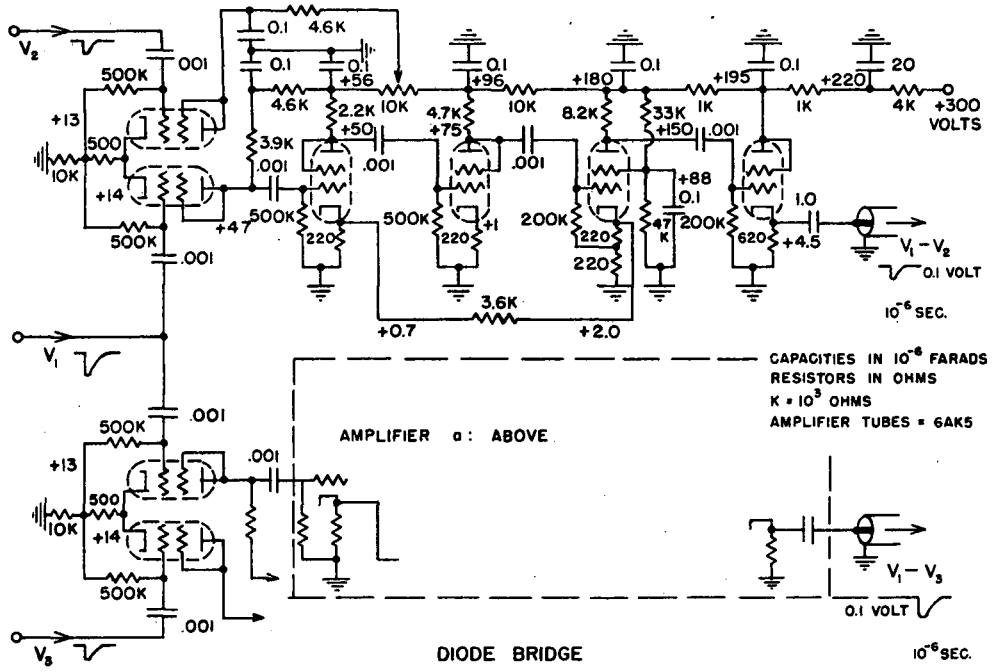

DIODE BRIDGE
DIFFERENTIAL AMPLIFIERS

FIG. 9

MU-5476

show zero output under conditions of balance. A filter which attenuates the initial charging pulse S_1 is provided by the series resistance R_1, the shunt capacity of the amplifier, and C_2, C_3. A positive signal S_2, coinciding with S_1 in time, effectively raises the forward resistance of the diode, causing less charging current to flow. The negative difference signal $(V_1 - V_2)$ is amplified and is a measure of the coincidence event. Similarly a signal S_1 and S_3 causes a negative difference signal $(V_1 - V_3)$. A 10^{-6} second coincidence may then be formed between the amplified signals $(V_1 - V_2)$ and $(V_1 - V_3)$, using conventional apparatus. The final coincidence represents a fast triple coincidence S_1, S_2, S_3.

If S_1 is absent, a positive signal S_2 or S_3 produces, in the ideal case, no net charge on C because the diode does not conduct in the backward direction. Actually, a fraction of S_2 is fed through because of the capacitance across the diode. In practice, it was found difficult to obtain positive 10^{-9} second signals which were free from a negative component (overshoot). The overshoot is due to the shorted-line, pulse-clipping technique which selects the 10^{-9} second component of the signal from the phototube. The diode conducts the negative component of S_2 and leaves C with a charge which is, fortunately, of opposite polarity to the charge left by a coincidence signal S_1, S_2. Therefore, if V_1 is zero, $(-V_2)$ is a positive difference signal which may be rejected in the later amplifying stages by ordinary methods. Furthermore, $(-V_2)$ may be made quite small compared to the coincidence signal $(V_1 - V_2)$ by adjusting the amplitude of S_2 to 1/2 to 1/3 the amplitude of S_1. For example if S_1 is 0.6 volt, S_2 may be made as low as 0.06 volt. The lower limit is set by the noise energy inherent in the first stages of the differential amplifier. Smaller signals will operate the circuit if their pulse length is 10^{-8} seconds.

The differential amplifier, Figure 9, has a balance adjustment R. The amplifier inputs are connected together and to a common signal point such as V_2. Resistance R is varied in each amplifier until zero output is obtained. The remaining part of the amplifier is conventional in design. The rise time of the amplifier is about 2×10^{-7} seconds; the voltage gain is approximately 500. A photograph of the construction of the bridge unit and the two amplifiers is shown in Figure 10.

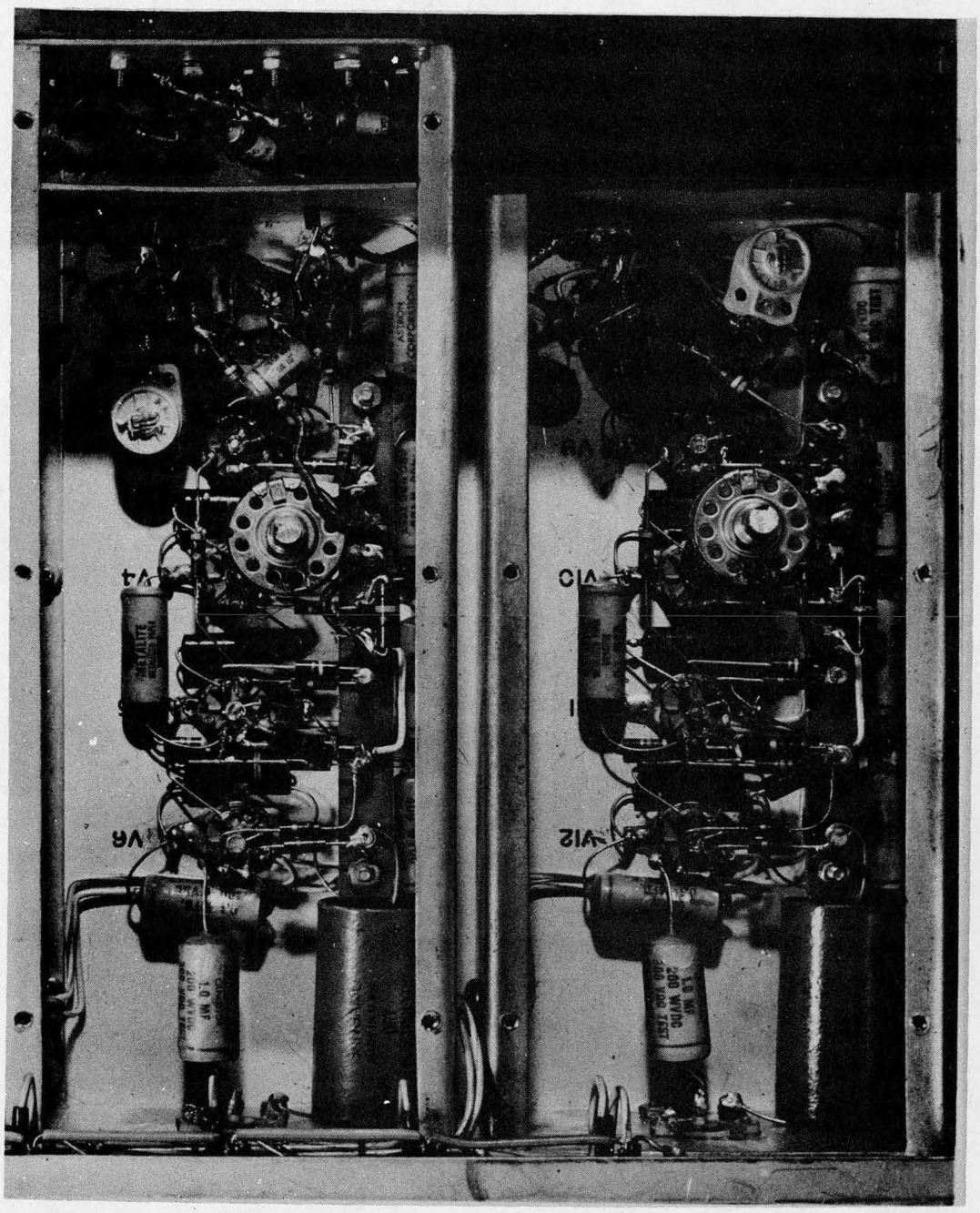

Fig. 10 Wiring and construction of diode bridge and differential amplifiers. Bridge unit is in upper left corner.

The analogy of the diode bridge coincidence unit to the classic Wheatstone bridge is evident: the battery voltage is S_1; the galvanometer across the bridge is the difference amplifier; the balance condition is changed by the variable arm resistance D; the sensitivity is increased by increasing S_1.

A cable impedance of 50 Ω (Rg - 8 μ) was selected because the available cable connectors were 50 ohms. It is necessary to minimize the signal reflections from the several joints in the variable length cable to front counter of the time-of-flight detector. The wave velocity in the cable was checked by the standing wave method over a wide range of frequencies (100 to 1,000 megacycles) and was constant within ± 1 percent. Because of the small wave velocity dispersion, the group velocity of a 10^{-9} second pulse was considered as equal to the measured wave velocity. The measured value is $(1.982 \pm 0.001) \times 10^{10}$ cm sec^{-1}, or β cable $= v/c = 0.662$.

3. Photomultiplier Pulse Limiter

The current pulses from the photomultiplier scintillation counter are not, in general, of uniform size or shape. The non-uniformity is particularly noticeable when observing the 10^{-9} second component of the signal. The difficulty is due to several reasons: (a) statistical fluctuations of the small number of photoelectrons released from the photoelectric surface in the first 10^{-9} seconds. (b) Non-uniform efficiency of light collection from various parts of the scintillator. (c) The amount of fluorescent light depends on the properties of the ionizing particle. In working with 10^{-9} second apparatus exposed to the background radiation from the target and neutron beam collimation system, the efficiency of the coincidence circuit for counting minimum ionization particles is greatly improved by making the circuits insensitive to signal height or shape. Since the balancing conditions of the diode bridge circuit depend somewhat on signal size and shape, a limiter and a pulse-shaping network were built at the phototube base. (See Figure 11.) The average negative signal from the photomultiplier anode is observed to turn off the plate current of the 6AH6 limiter tube in about 10^{-9} seconds. If the capacity C of the grid circuit is 10^{-11}

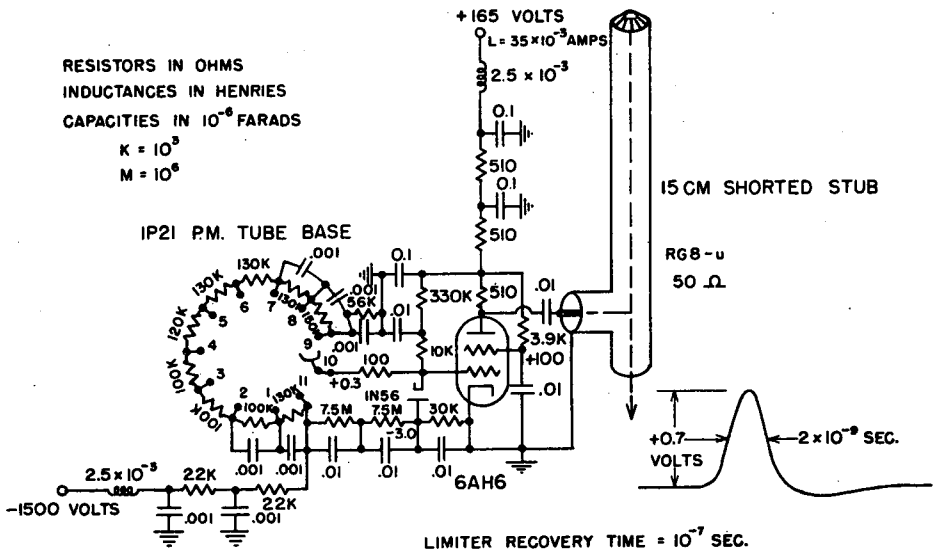

PHOTOMULTIPLIER, PULSE LIMITER
AND SHAPING CIRCUIT

FIG. 11

MU-5477

farads, the peak current from the p. m. is approximately C ($\Delta V/\Delta T$) or 0.03 amperes. The input capacity is prevented from charging greater than minus three volts by the biased IN56 diode, which conducts the charging current to ground. The grid recovery time is RC = $(10^4)(10^{-11})$ = 10^{-7} seconds. The positive 10^{-7} second current pulse in the plate circuit of the limiter tube is differentiated by a 15 cm. 50 ohm, shorted line. The resultant 0.7 volt 10^{-9} second positive pulse, which is fed to the coincidence circuit, is shown in Figure 11. The constructional details of the unit are quite important, in order to keep the circuitry critically damped. Figure 12 is a photograph of the wiring and construction of the limiter.

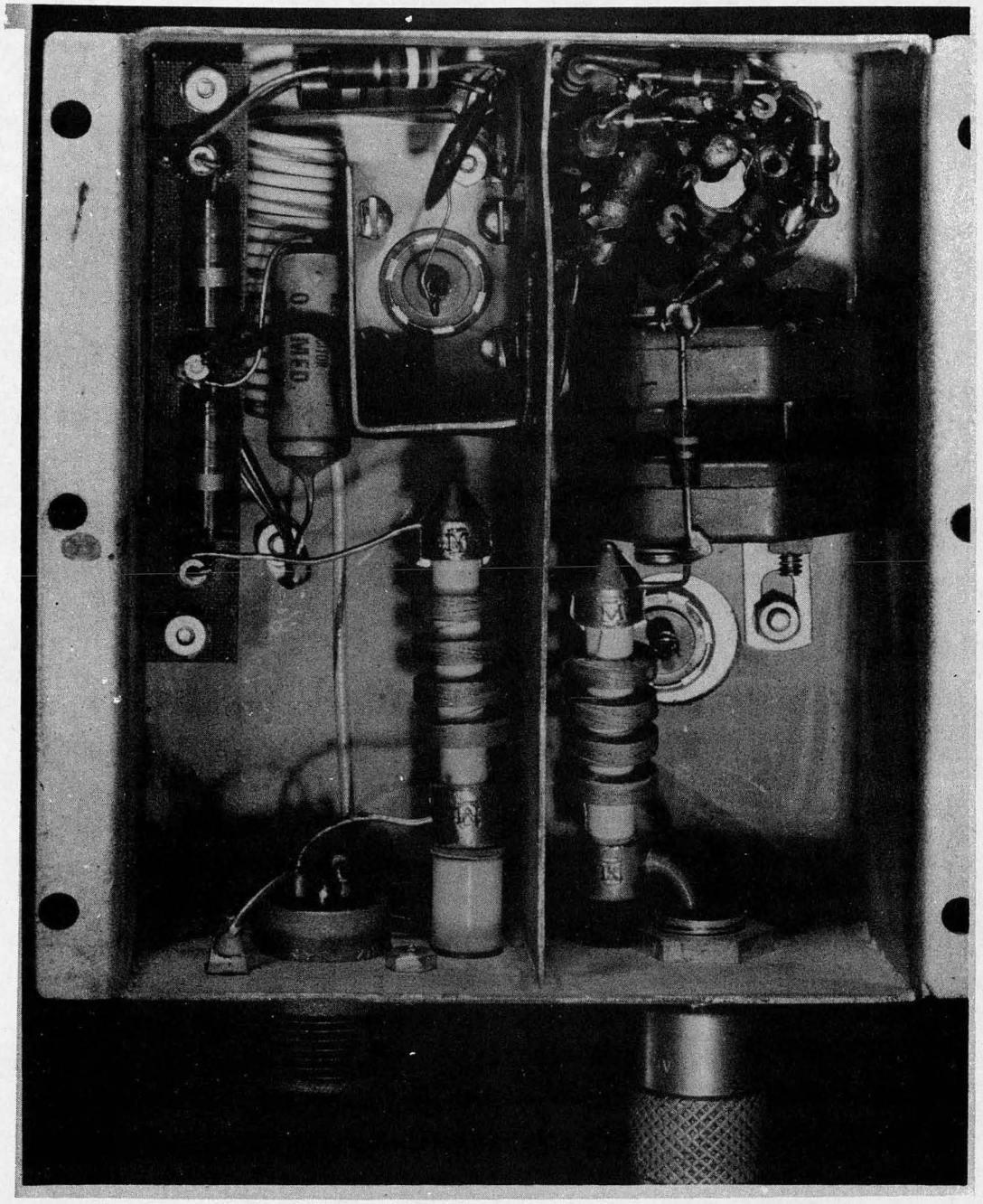

Fig. 12 Wiring and construction of photomultiplier pulse limiter.

IV. PROCEDURE FOR MESON IDENTIFICATION

The identification of mesons produced by neutron bombardment was, of course, the main experimental problem to be solved, before attempting the angular distribution. In October, 1951, mesons (40 to 80 Mev) and medium energy protons (80 to 150 Mev) were observed at 90° to carbon, using a simple time-of-flight detector and the range of the particle in an absorber placed in front of the rear counter. If a meson and proton have the same velocity, the range Rp of the proton in material is:

$$Rp = \frac{\text{Proton Mass}}{\text{Meson Mass}} \times (\text{range of meson}) \approx 6.7\ R_{\pi}$$

The 90° time-of-flight data will be discussed in Section VII in connection with the absolute cross section determination.

Identification of mesons detected by the magnet time-of-flight system (Section III) was performed at 15° to the beam with counting rates of about 10 per minute. In the following a brief account is given of the equipment calibration and the results of several tests for pions:

A. Equipment Calibration

1. Magnetic Field and Energy Resolution

The energy resolution is determined principally by the momentum selection defined by the geometry of the counters and the aperture of the magnetic field. The water cooled magnet[20] has a 20 cm. diameter pole face and a 7.5 cm. gap. The entrance to the magnet was collimated to 6 x 9 cm. The coils provide a maximum of 5×10^4 ampere turns. Approximately 10^5 watts of power at 500 amperes was supplied by a motor generator set. In the central region, the field was about 1.5×10^4 gauss. The deflection of a 70 Mev meson is about 30°. Larger deflections would have been desirable in order to reduce the background of scattered protons at the forward angles.

Meson trajectories were initially estimated by use of a current-carrying wire, stretched from the target through the magnet, and through the position of the rear counters. The analogy of the forces on the wire, to the forces on a moving charged particle in a magnetic field, allow one to derive:

$$H\rho = \frac{10\ T}{I} = \frac{p\ c}{e}$$

Where $H\rho$ is in gauss CM.

T - wire tension in dynes
I - current in amperes
p - momentum of charged particle in grm. cm sec^{-1}
e - charge of particle in e.s.u.
c - velocity of light in cm sec^{-1}

The assumption is that the tension in the wire is not due to the weight of the wire between the suspended ends. Extreme trajectories were explored for various parts of the target and rear counter areas. At 70 Mev, the limits were ± 25 Mev. A gaussian distribution (Figure 13) centered at 70 Mev with $1/e = \pm 12$ Mev (probable error ± 6 Mev), was assumed for the energy resolution.

2. Time Resolution and Counter Efficiency

The operating potential for each photomultiplier counter was adjusted to obtain a relative standard counting rate from a 10 mR, Co^{60}, γ-ray source. The individual potentials varied from minus 1400 to 1800 volts. The time for the multiplied electrons to travel through the dynode accelerating structures, depends upon the accelerating potential. A variation of 100 volts in a total supply of 1500 volts produces about a $\pm 10^{-9}$ second variation. The two γ-rays from Co^{60} are emitted almost simultaneously, and provide a convenient means of aligning two counters in time with respect to the coincidence circuit. The adjustment of the cable lengths to the 18 counters was made to an accuracy of $\pm 3 \times 10^{-10}$ seconds.

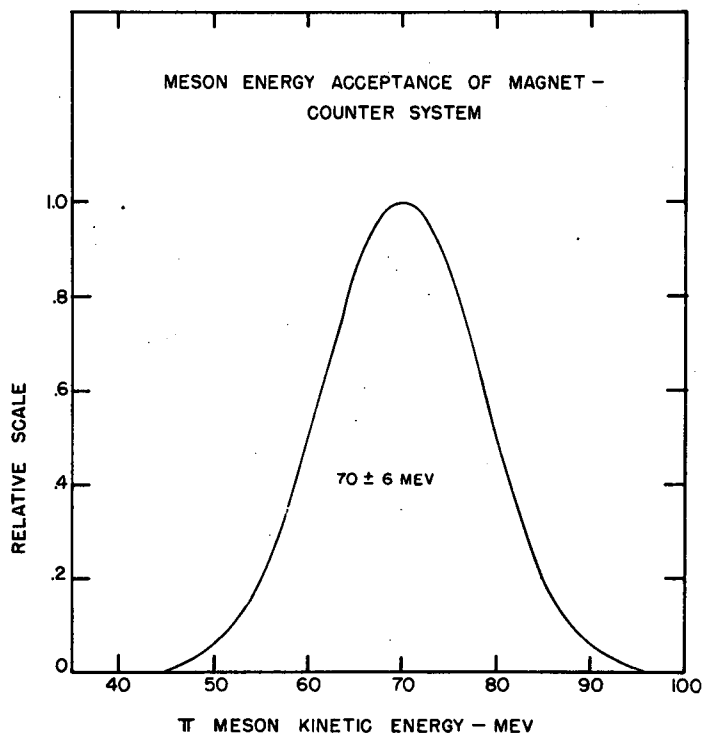

FIG. 13

MU-5410

The relative efficiency and time resolution of systems A and B were measured by exposing the front and rear counter sets, with a few centimeters separation, to the high energy protons from the target in the forward direction. These data were taken near the end of the meson angular distribution run. An absolute scale of 0.9 for the efficiency of the slow (s) doubles circuit was a best estimate based upon earlier measurements, not shown here. The results are given in Figure 14. Curves 1, 2, 3, 4, 5, were read from scalers 6, 5, 4, 11, 10 of Figure 7 for system A. Similar results were obtained for system B. The resolution curves are approximately three times broader than for a simple double coincidence system using small scintillators, operating at the same efficiency. (See III-C-1).

At 70 Mev meson has $\beta_\pi = 0.75$. The cable velocity is $\beta_c = 0.662$ when the counters are in place on either side of the magnet, the separation d is 205 cm. Therefore, the cable length to be added to the front counter to form a coincidence is:

$$L = d\left(\frac{\beta_c}{\beta_\pi}\right) = 180 \text{ CM.}$$

3. Solid Angle

The front counter is placed 45 cm from the center of the target. It is assumed that the magnetic field does not appreciably alter the inverse square law for the intensity of the mesons. The solid angle of system A or B is therefore,

$$\Delta\Omega = \frac{180}{(250)^2} = 2.9 \times 10^{-3} \text{ steradians.}$$

4. Relative Monitor Efficiency

The relative efficiency of the coincidence monitor (No. 1) is maintained at a constant value by periodic checks with the simultaneous γ-rays from 10 mR - Co^{60} source (5.3 yr. half life). The integral bias curve obtained with Co^{60} coincidences is considerably sharper than the curve produced by the scattered protons coincidences.

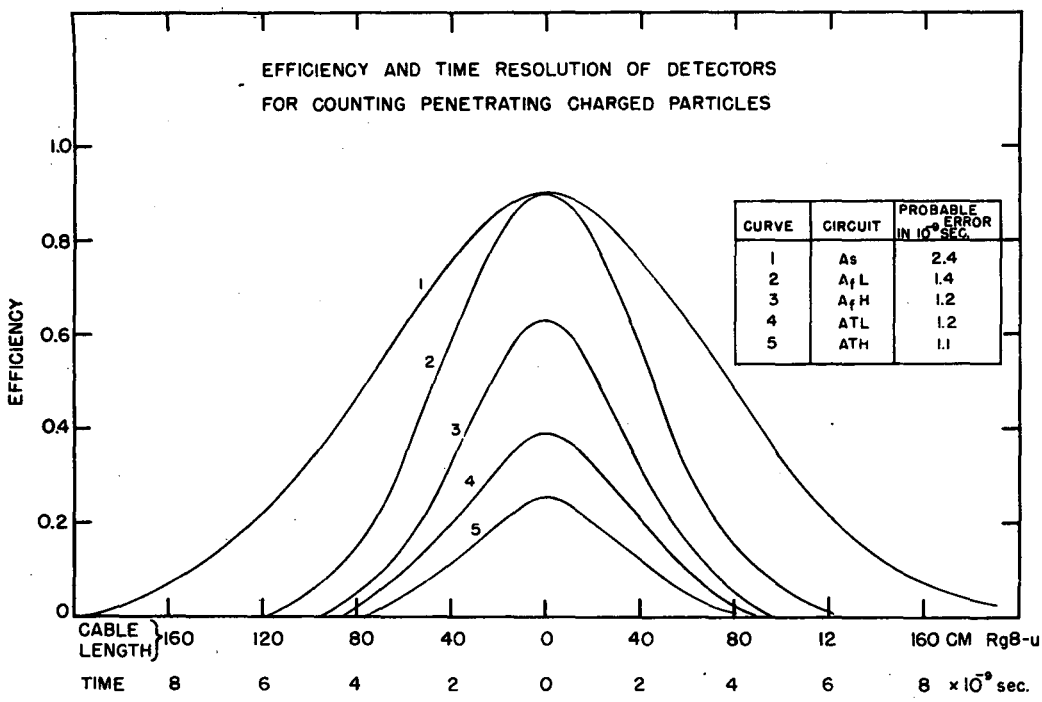

CURVE	CIRCUIT	PROBABLE ERROR IN 10^{-9} SEC.
1	As	2.4
2	$A_f L$	1.4
3	$A_f H$	1.2
4	ATL	1.2
5	ATH	1.1

FIG. 14

MU-5411

B. Tests for Mesons

The following tests were made with the more numerous negative mesons at 15°. The low rate of positive mesons prevented any direct identification. The tests are essentially (1) momentum, (2) velocity, (3) range. The results are shown in Figures 15, 16, 17, respectively, in terms of the relative beam monitor reading. One monitor unit represents about 15 minutes of cyclotron time.

1. Momentum Test

The important results are: the polarity of the field was correct for counting negatively charged particles; most of the particles disappear with field off indicating the momentum is compatible with a 70 Mev meson. Those particles which do not disappear with field off were identified as a mixture of scattered high energy protons and accidental coincidences. These background counts are assumed to be the same with field on or off, and were subtracted from the meson data. Figure 18 is a summary of the background data, sampled at regular intervals during the experiment at various laboratory angles. Beyond 75° the background was not measurable and it was assumed to be less than one per hour.

2. Velocity Test

With the magnet current at 500 amperes, the cable lengths to the front counter (A_1 and B_1) were varied. One obtains the same time resolution curve as discussed in A-2 with scattered protons using the triples coincidence data. This is expected since the energy resolution of the time-of-flight system is considerably broader than for the magnetic channel. That is,

$$\frac{\Delta E}{E} = \frac{\pm c \, \Delta \tau}{d} \sqrt{\gamma_\pi^2 - 1} \; (\gamma_\pi + 1)$$

$$\text{where } \gamma_\pi = 1 + \frac{\text{meson kinetic energy}}{\text{meson rest energy}} .$$

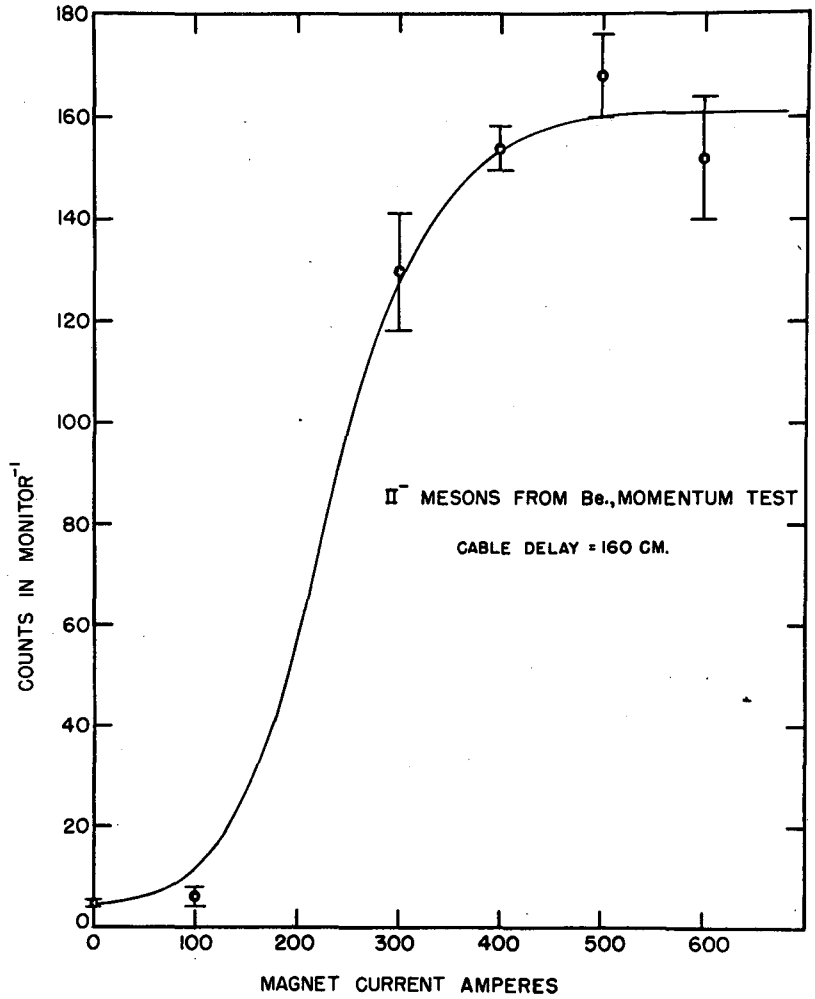

FIG. 15

MU-5344

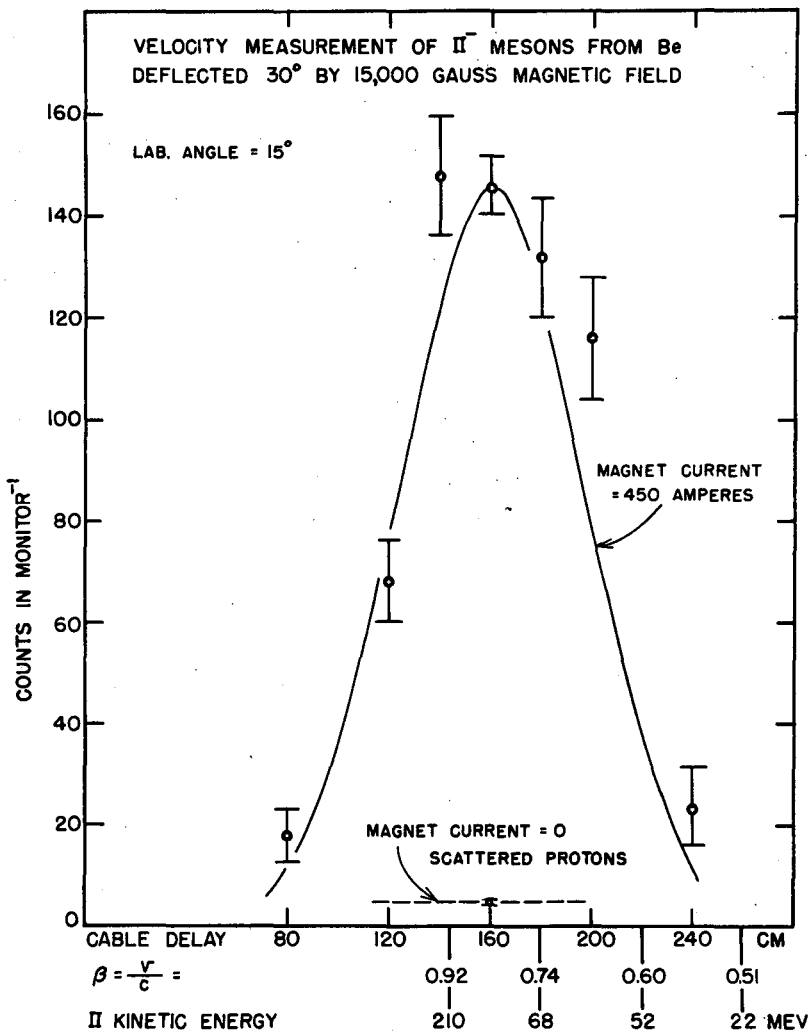

FIG. 16

MU-5345

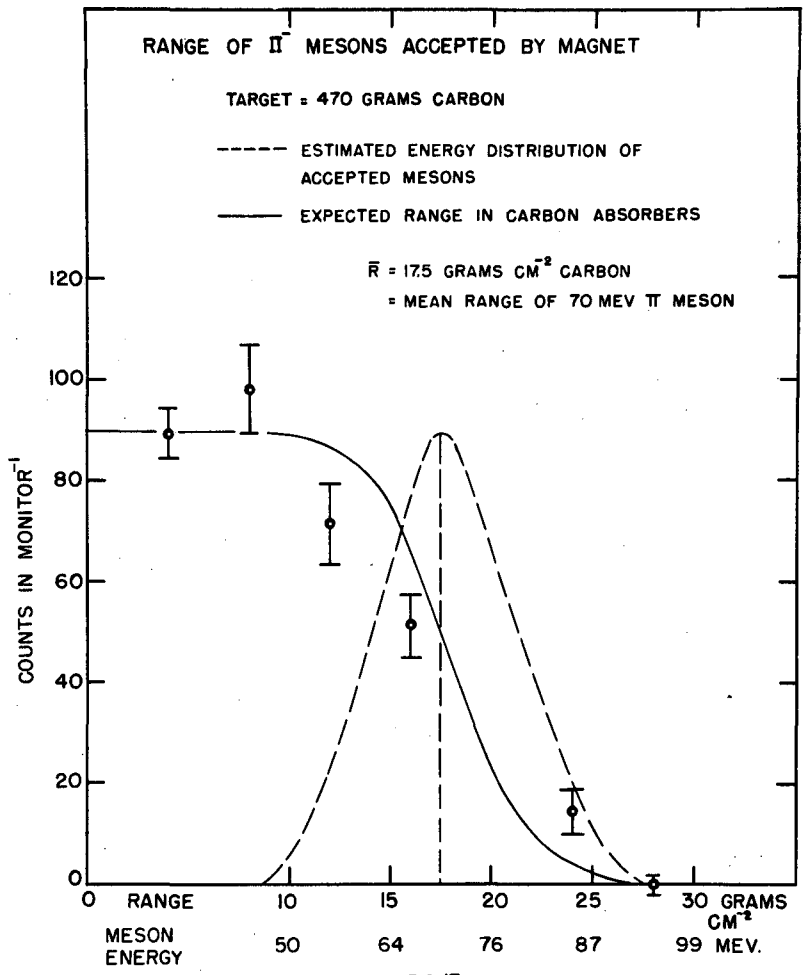

FIG. 17

MU-5346

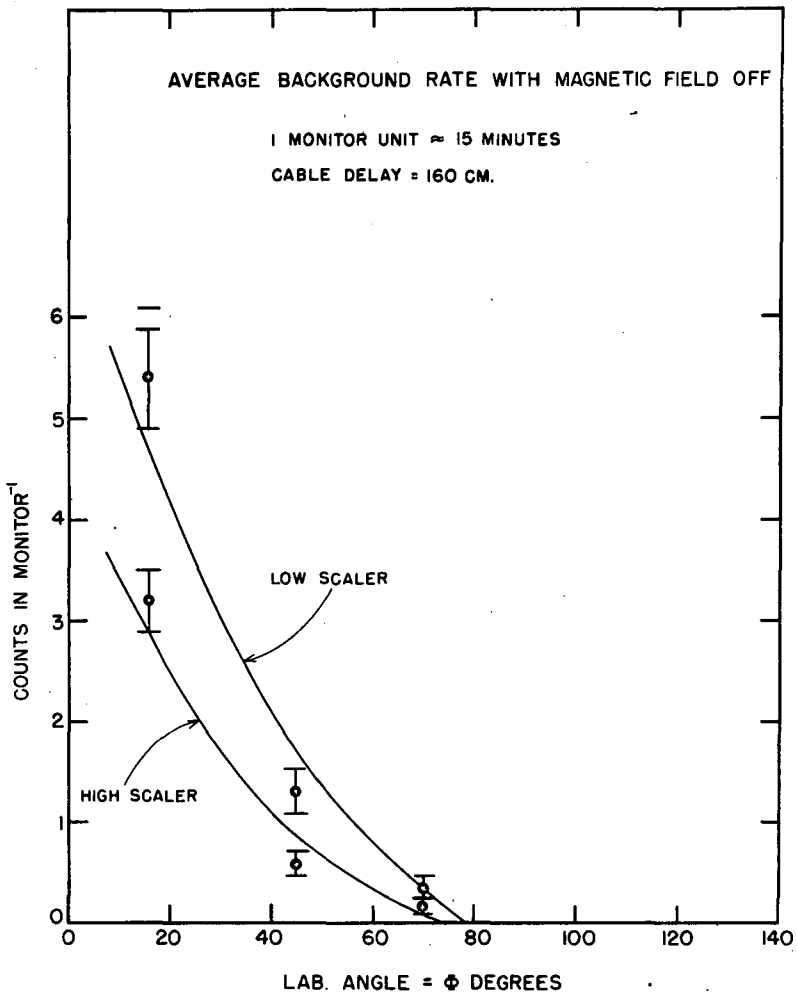

FIG. 18

MU-5347

If $d = 205$ cm

$\Delta\tau = 1.2 \times 10^{-9}$ sec

$\gamma_\pi = 1 + 70/140 = 1.5$

Then $\Delta E/E \approx \pm 0.5$

whereas for the magnetic channel $\Delta E/E \approx \pm 0.1$.

The doubles circuits now record mostly accidental coincidences, and are good indication of the relative performance of the various counter sets.

3. Range Test

With the magnet current and velocity set for 70 Mev meson, carbon absorbers were placed before the rear counters. The geometry is not perfectly poor so that some of the mesons are expected to scatter and miss the rear counter. The mean range is about 17.5 gram cm^{-2} of carbon which corresponds to a 70 Mev pion. The slope of the range curve is in agreement with a 1/e width of ± 12 Mev, centered at 70 Mev, for the meson energy. The angular distribution data was taken without the carbon absorbers. The rear counters are equivalent to 4 grams cm^{-2} of carbon absorber.

4. Target Data

The target volume was made as large as possible to maximize the counting rate. The dimension of the Carbon and Be targets were each equal to 300 cm^3 with dimensions 10.3 x 3.8 x 7.6. The counting rates were linear (within statistics of ± 10 percent) with volumes up to 300 cm^3. The pions emerge perpendicular to the 10.3 x 7.6 face of the target. The neutron intensity is attenuated from 10 to 20 percent (depending upon target orientation), according to the total neutron cross sections[22] for C and Be. The weights of the Be and C targets are 554 and 470 grams, respectively. There are 246L protons in Be and 235L protons in C, where L is Avogadro's number. Therefore, to adjust the observed mesons to correspond to observations from targets containing the same number of alpha particles or protons, the carbon data must be multiplied by 1.049.

5. Electron Contamination

A 157 Mev electron has the same momentum as a 70 Mev pion; however the mean range of the electron is about 60 gm cm^{-2} of carbon. From the range curve for negative mesons, the number of 157 Mev electrons must be very small. The source of high energy electrons can be the decay γ-rays from a moving neutral meson.[21] The γ-ray makes an electron pair in the target, and the electron or positron may carry off most of the γ-ray energy. The ratio of positrons to positive mesons may not be small, and for this reason the low positive meson yield from C and Be is in some doubt. However, at 90° the agreement of the ratio data measured here, with the measurement made by nuclear emulsion detectors[5] which were probably insensitive to electrons, indicates that the positron contamination is probably not larger than 10 percent to 20 percent of the positive meson yield. In the following data no attempt was made to correct for electron or positron contamination.

V. EXPERIMENTAL RESULTS

The angular distributions of 70 ± 6 Mev charged mesons from C^{12} and Be^{9} were measured during July 6, and 7 and September 5, 6, 7, 1952. Some of the data were re-measured during the latter run to re-establish the relative efficiency of the detector. System A was not used at 15 and 30 degrees, because it would have projected into the neutron beam. From 45 to 125 degrees both systems were employed. At periodic intervals, the current was reversed in the magnet coils, to insure that A and B were recording properly. The data from A and B are combined with equal weights. The rate of positive and negative counts per unit monitor are shown in Table I. The data have been corrected for background counts. The two values for each target at each angle are the low and high bias counts as explained in III-B. The targets contain approximately the same number of protons, and may be adjusted for equal target protons by multiplying the carbon data by 1.049. (See IV-B-4). Statistical probable errors are quoted.

A. Negative to Positive Ratio

The negative to positive ratio is the most direct information to be obtained. The mesons have, within close limits, the same mass,[23] lifetime,[24] energy and efficiency for detection. The ratios, computed from Table I, are plotted in Figures 19 and 20 as a function of observation angle. The meson energy, corrected for energy loss in the target and front counter, is 85 ± 8 Mev. The angular resolution ± 6° is determined by the Coulomb scattering in the target. The detector geometrical resolution is only ± 2.5°, and the Coulomb scattering of a 70 Mev meson in 1 cm of carbon is ± 1.8 degrees.

TABLE I

RELATIVE YIELDS OF POSITIVE AND NEGATIVE PIONS FROM Be AND C. THE NUMBERS LISTED ARE CORRECTED COUNTS PER UNIT MONITOR RESPONSE

TARGET	554 g. Be^9		470 g. C^{12}	
ANGLE DEGREES	π^+	π^-	π^+	π^-
	4.6 ± 0.9	148.0 ± 3.0	4.0 ± 0.7	89.0 ± 3.0
15	3.4 ± 0.7	103.0 ± 3.0	3.6 ± 0.6	62.0 ± 3.0
		116.0 ± 5.0		73.0 ± 4.0
30		79.0 ± 4.0		53.0 ± 3.0
	0.68 ± 0.29	53.0 ± 1.0	1.2 ± 0.4	39.0 ± 1.0
45	0.59 ± 0.21	31.0 ± 1.0	1.3 ± 0.3	28.0 ± 1.0
	0.90 ± 0.30	25.0 ± 1.0	1.2 ± 0.3	22.0 ± 1.0
60	0.95 ± 0.26	18.0 ± 1.0	0.8 ± 0.3	15.0 ± 1.0
	0.55 ± 0.24	14.0 ± 1.0	0.9 ± 0.3	11.0 ± 1.0
75	0.42 ± 0.18	10.0 ± 1.0	0.7 ± 0.2	8.0 ± 0.6
	0.13 ± 0.09	10.8 ± 0.8	0.58 ± 0.20	7.6 ± 0.7
90	0.13 ± 0.09	5.5 ± 0.6	0.14 ± 0.09	4.9 ± 0.5
	0.0 ± 0.1	4.8 ± 0.5	0.30 ± 0.14	4.7 ± 0.5
110	0.0 ± 0.1	3.0 ± 0.5	0.15 ± 0.10	2.8 ± 0.5
	0.29 ± 0.14	4.5 ± 0.5	0.72 ± 0.22	3.3 ± 0.5
125	0.14 ± 0.09	2.3 ± 0.4	0.58 ± 0.20	2.2 ± 0.4

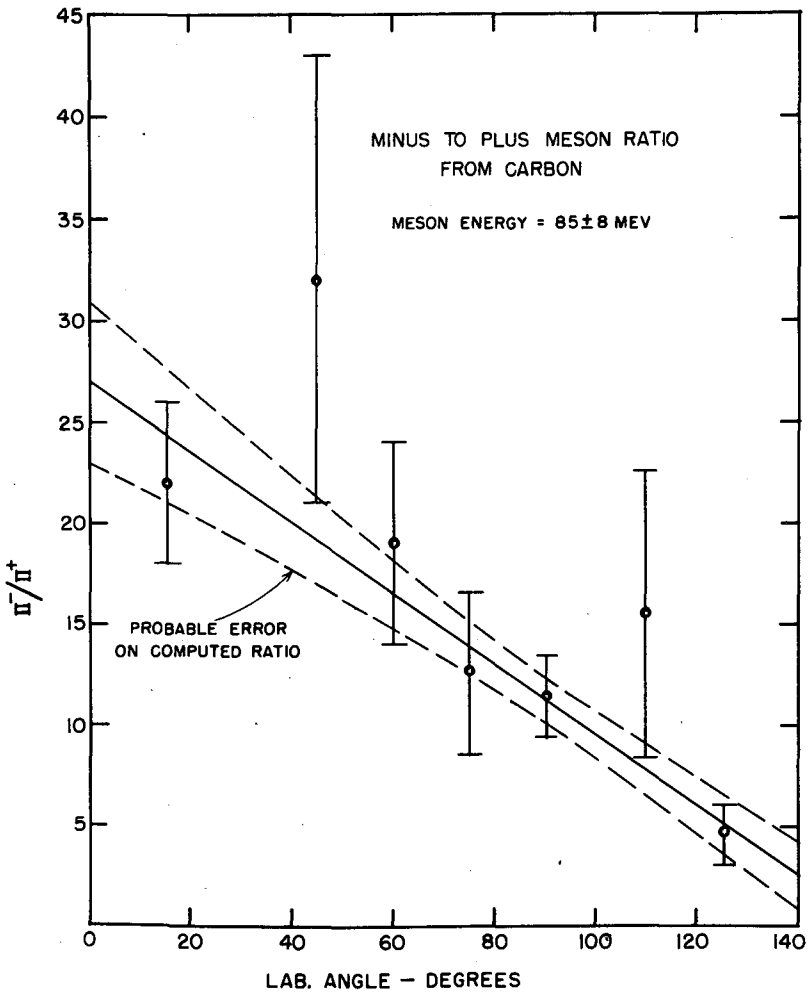

FIG. 19

MU-5348

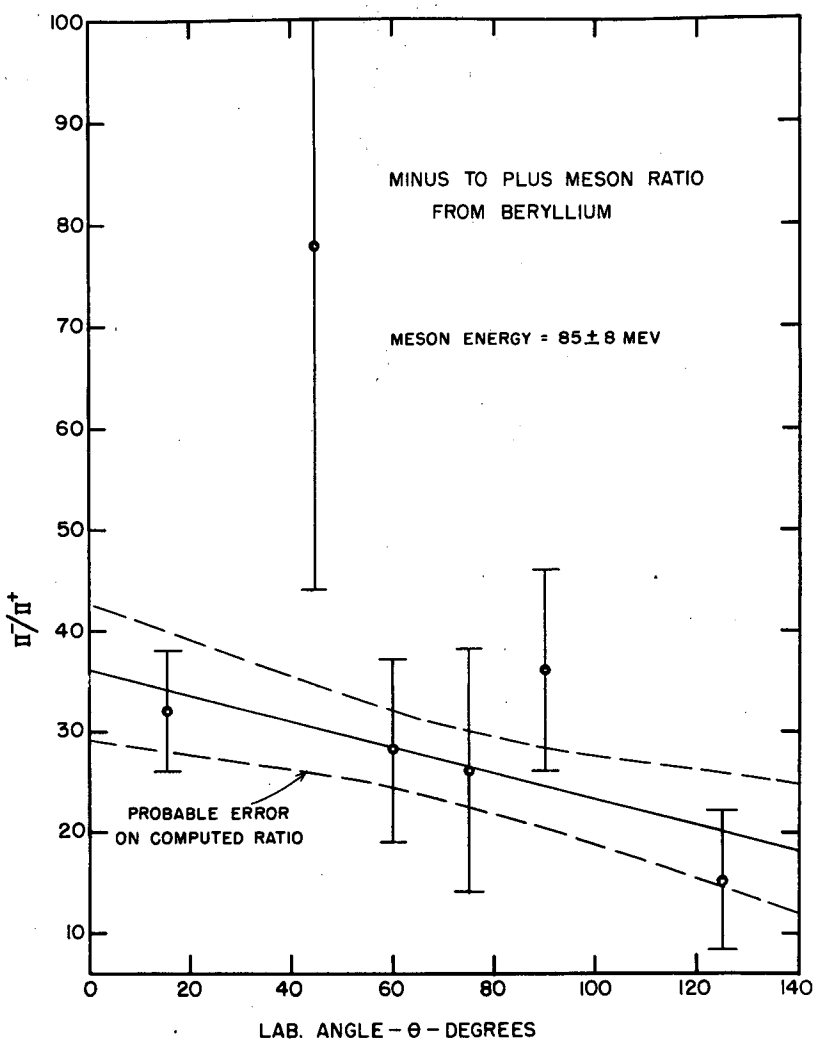

FIG. 20

MU-5349

The low bias data were fitted by a straight line by the method of least squares,[31] on the assumption of no error in the angular measurement. The ratio of the probable errors on the basis of external consistency (r_e) and internal consistency (r_i) was $r_e/r_i = 0.7$ for Be and 0.6 for carbon. The evidence is that a straight line is a reasonable fit to the experimental points and that the probable errors assigned to the measured ratios at each angle are not too small. The error of the fitted ratio is, of course, smaller than the error of any one measurement because of the weights carried by the adjacent points. The weight of a data point is proportional to the inverse square of the probable error. The ratios computed by the least squares method are given in Table II, and represent the best estimate consistent with the experimental data. Reduction of the high bias data gave similar results, but with slightly greater error due to the fewer number of counts. In all the following, the data from the low bias counts are used.

At 90°, the carbon ratio may be compared with the answer obtained by Bradner, et al.,[5] who detected the mesons by their characteristic track endings in nuclear emulsions. Their value is $\pi^-/\pi^+ = 12.6 \pm 1.5$ for 50 → 65 Mev. Our value is 11 ± 1 for 85 ± 8 Mev. The agreement of the measurement, although at different energies, seems to indicate that the contamination of the positive mesons by high energy positrons is not very large. (See IV-B-5).

The Be ratio is about twice the carbon ratio at all angles. The 90° ratio data have been weighted by an earlier reliable measurement taken with a similar system. However, because of different relative monitor unit, the individual π^+ and π^- counts are not shown in Table I.

TABLE II

TARGET ANGLE DEGREES	BERYLLIUM π^-/π^+	CARBON π^-/π^+
0	36 ± 7	27 ± 4
30	32 ± 5	22 ± 3
60	28 ± 4	16 ± 2
90	24 ± 4	11 ± 1
120	21 ± 6	6 ± 1

TABLE III

ANGLE DEGREES	$\pi^-_{Be} - \pi^-_{2/3\,C}$	$\pi^+_{Be} - \pi^+_{2/3\,C}$	$\pi^+_{Be}, \pi^+_{2/3\,C}$ WEIGHTED AVERAGE
15	55 ± 5.0	+ 0.4 ± 1.1	4.4 ± 0.6
30	40 ± 7.0		
45	12 ± 2.0	- 0.5 ± 0.5	0.89 ± 0.23
60	2 ± 2.0	- 0.4 ± 0.4	1.1 ± 0.2
75	2 ± 1.0	- 0.3 ± 0.4	0.70 ± 0.18
90	3 ± 1.0	- 0.5 ± 0.2	0.70 ± 0.08
110	0 ± 0.8	- 0.3 ± 0.2	0.13 ± 0.08
125	1 ± 0.7	- 0.5 ± 0.3	0.41 ± 0.12

B. Qualitative Angular Distribution Results

The negative and positive yields change most rapidly in the region 0 to 60°. The increase of π^-/π^+ ratio at the forward angles indicates that the angular distributions of the pions are not the same; the positive yield seems to be a more uniform distribution. On a relative basis, the Be target consists of five neutrons and four protons (1 Be nucleus); the carbon target consists of four neutrons and four protons (2/3 carbon nucleus). According to the alpha particle model of light nuclei,[9] it is expected that a subtraction of the target data will show:

(a) The negative mesons produced in a neutron-neutron collision.

(b) No net positive yield, if the protons in the two targets have equal production efficiency.

The subtracted data are listed in Table III. The negative pion difference is most prominent in the 15 to 60 degree region. The positive pion difference is zero within statistics at each angle; however, a weighted average over all angles observed indicates a slightly greater yield for carbon, but probably the same angular distribution as Be. Because of the poor statistics the positive pion yields due to the four protons in each target were averaged, and are also shown in Table III.

VI. CORRECTION OF ANGULAR DISTRIBUTION DATA

The experimental data are the angular distributions of 85 ± 8 Mev charged pions from C^{12} and Be^9 from 15 to 125 degrees in units of counts per monitor. There is, at present, a complete lack of experimental information for the energy spectra of mesons produced by neutron bombardment of these targets. On the assumption that the general characteristics of these spectra may be computed as a function of angle (ϕ) it is of interest to reduce the angular distribution data to units of the differential cross section $d\sigma(\phi)/d\Omega$ in CM^2 steradian^{-1} nucleus^{-1}. In a relative manner, this requires a fold of the detector energy acceptance into the computed energy spectra, in order to correct the data for the number of mesons not counted at other energies. It will be shown from the kinematics associated with a computation of the spectra, that there is a fairly well defined center-of-mass for the incoming neutron and the moving target nucleon which will allow the laboratory angular distribution to be transformed to a most probable center-of-mass frame.

With less accuracy, the absolute scale for the cross section will be assigned from (1) the beam intensity measurement, (2) time-of-flight measurement of mesons at 90°, without use of magnet, (3) corrections for decay in flight, scattering loss, efficiency and solid angle of the detector. In this section the relative corrections are discussed in parts A and B; measurements and computations for an absolute scale are reviewed in C and D.

A. Energy Spectra Computations

The general features of meson energy spectra from carbon bombarded by 340 and 380 Mev protons have been computed by Henley[25] and Passman, Block and Havens,[26] for 0 and 90 degrees. Their interpretation is based, in part, upon the properties of the more simple, fundamental reaction ($p + p \rightarrow \pi^+$) which has been studied in some detail.[26, 3] In this reaction the possible products are $p + p \rightarrow \pi^+ + p + n$ or

$\pi^+ + d$. The experimental results are (a) the production is mainly concentrated in a narrow spectrum around the maximum energy compatible with deuteron formation, (b) the cross section increases with the available energy,[26, 27] (c) in the center-of-mass system of the colliding nucleons, the mesons are emitted into a $\cos^2\theta$ distribution. In the case of meson production from complex targets, it is assumed that the production proceeds through the same elementary process, but now the target proton is in motion,[10] because of the binding forces in the carbon nucleus. The effect of the target nucleon momentum distribution is to (a) increase the energy available in the reaction, (b) broaden the observed meson energy spectrum, (c) distribute the magnitude and direction of the center-of-mass velocity vectors. Other difficulties and refinements are discussed in the references. In a simplified picture, the remaining nucleons carry off momentum equal and opposite to the momentum of the struck nucleon and do not interact with the outgoing meson.

1. Collision Model

In attempting to compute meson spectra from a carbon target, one is immediately impressed by the complexity of the problem, and by the effort put forth by previous investigators. In order to make any progress toward the solution of meson spectra at angles ranging from 15 to 125° to the neutron beam, it was necessary to work with the simplest assumption for the collision model, and to use approximate methods wherever possible.

The predominant elementary process in neutron bombardment is assumed to be $n + n \rightarrow \pi^- + d$. This is a two-body problem, and the solution of the equations for conservation of energy and momentum yield an unique answer for the meson energy and angle for a given neutron-neutron collision. The problem then is to consider the effect of the neutron beam energy spectrum,[2] reproduced in Figure 21, the momentum distribution of the target nucleons,[10] shown in Figure 22, and the excitation function,[27] reproduced in Figure 23. In the excitation function, the curve has been drawn through the points measured by Schulz and Steinberger and extended by a straight line into the unmeasured energy regions,

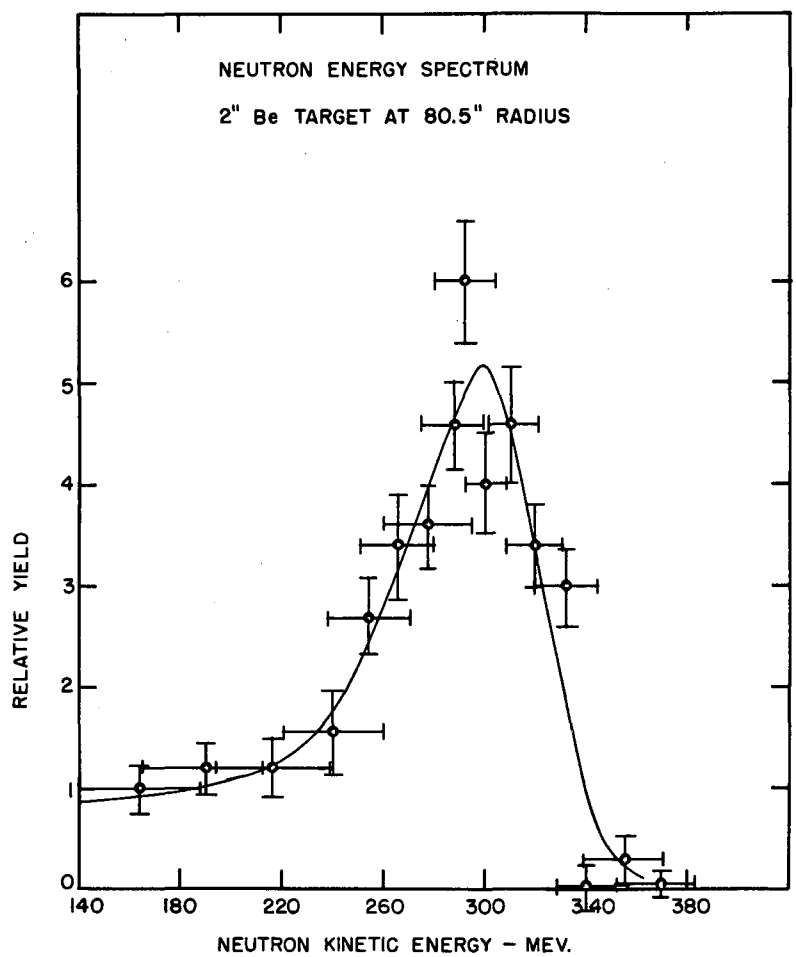

FIG. 21

MU-5350

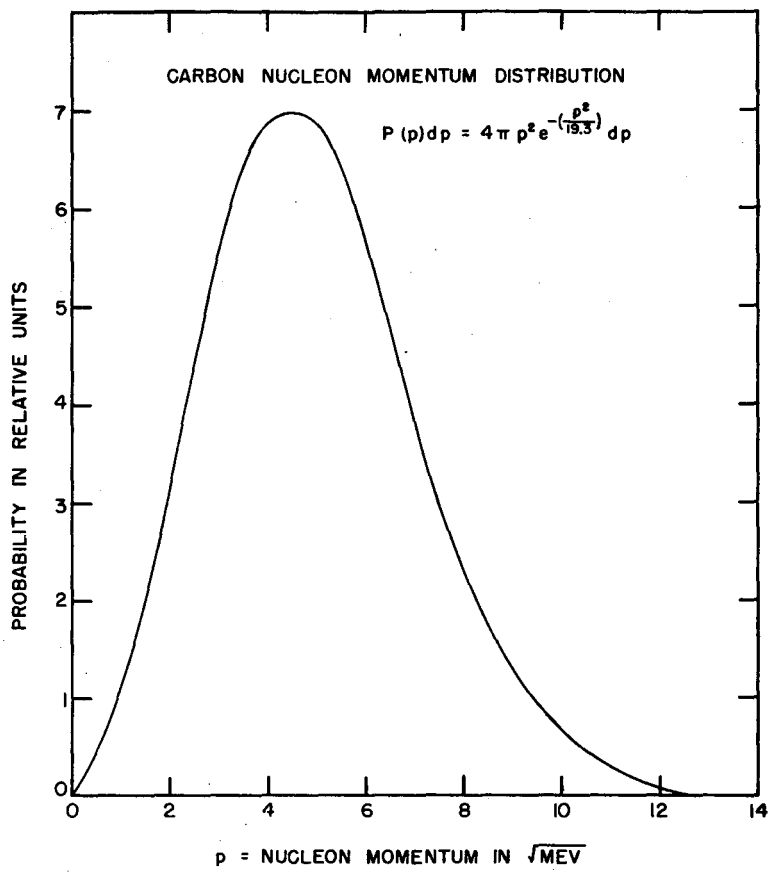

FIG. 22

MU-5478

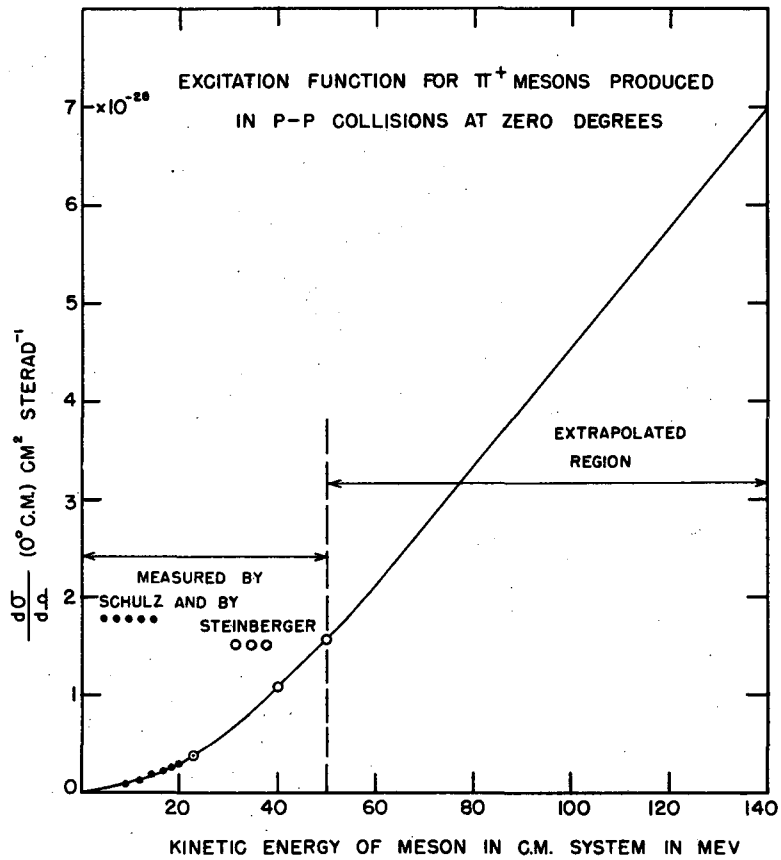

FIG. 23

MU-5479

since the larger excitation energies will be used in the energy spectra computations. It is assumed that the excitation curve is independent of the meson angle.

The probability that a meson is created depends, through the excitation function on the kinetic energy ($T_\pi^\prime$) of the meson in the center-of-mass system of the colliding nucleons (i.e., on the energy available). As a first step, $T_\pi^\prime$ was computed for the range of expected momenta of the colliding nucleons. A discussion of the conservation of energy and momentum relations, and the energy available for the reaction are presented in Appendix A. Neutron beam energies (T_1) of 270, 300, 340 Mev, were selected to collide with target nucleon energies (T_2) of 0 to 100 Mev, at angles (α) from 180 to 90 degrees. A head-on collision is when $\alpha = 180^\circ$. The various $T_\pi^\prime$ are shown in the polar plots 24, 25, 26 for lines of constant T_2. For example, if the beam energy is 300 Mev, and if the collision occurs at $\alpha = 150^\circ$ with a 40 Mev target neutron, the meson energy is 57 Mev in the C. M. system. Assuming the nucleon momentum distribution is spherically symmetric in coordinate space, the probability of a collision at angle α in range $d\alpha$ is $1/2(\sin \alpha)\, d\alpha$. The first conclusion is that if $\bar{\alpha}$ is the most probable collision angle, then $180^\circ > \bar{\alpha} > 120^\circ$. A collision angle less than about 120° does not produce mesons because the available energy drops below $m_\pi C^2$. The exact value of this cut-off angle changes rather slowly with T_1, in the range 270 to 340 Mev.

2. Most Probable Collision

In order to further define the most probable collision, the independent probabilities that a neutron has an energy T_1, T_2, and a collision angle α, and that a meson of $T_\pi^\prime$ has been created in the C. M. system, must be multiplied into the curves for $T_\pi^\prime$. The results are shown in the polar plots 27, 28, 29. These plots show the relative meson yield in the center-of-mass system for the various nucleon energies and angles of collision in the laboratory system. The sin α factor favors collisions at 90°; the excitation function favors head-on

MESON ENERGY IN C.M. SYSTEM

BEAM ENERGY = 270 MEV

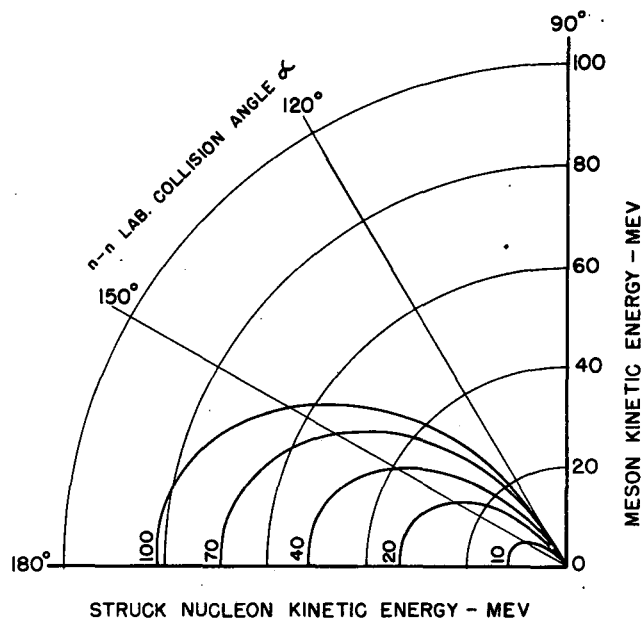

FIG. 24

MU-5351

MESON ENERGY IN C.M. SYSTEM

BEAM ENERGY = 300 MEV

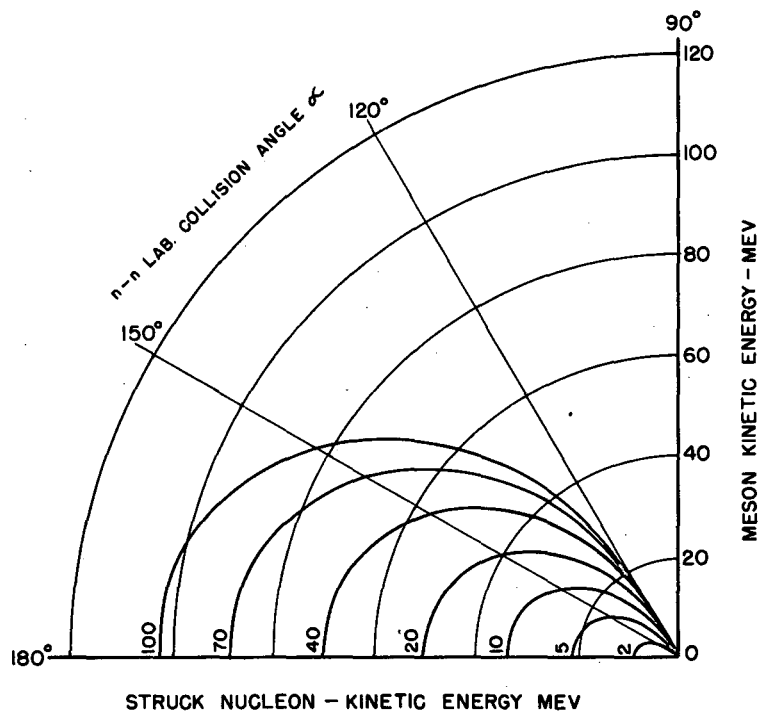

FIG. 25

MU-5352

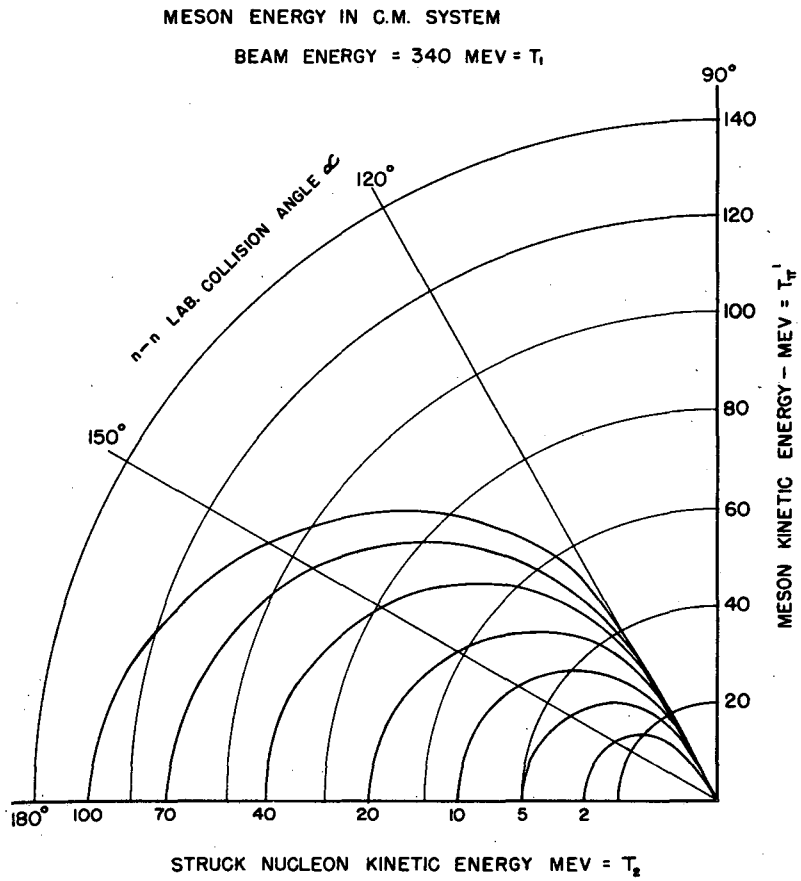

FIG. 26

MU-5480

RELATIVE YIELD OF MESONS

BEAM ENERGY = 270 MEV

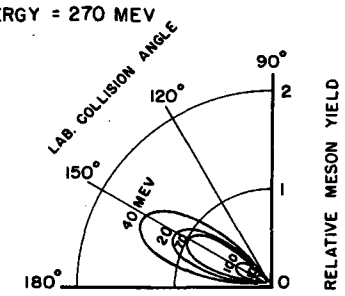

STRUCK NUCLEON – LINES OF CONSTANT K.E.

THE DISTRIBUTION OF NUCLEON ENERGIES SHOWN IN FIG. 22 HAS BEEN USED TO WEIGHT THE YIELDS

BEAM ENERGY = 340 MEV

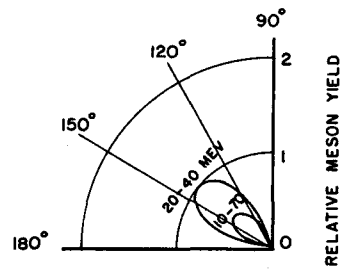

STRUCK NUCLEON – LINES OF CONSTANT K.E.

FIG. 27

MU-5481

RELATIVE YIELD OF MESONS IN C.M. SYSTEM

BEAM ENERGY = 300 MEV

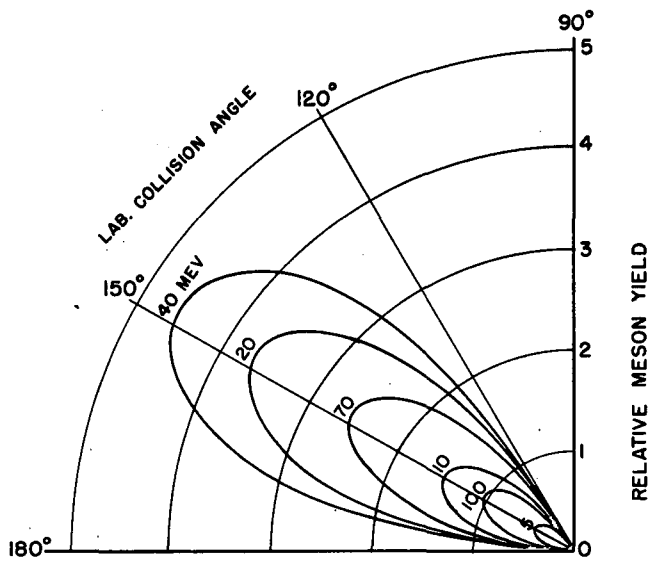

STRUCK NUCLEON LINES OF CONSTANT K.E.

FIG. 28

MU-5353

RELATIVE YIELD OF MESONS IN C.M. SYSTEM

BEAM ENERGY = 320 MEV

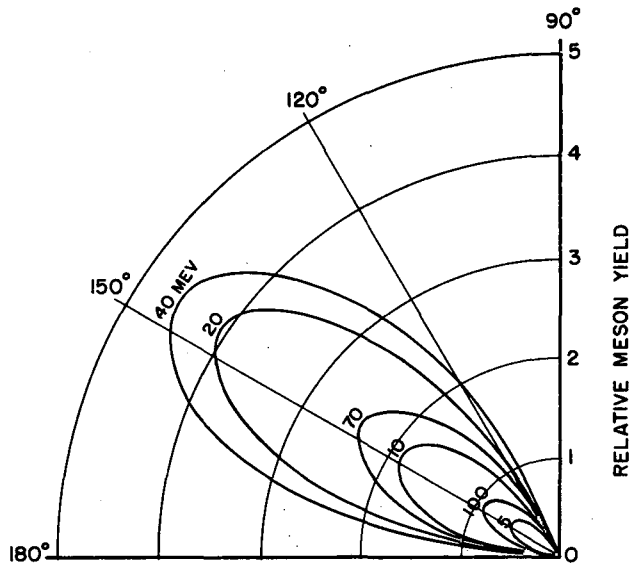

STRUCK NUCLEON – LINES OF CONTANT K.E.

FIG. 29

MU-5354

collisions, as well as the larger energies for T_1 and T_2. Finally, the momentum distribution returns the yield probability to a low value for large T_2 and for any T_1. From these polar plots the following facts are inferred:

(a) About 60 percent of the neutrons in the energy spectrum above 200 Mev are effective in producing mesons. This is seen by plotting the maximum relative yield of mesons in the C. M. system as a function of the neutron energy and comparing with the neutron spectrum. (See Figure 30.) The most effective energy is 310 Mev.

(b) The most probable collision angle, $\bar{\alpha}$, remains fairly constant for all collisions. $\bar{\alpha} = 146^{\circ}$, from Figure 31.

(c) The probable center-of-mass energy for the meson is about 50 to 60 Mev, Figure 32, which is large compared to 20 Mev, the maximum energy for a meson made by a 340 Mev proton and a target proton at rest.

(d) No mesons are made in exact head on collisions or for α less than 120°.

The collision parameters are determined more closely by computing weighted average values and their probable errors, where the weights are determined by the relative meson yield. The results are:

$$\bar{T}_1 = 310 \begin{smallmatrix} + 20 \\ - 30 \end{smallmatrix} \text{ Mev} \qquad \bar{T}'_{\pi} = 52 \pm 20 \text{ Mev}$$

$$\bar{\beta}'_{\pi} = 0.68 \pm 0.08$$

$$\bar{T}_2 = 40 \begin{smallmatrix} + 30 \\ - 25 \end{smallmatrix} \text{ Mev}$$

$$\bar{\alpha} = 146 \pm 10 \text{ degrees}$$

The total momentum $(\vec{p}_1 + \vec{p}_2)$ or center-of-mass velocity makes an angle $\tau = 15 \pm 6$ degrees with respect to the neutron beam (laboratory axis). The center-of-mass velocity projected onto the laboratory axis is $\bar{\beta}_{cm} = 0.27 \pm 0.04$. A most probable collision in terms of momentum vectors is shown in Figure 33. It is evident that the allowable values for the center-of-mass motion are fairly restricted by the requirements for meson production.

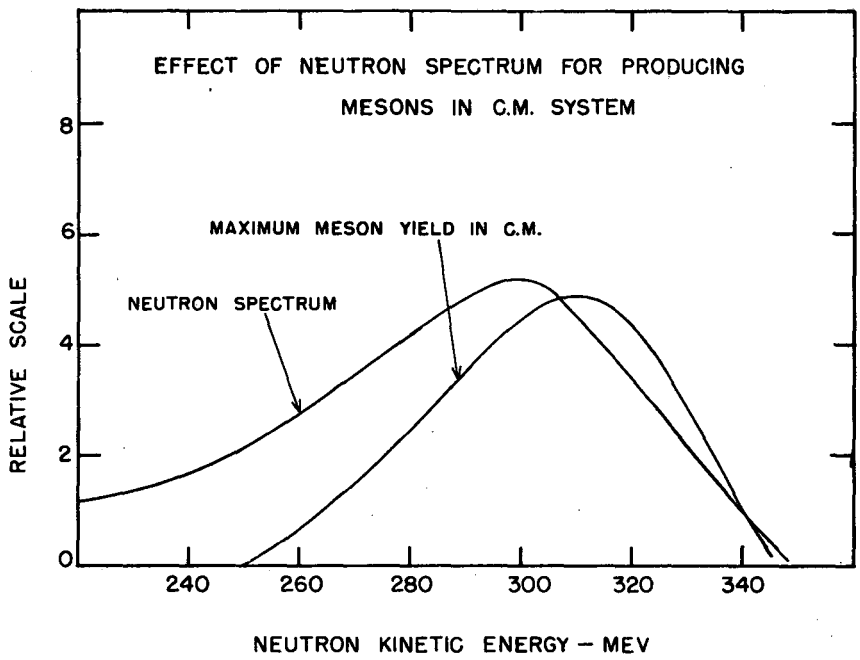

FIG. 30

MU-5482

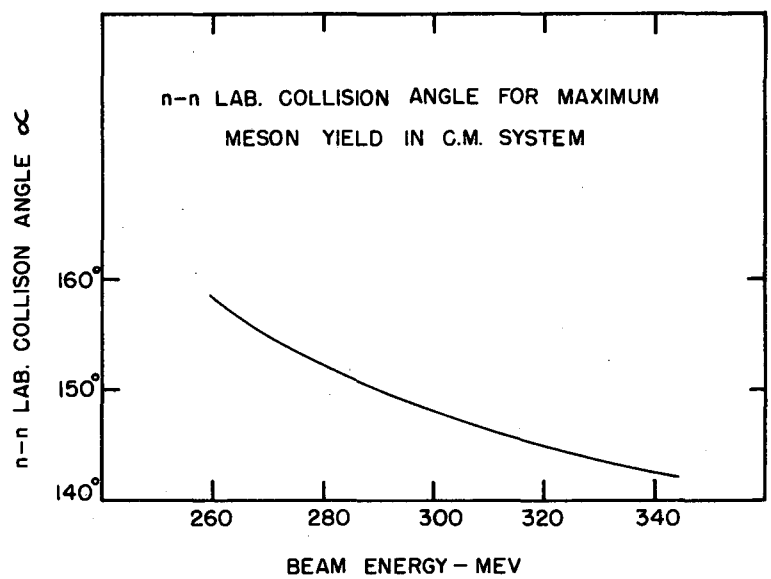

FIG. 31

MU-5483

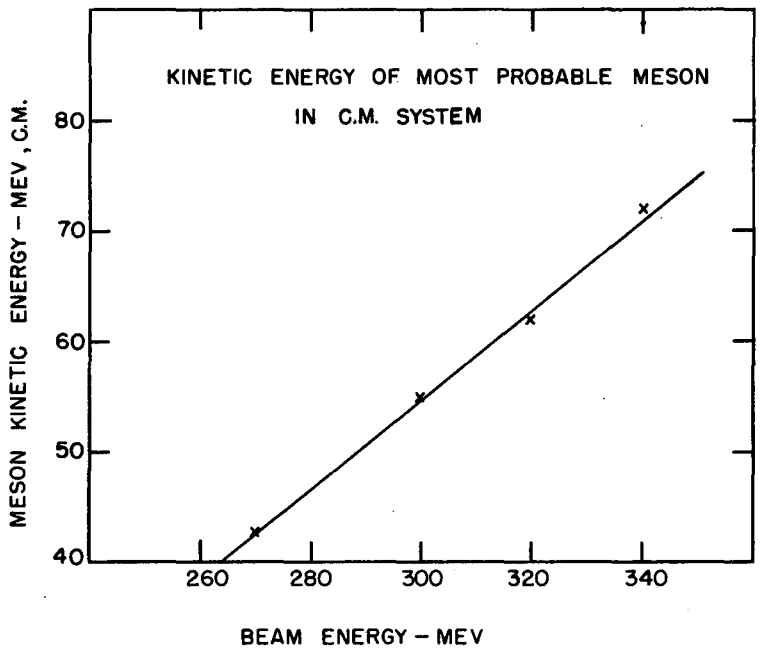

FIG. 32

MU-5484

WEIGHTED AVERAGE MOMENTA OF COLLIDING NUCLEONS
FOR MAXIMUM MESON YIELD IN C.M. SYSTEM

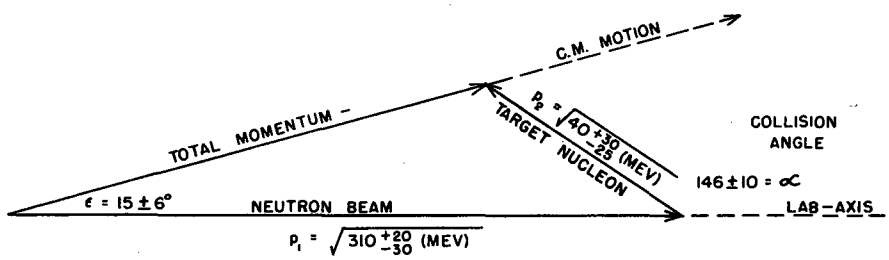

$\beta_{C.M.} = 0.27 \pm 0.04$ (PROJECTED ON LAB-AXIS)

$T_\pi' = 52 \pm 20$ MEV = MESON K.E. IN C.M.

$\beta_\pi' = 0.68 \pm 0.08$ = MESON β IN C.M.

FIG. 33

MU-5485

3. Construction of 90° Meson Spectrum

At 90° the kinematical formula for the meson energy are somewhat easier to evaluate. The spectra in the laboratory system are constructed by summing overall collisions which contribute to the meson production at a particular angle of observation. In part (2) above, it was inferred that the mean center-of mass velocities form a cone ± 15°, about the beam axis. A particular meson energy in the C. M. system is, therefore, not an unique value when transformed to the laboratory system. An approximation is to restrict the collisions to a plane perpendicular to the plane containing the beam and the observed meson. One then obtains an average value of the meson laboratory energy for collisions on the cone, i.e., for collisions around the beam axis. Next, holding T_1 and T_2 constant in their perpendicular plane, the collision angle α is varied and the resultant meson energy computed. The relative number of mesons contributing to a particular energy is just the relative center-of-mass yield factor computed as a function of α, T_1 and T_2. Finally, holding T_1 constant, the process is repeated for other values of T_2 in equal steps so that the results may be summed over all T_2. The curves plotted and summed are shown in Figure 34, and are quite instructive in that they show the relative contribution to the total spectra made by the various target nucleon momenta. A comparison of Figure 34 with the measured spectra of π^+ mesons from carbon bombarded by 340 Mev protons,[4] indicates the general features of the meson spectra from carbon have been predicted at 90°.

Spectra for T_1 = 270 and 330 Mev were also computed at 90°, but when weighted by the neutron spectrum and combined with the T_1 = 300 Mev results, there was little change in the spectrum shape. In computations for other angles, T_1 = 300 Mev was used.

4. Spectra at Other Angles

It was observed in the computation of the 90° spectra, that the partial spectra contributed by a constant nucleon momentum when the collision angle α was varied, could be defined at these meson energies:

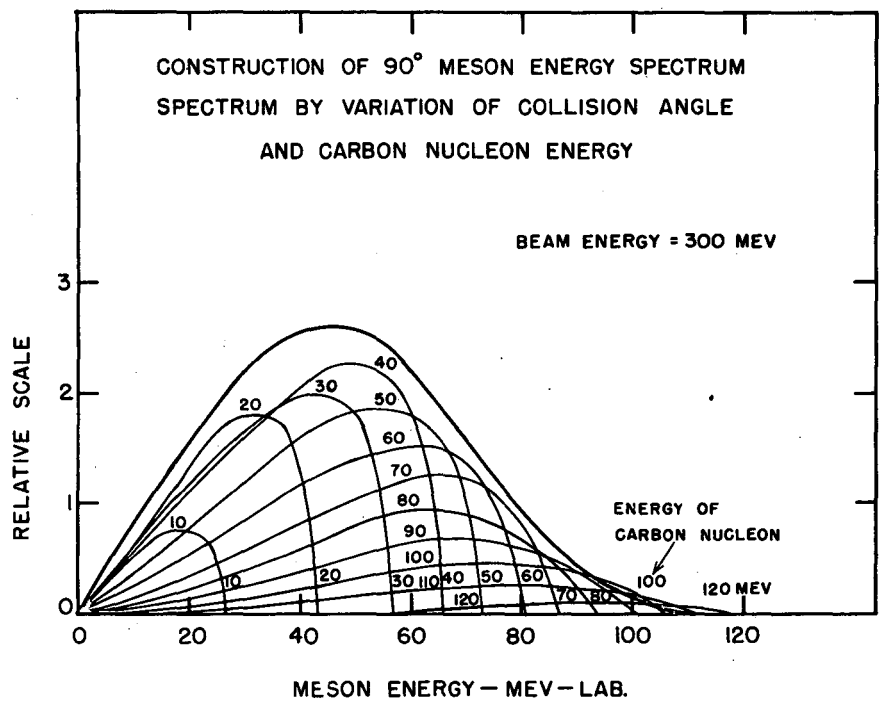

FIG. 34

MU-5486

(a) When $\alpha = 180^{\circ}$, the meson energy is a maximum (T_{π} max), but the meson probability is zero because of the sin α term.

(b) When $\alpha = 150^{\circ}$, the meson energy has a most probable value ($\overline{T}_{\pi}$) and the meson probability is a maximum.

(c) When $T_{\pi} \rightarrow 0$, as $\alpha \rightarrow 120^{\circ}$, the probability also approaches zero, because of the excitation function.

The values of T_{π} (max) and $\overline{T}_{\pi}$ as a function of meson angle of emission ϕ in the laboratory system have been computed for various T_2 and are shown in Figures 35 and 36. From these plots and the relative yield factors in Figure 28 for $T_1 = 300$, meson spectra at any angle can be graphically constructed. Again, a check with the measured π^+ spectra from carbon bombarded by 340 Mev protons at 0° and 180°,[29] shows that the general features of the computed spectra are correct, when the differences in the neutron and proton beam energies have been considered. The computed spectra, normalized to the same peak value, are shown in Figure 37.

B. Relative Efficiency of Detector - Target System

It is apparent that due to the change in the meson energy spectrum as the angle of observation (ϕ) is varied, a detector with a fixed energy acceptance will have a relative efficiency f (ϕ) for recording the total number of mesons at each angle. The problem here is to determine f (ϕ), assuming the general features of the computed spectra (Figure 37) are correct. Again a graphical rather than an analytical analysis has been performed in order to reduce the labor of computation. As the mesons proceed out of the target and into the detector system, the spectrum is modified by the energy dependent factors: (1) energy loss in the target and front counter, (2) Coulomb scattering in the front counter, and (3) decay in flight.

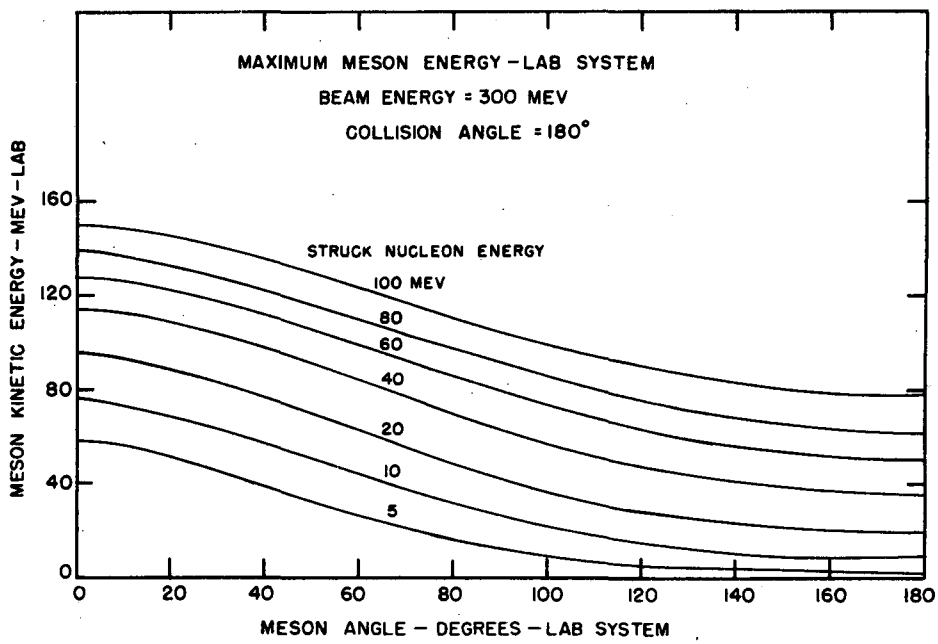

FIG. 35

MU-5412

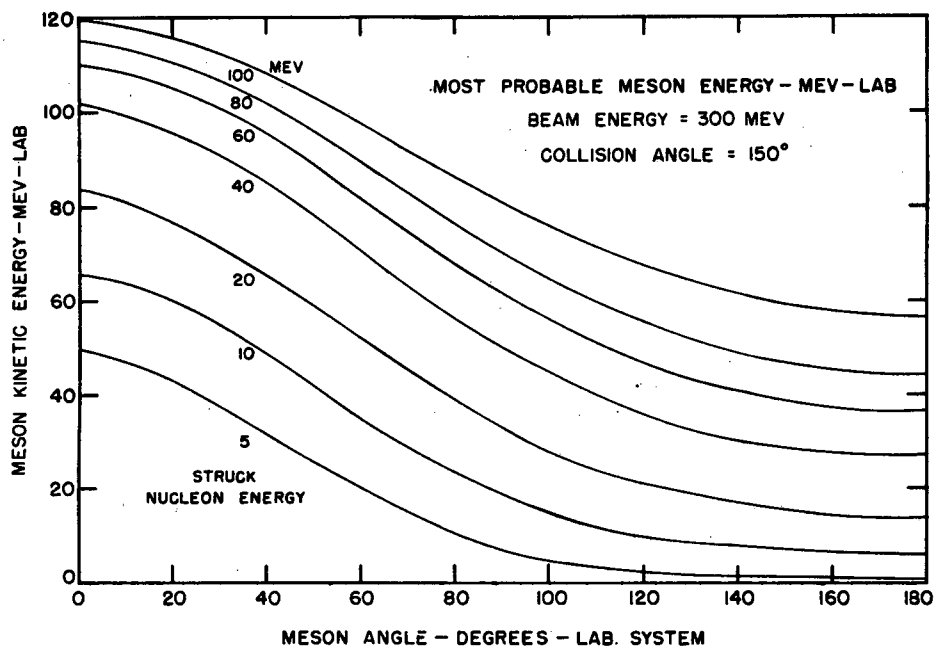

FIG. 36

MU-5413

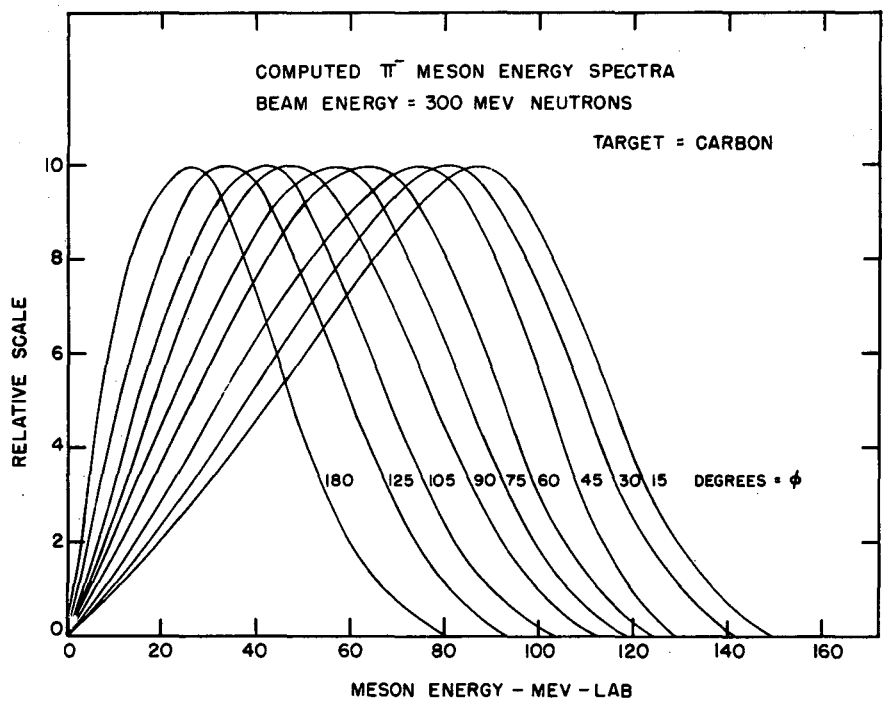

FIG. 37

MU-5414

1. Energy Loss

The thickness of the Be and C target in the direction of meson travel is 3.8 cm. The front counter is a 1 cm thick stilbene crystal, considered equivalent to 1 cm of carbon. Be and Carbon have closely the same stopping power. The rate of meson energy loss in carbon was computed from the range - energy curves of Aron, et al.,[29] for protons in carbon, using a ratio $(m_p/m_\pi) = 6.7$. The spectrum changes were estimated by considering the energy loss for those mesons which originate at various depths in the target. The spectrum is shifted to a lower energy, and the total number of mesons is less, because the lower energies are stopped in the target and the counter. The energy loss effect is relatively most severe at the wide laboratory angles.

2. Coulomb Scattering

Loss of mesons due to multiple scattering[30] in the front counter is small because the mean squared scattering angle $\overline{\theta^2}$ of a 70 Mev meson in 1 cm of carbon is 3.14 (degrees),[2] which is less than the angular spread of the meson trajectories allowed by the geometry of the system. A useful formula for meson scattering in carbon is:

$$\overline{\theta^2} = \frac{13\ t}{\beta^4\ E^2\ (\text{Mev})^2}$$

where t - Carbon thickness in cm.

E - Total energy of meson in Mev.

β - Velocity of meson in units of C, the velocity of light.

The change in $\overline{\theta^2}$ for various observation angles is very small because the mean detection energy remains approximately constant.

3. Meson Decay in Flight

The π meson decays by the process $[\pi \rightarrow \mu + \nu$ (neutrino)] with a mean life 2.5×10^{-8} seconds. The μ meson has about 4 Mev kinetic energy[23] in the π meson rest frame. In the laboratory system, most of the decay μ mesons from 70 Mev π mesons make an angle greater than $\pm 10^{\circ}$ with respect to the original π direction. Since the angle subtended by the rear counter set, for most of the points along the flight path, is

less than $\pm 10^{o}$, only a small number of μ mesons will enter the rear counters. Therefore, if a π decays in flight, the probability is large that it will not be recorded.

If N_o is the initial number of π mesons leaving the target, then the number N surviving the flight path d is:

$$N = N_o e^{-t/\tau}$$

where $\tau = 2.5 \times 10^{-8}$ sec.

t = proper time in π frame

$$t = (t_{lab})\, \gamma_\pi^{-1} = (d/c)\, (\gamma_\pi^2 - 1)^{-1/2}$$

The relative change in N/N_o is small as the observation angle is varied because the mean detection energy is approximately constant.

4. Conclusions

In order to illustrate the effect of the corrections (1, 2, 3), the modified computed spectra are shown for 0° and 90° in Figures 38 and 39. Finally, the energy resolution curve (Figure 13) was folded into the remaining spectra. At 0°, $f(0^o) = 0.18$; at 90°, $f(90^o) = 0.09$. Intermediate angles from 0° to 180° were analyzed in the same fashion and the relative efficiency $f(\phi)$ of the detector is plotted in Figure 40. To obtain the absolute efficiency $\epsilon(\phi)$, the efficiency of the counters for recording penetrating charged particles must be included. For the low bias counts the counter efficiency is 0.4. Therefore, $\epsilon(\phi) = 0.4\, f(\phi)$.

Although the absolute efficiency is rather low (0.072 at best) for detecting the complete meson spectrum, it is important to note that between $\phi = 0$ and 75 degrees the change in relative efficiency is small compared to the change observed in the π^- counting rate.

C. Beam Intensity Measurement

From the analysis of meson production probabilities for various neutron energies (VI-A-2) it was estimated that 60 percent of the neutron intensity above 200 Mev is effective for meson production in

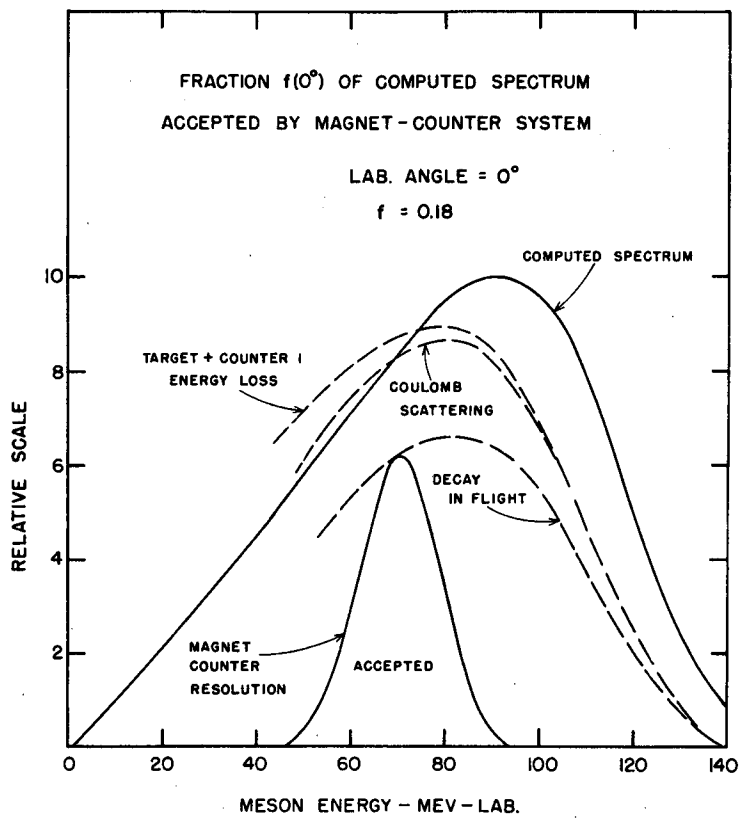

FIG. 38

MU-5415

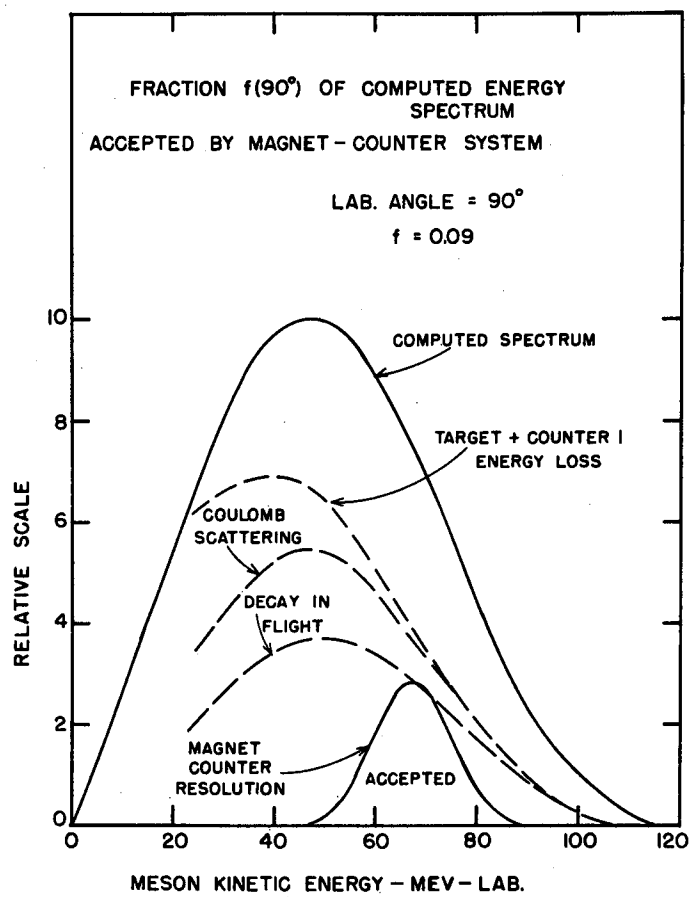

FIG. 39

MU-5355

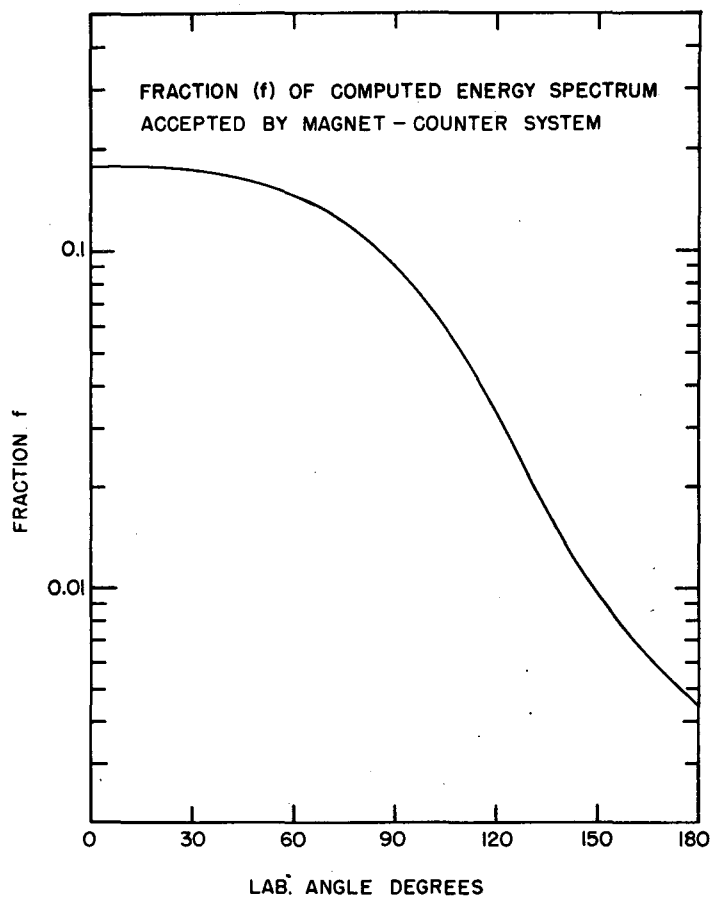

FIG. 40

MU-5356

carbon, and the effective neutron energy is $310 \begin{smallmatrix}+20\\-30\end{smallmatrix}$ Mev. The next problem is to determine the intensity of the neutron beam above 200 Mev, in units of neutrons CM^{-2} $monitor^{-1}$, where the relative monitor unit is the same for the meson angular distribution data.

The procedure is to set up a n - p scattering experiment similar to Segrè, et al.,[12] who used the same neutron beam, limited to energies above 200 Mev, to measure the n - p differential scattering cross section. The hydrogeneous target (CH_2 - C) was placed 20 feet downstream from the meson target, and the intensity measurement run concurrently with the meson experiment. The geometry of the 150 Mev proton threshold detector is shown in Figure 41. The scattering angle is $\phi = 33^o$. The differential cross section for scattering protons into a fixed solid angle $d\Omega$ at $\phi = 33^o$ is given[12] as:

$$\frac{d\sigma}{d\Omega}(33^o) = (6.5 \pm 0.8) \times 10^{-27}\ cm^2\ sterad.^{-1}$$

Let N = proton counts in $monitor^{-1}$

n = neutrons above 200 Mev in cm^{-2} $monitor^{-1}$

H = total protons in target

$\Delta\Omega$ = detector solid angle in steradian

ϵ = detector efficiency

$$\text{Then } N = nH\left(\frac{d\sigma\ (33^o)}{d\Omega}\right)\ \Delta\Omega\epsilon$$

Four photomultiplier scintillation counters were used for the proton detector. The small ($1 \times 1\ cm^2$) outer counters 1, 2 are used to measure the efficiency of the larger ($4 \times 5\ cm^2$) inner counters 3, 4 separated by the 1/2 inch tungsten absorber. The efficiency of 3, 4 is given by the ratio of events 1, 3, 4, 2 to events 1, 2. By moving counters 1, 2 over various sections of 3, 4 an average efficiency of $\tau = 0.75 \pm 0.05$ was obtained. This agrees with the transmission factor 0.74 for

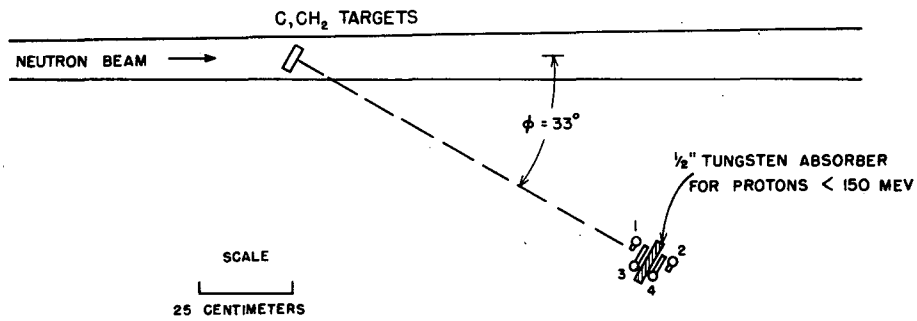

NEUTRON BEAM INTENSITY MEASUREMENT
BY N-P SCATTERING

FIG. 41

MU-5416

the tungsten absorber at 33° as measured by Segrè, et al.[12] The efficiency of 3, 4 without the tungsten, is about 90 percent. The coincidence apparatus is similar to that described for the meson detector. The values obtained with counters 3, 4 and their standard deviations are:

$$N = (4.25 \pm 0.08) \times 10^3 \text{ proton monitor}^{-1}$$
$$H = 2.04 \times 10^{25} \text{ protons}$$
$$\Delta\Omega = 1.81 \times 10^{-3} \text{ sterad.}$$
$$\bar{\epsilon} = 0.75 \pm 0.05,$$

Therefore,

$$n = (2.36 \pm 0.34) \times 10^7 \text{ neutrons cm}^{-2} \text{ monitor}^{-1}.$$

The meson target is at 50 feet from the neutron source. The n - p scattering target at 70 feet. In addition, the meson target attenuated the neutron beam at the n - p scattering target by 0.93. The neutron flux at the meson target, and its probable statistical error is:

$$n' = (5.0 \pm 0.5) \times 10^7 \text{ neutrons cm}^{-2} \text{ monitor}^{-1}$$

Since one monitor unit requires 15 minutes, the average neutron intensity above 200 Mev is about 5×10^4 neutron cm^{-2} sec^{-1}. The effective neutron intensity for meson production in carbon is:

$$(3.0 \pm 0.3) \times 10^7 \text{ neutrons cm}^{-2} \text{ monitor}^{-1}.$$

D. Differential Cross Sections at 90°

The differential cross sections at 90° for meson production will be discussed first, because at this angle it was possible to remeasure the meson yield, without the use of the magnetic field. The data thus obtained with two different detection efficiencies, will increase the reliability of the final cross section computations.

1. Time-of-Flight Data at 90°

The time-of-flight data at 90° was recorded immediately after the angular distribution measurement, in order to preserve the efficiency and time calibration of the detector as described in (IV-A-2).

The counters were placed along a 90° line through the target, and the magnet was removed from the central region. The position of the front counter was changed from 45 to 35 cm, to decrease the Coulomb scattering effect, and the rear counters A and B were placed adjacent, at 310 cm. from the front counter.

A relative spectrum efficiency ($g = 0.18$) for the time-of-flight counter was constructed from the computed meson spectra as in (VI-B). The constructed results are shown in Figure 42. At 30 Mev, the mesons are completely attenuated by the 4.0 gram cm^{-2} of carbon equivalent in the rear counters. Loss by decay in flight is relatively larger, but it is compensated by the wider energy resolution.

The experimental data for the carbon and Be targets are shown in Figures 43 and 44. The counting rates per monitor are a function of the cable length in cm. to the front counter. As a reference the non-linear scales for β and the kinetic energies in Mev of the meson and proton are also shown along the abscissa. There is evidence for electrons, mesons and protons. The solid lines are the estimated velocity spectra when the effect of the time resolution has been considered. The dotted curves indicate the extra width due to time resolution, on each spectrum.

The electrons and positrons are assumed to have kinetic energies below 150 Mev because of the agreement of the charged meson ratio measurement with the nuclear emulsion data.

The mesons with $\beta \approx 0.7$ are mostly negative because of the large measured negative to positive ratio. In the region 50 to 70 Mev the contamination due to electrons and protons is probably small. The average counts at cable lengths 270 and 310 cm. will be considered as the total number of mesons in the computed accepted spectra.

The protons below 65 Mev are cut off by the 4.0 gram cm^{-2} equivalent of carbon absorber in the rear counter. In the region 65 to 150 Mev the proton spectrum is seriously modified by the energy loss in the target. About 10 percent of the protons in their energy range are expected to escape from the target. The protons are assumed to result

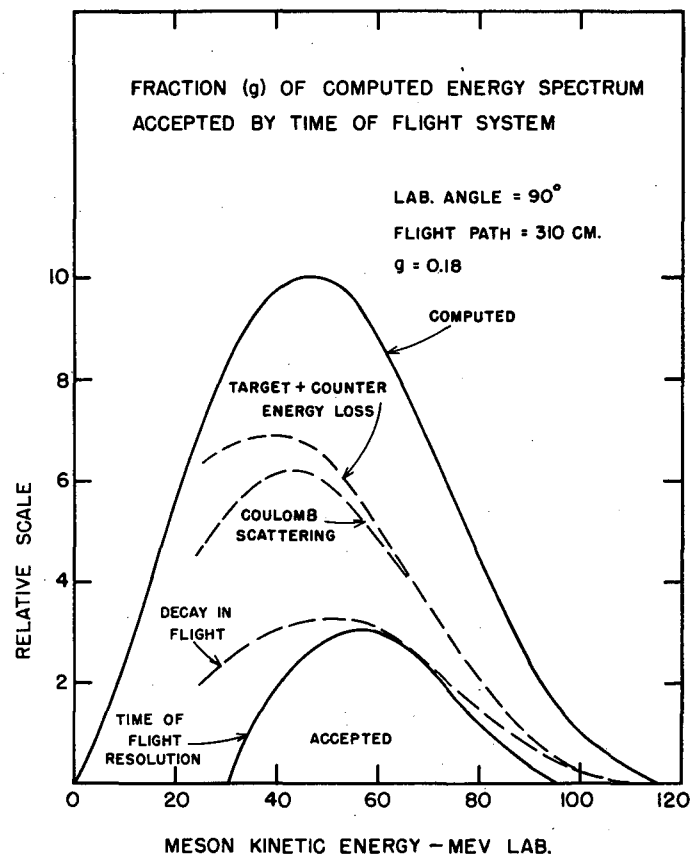

FIG. 42

MU-5357

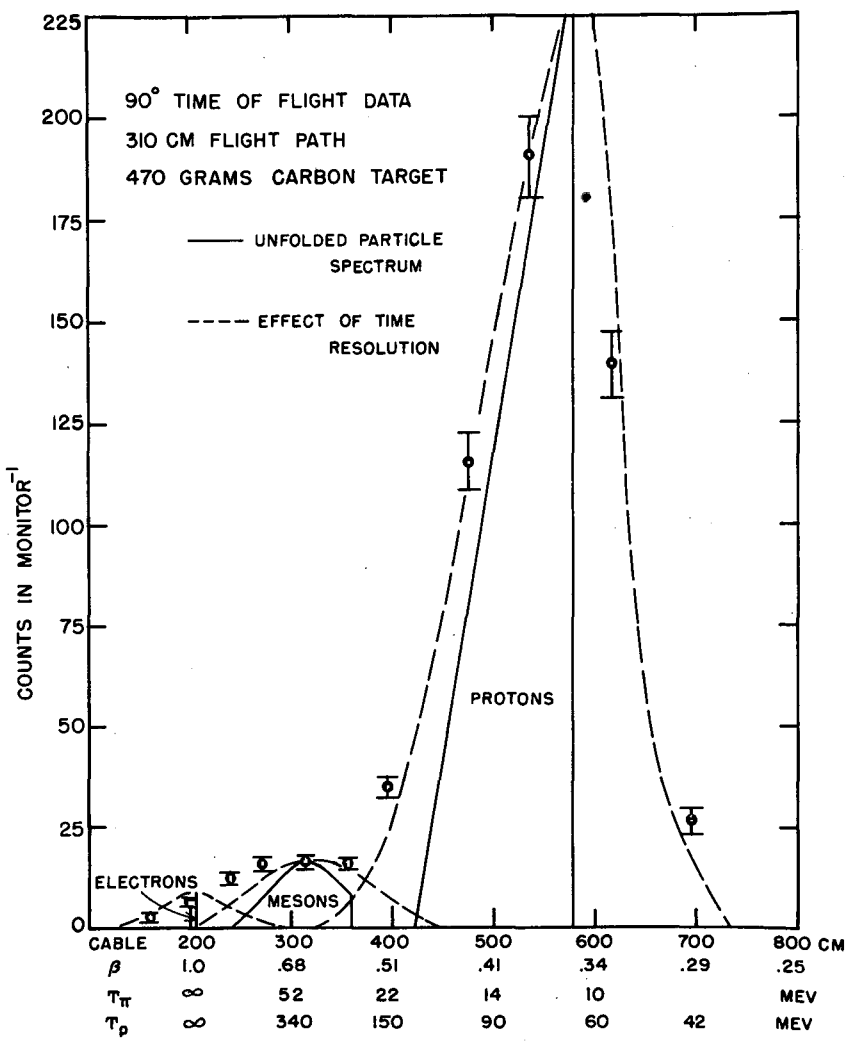

FIG. 43

MU-5358

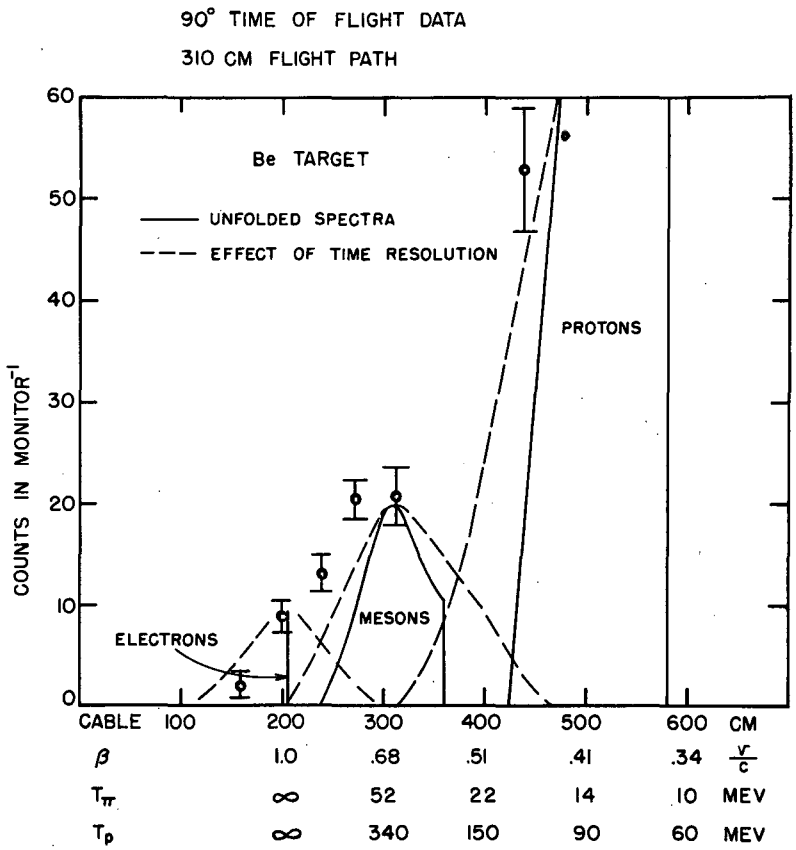

FIG. 44

MU-5359

from a collision between the incoming neutron and the moving target proton. Conservation of energy and momentum allow a 120 Mev proton to be emitted at 90° to an incoming 300 Mev neutron, which collides at an optimum angle with a 100 Mev target proton. However, in order to measure the proton spectra at this angle, much thinner targets and counters must be used.

2. Computation of $d\sigma/d\Omega\,(90^{o})$

The differential cross section for production of mesons of any energy in the laboratory system at angle ϕ, into a solid angle $d\Omega$ is $d\sigma/d\Omega\,(\phi)$ in units of cm^2 $steradian^{-1}$ $nucleus^{-1}$. The relationship to the observed counting rate per monitor is,

$$\frac{\text{counts }(\phi)}{\text{monitor}} = n\, N_T\, [\, d\sigma/d\Omega\,(\phi)\,]\ \Delta\Omega\, \epsilon(\phi)$$

where n = effective neutron intensity for meson production in carbon

$= (3 \pm 0.3) \times 10^7$ neutron cm^{-2} $monitor^{-1}$ (VI-C)

N_T = total number of target nuclei (IV-B-4)

$\Delta\Omega$ = detector solid angle (IV-A-3)

$\epsilon(\phi)$ = absolute efficiency (VI-B-4)

The numbers for the two systems are summarized in Table IV. (TF = Time-of-flight system, TF + M = TF + Magnet system). In performing the Be^9 - 2/3 C^{12} counting rate, it must be remembered that the targets are equalized to the same number of protons when the carbon counts are multiplied by 1.049.

3. Conclusions

It is evident that π^- mesons made in a $(n + n \rightarrow \pi^-)$ process are detectable in each detector system, at 90°, <u>independent</u> of any corrections for the efficiency of the system. In addition there is the π^- yield with better statistics from C or Be which may be considered to be from an n - n collision because of the large π^-/π^+ ratio.

The weighted average results are the best estimate for the differential cross section at 90° and are shown in Table V, with the assumed process. The reliability of the differential cross sections to

TABLE IV

π^- DIFFERENTIAL CROSS SECTION AT 90° LABORATORY SYSTEM

Detector System	Target	Observed Meson	Counting Rate in Monitor^{-1}	Absolute Efficiency $\epsilon(90°)$	$\Delta\Omega$ Sterad.	$[d\sigma/d\Omega\,(90°)]$ in 10^{-28} cm^2 st^{-1} nucleus^{-1}
TF	C^{12}	$\pi^- + \pi^+ \approx \pi^-$	16.5 ± 1.4	$(0.18)(0.4)$	3.0×10^{-3}	1.07 ± 0.14
	Be^9	$\pi^- + \pi^+ \approx \pi^-$	20.9 ± 1.7	$(0.18)(0.4)$	3.0×10^{-3}	0.86 ± 0.11
	Be^9-2/3C^{12}	π^-	$\left[\begin{array}{l}(20.9 \pm 1.7)\\ -(17.3 \pm 1.5)\end{array}\right]$	$(0.18)(0.4)$	3.0×10^{-3}	0.15 ± 0.10
TF + M	C^{12}	π^-	7.6 ± 1.1	$(0.09)(0.4)$	2.9×10^{-3}	1.05 ± 0.18
	Be^9	π^-	10.8 ± 0.8	$(0.09)(0.4)$	2.9×10^{-3}	0.95 ± 0.14
	Be^9-2/3C^{12}	π^-	$\left[\begin{array}{l}(10.8 \pm 0.8)\\ -(8.0 \pm 0.8)\end{array}\right]$	$(0.09)(0.4)$	2.9×10^{-3}	0.25 ± 0.10

TABLE V

WEIGHTED AVERAGE π^- DIFFERENTIAL CROSS SECTION AT 90° LABORATORY SYSTEM

Target	Process	$[d\sigma(90°)/d\Omega]$ in 10^{-28} cm^2 st^{-1}
C^{12}	$n + C^{12} \rightarrow \pi^-$	1.06 ± 0.11 nucleus^{-1}
Be^9	$n + Be^9 \rightarrow \pi^-$	0.90 ± 0.09 nucleus^{-1}
Be^9-2/3C^{12}	$n + n \rightarrow \pi^- + d$	0.20 ± 0.07 Neutron^{-1}

be assigned to the angular distribution in data in the next sections on the basis of f (ϕ) has been considerably reinforced by the 90° time-of-flight data.

It should be observed that $[d\sigma/d\Omega\,(90^{\circ})]_{\pi^-} = (1.06 \pm 0.11) \times 10^{-28}$ cm^2 ster.$^{-1}$ for 300 ± 30 Mev neutrons on carbon is close to the value obtained by Richman, et al.[4] for π^+ mesons for 340 Mev protons on carbon. They obtained $[d\sigma/d\Omega\,(90^{\circ})]_{\pi^+} = (2.3 \pm 0.5) \times 10^{-28}$ cm^2 ster^{-1}.

VII. CORRECTED ANGULAR DISTRIBUTION DATA

The corrected angular distribution yields are obtained by dividing the experimental data (Table I, III) by the absolute efficiency ϵ (ϕ) as defined in (VI-B-4). If the absolute differential cross section were computed at each angle, the percentage error in the cross section would be increased to at least ten percent, because of the statistical probable error in the neutron intensity. However, the errors in the π^- data from C and Be are in general less than ten percent. Therefore, in order to preserve the relative angular information, the cross sections have been computed relative to 90°, and then normalized at this angle, by the absolute cross sections as determined in (VI-D). The statistical uncertainty in the absolute scale is ± ten percent for π^- from Be or C, about ± 30 percent for π^- from (Be - 2/3 C), and at least ± 30 percent for π^+, from Be and 2/3 C average results. The systematic errors and real errors in the numerous corrections for the absolute cross section will probably contribute the largest uncertainty, but unfortunately they are unknown.

A. Laboratory System

The computed differential cross sections [$d\sigma/d\Omega$ (ϕ)] for charged mesons from Be^9 and C^{12} are listed in Table VI. The uncorrected data (Table I, III) and the corrected data (Table VI) are plotted in Figures 45, 46, for π^- from Be^9; Figures 47, 48 for π^- from C^{12}; Figures 49, 50 for π^- from Be^9 - 2/3 C^{12}; and Figures 51, 52 for π^+ from Be^9, 2/3 C^{12} weighted average. It is evident from the relative shapes of the corrected and uncorrected angular distributions that the effect of the absolute efficiency ϵ (ϕ) has been relatively small in the region of good statistics (15 → 70°) and large in the region of bad statistics (70 → 125°).

TABLE VI

ANGULAR DISTRIBUTION OF CHARGED MESONS
IN LABORATORY SYSTEM

$[d\sigma(\phi)/d\Omega]_{lab.}$ sterad.$^{-1}$

ϕ (Degrees)	In 10^{-28} cm^2 nucleus^{-1}		In 10^{-29} cm^2 neutron^{-1}	In 10^{-30} cm^2 nucleus^{-1}
	π^- from Be^9	π^- from C^{12}	π^- from Be^9-2/3C^{12}	(Weighted Average) π^+ from Be^9 or 2/3 C^{12}
15	6.5 ± 0.2	6.2 ± 0.2	24.0 ± 2.0	19.0 ± 3.0
30	5.2 ± 0.2	5.2 ± 0.3	18.0 ± 3.0	----------
45	2.5 ± 0.1	2.8 ± 0.1	5.7 ± 0.9	4.1 ± 1.1
60	1.3 ± 0.1	1.8 ± 0.1	1.0 ± 1.0	5.7 ± 1.0
75	0.92 ± 0.06	1.2 ± 0.1	1.3 ± 0.7	4.7 ± 1.2
90	0.90 ± 0.09	1.06 ± 0.11	2.0 ± 0.7	1.8 ± 0.7
110	0.8 ± 0.1	1.2 ± 0.1	0 ± 1.0	2.2 ± 1.3
125	1.4 ± 0.2	1.6 ± 0.2	3.2 ± 2.2	13.0 ± 4.0

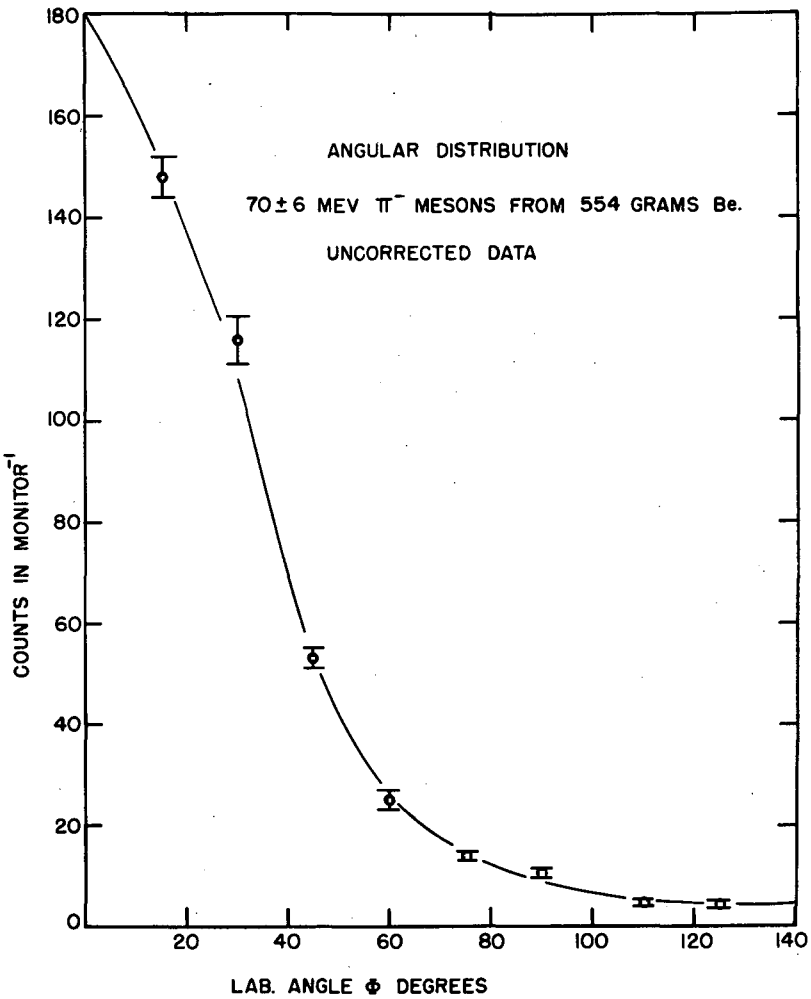

FIG. 45

MU-5360

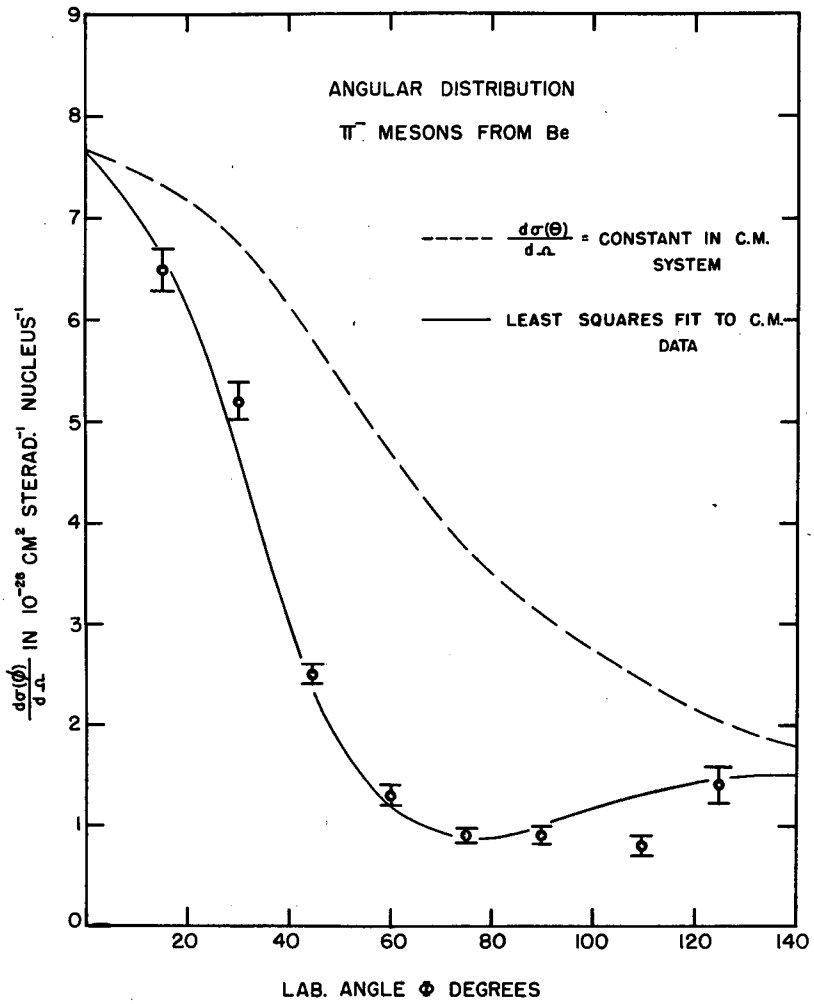

FIG. 46

MU-5361

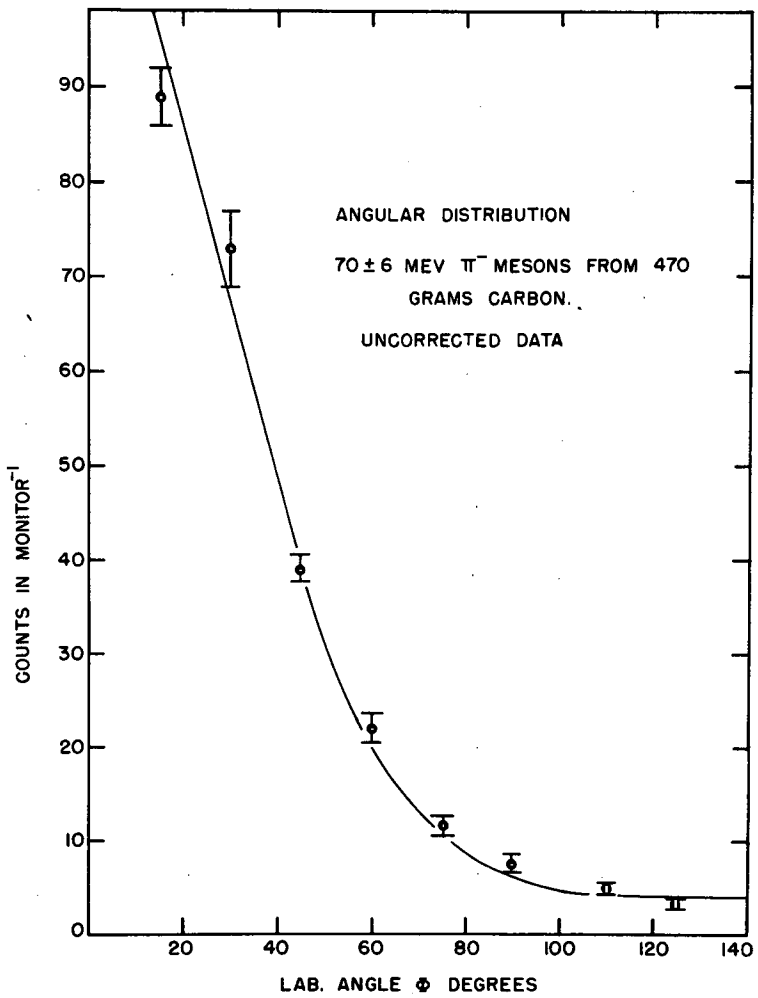

FIG. 47 MU-5399

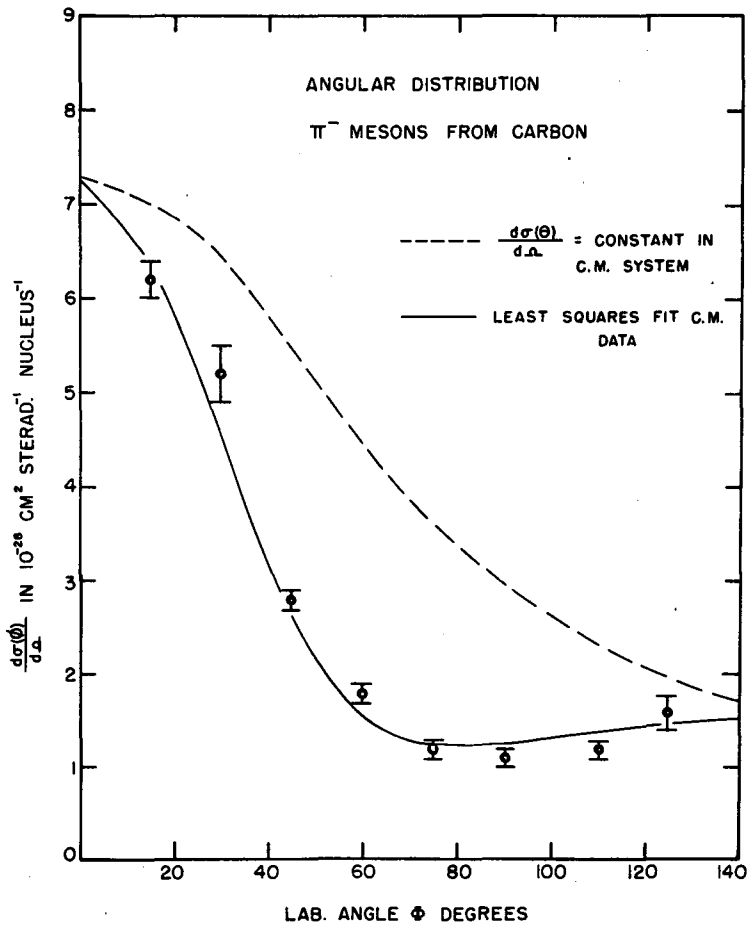

FIG. 48

MU-5400

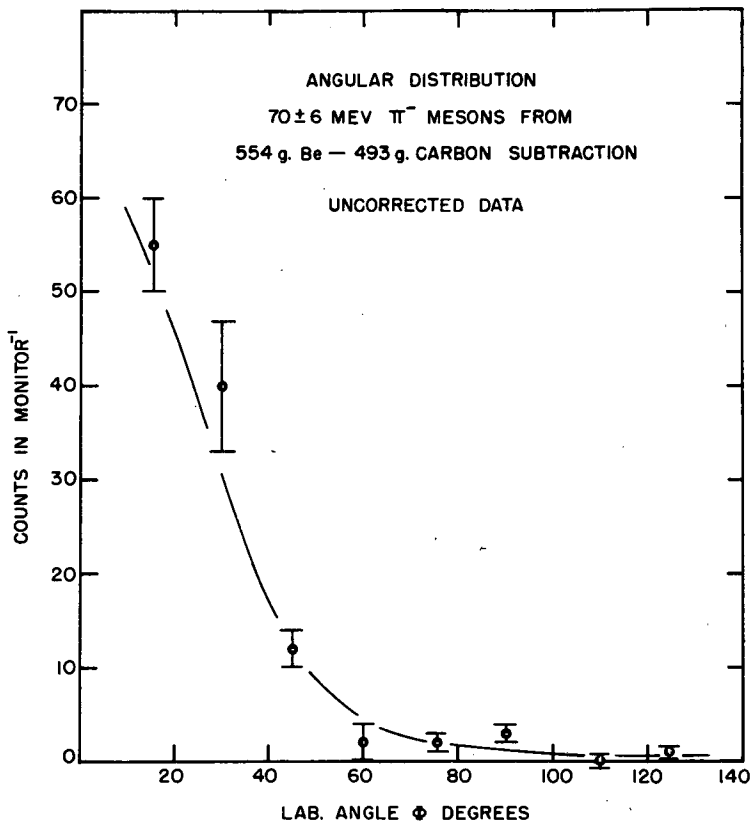

FIG. 49

MU-5401

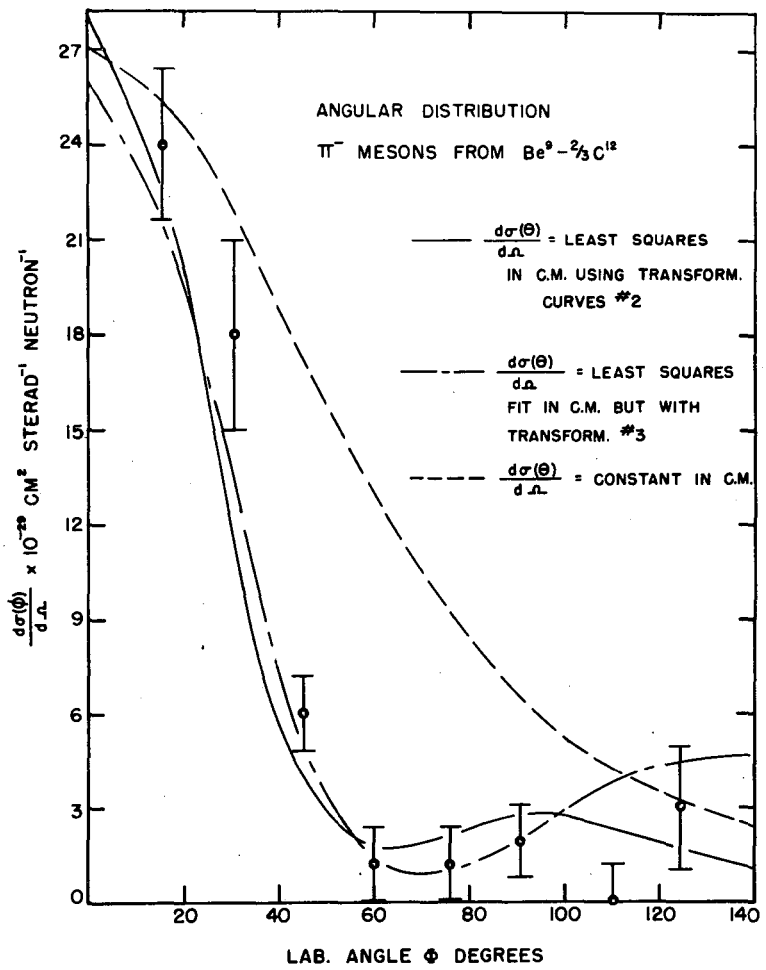

FIG. 50

MU-5402

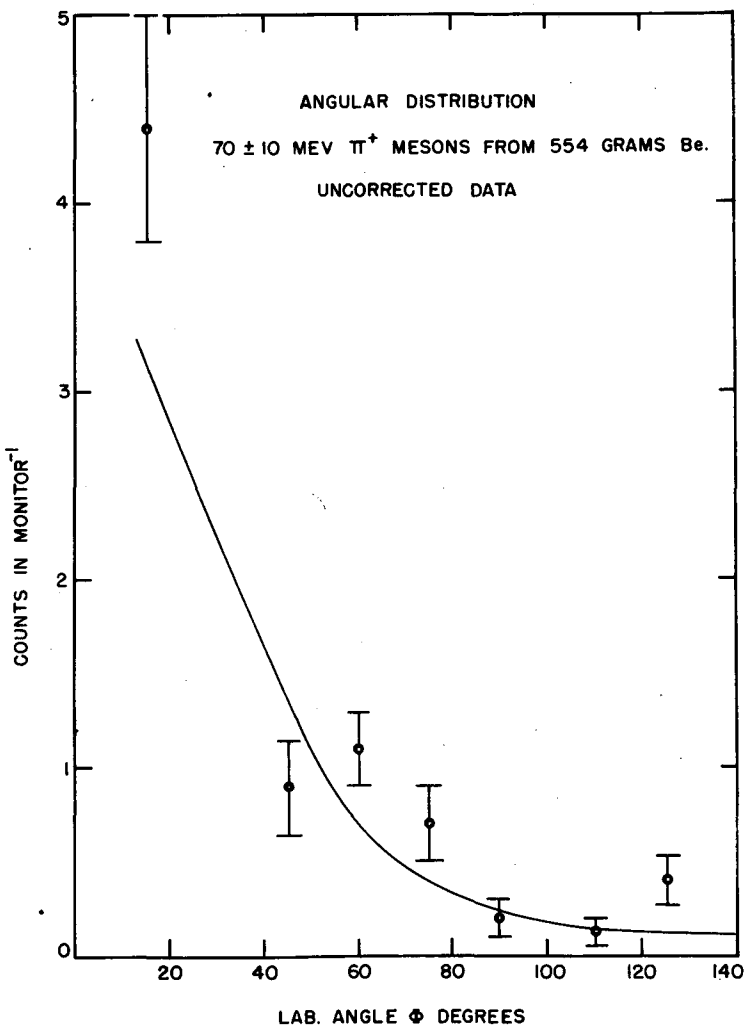

FIG. 51

MU-5403

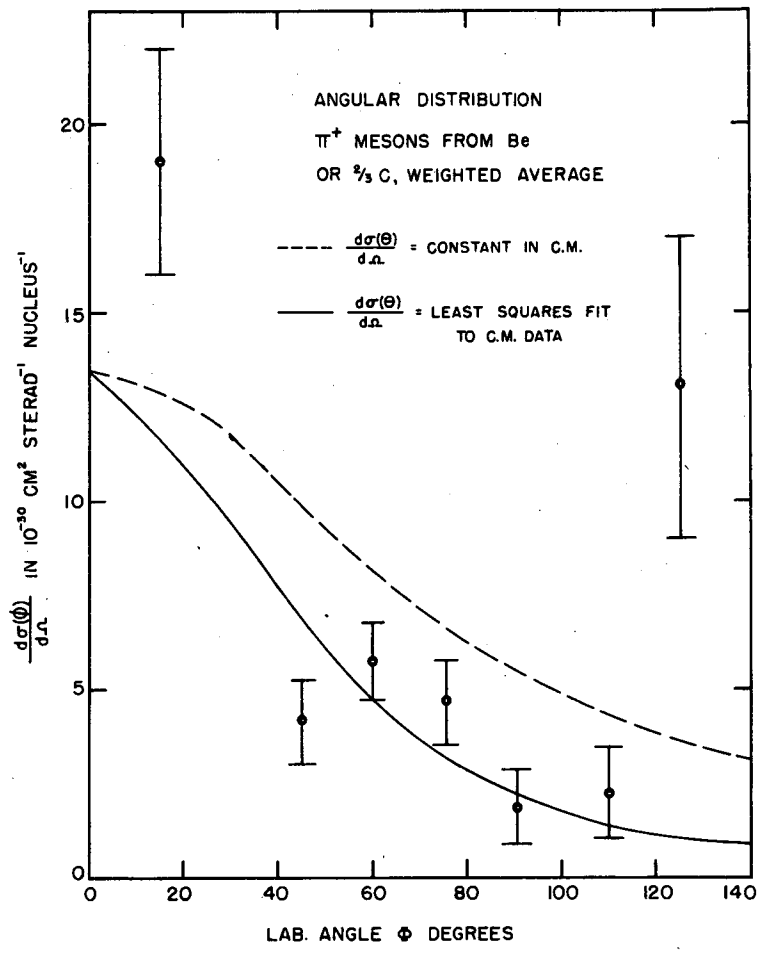

FIG. 52

MU-5404

B. Average Center-of-Mass System

To transfer the laboratory angular distribution into a center-of-mass system for the two moving, colliding nucleons, one must necessarily use average values for the center-of-mass velocity βCM and the meson velocity β'_π in the center-of-mass frame. (See Section VI.) The angle and intensity transformations:

$$\phi \quad \text{lab} \rightarrow \theta \quad \text{cm}$$

$$(d\sigma/d\Omega)\text{lab} \rightarrow (d\sigma/d\Omega) \quad \text{cm}$$

are derived in Appendix B, and are plotted in Figures 53 and 54 (curve 3). For comparison, the transformation for a target at rest (curve 1) and for a target only slightly in motion (curve 2) have been shown. Transformations by curve 1 are considered very improbable. As a guess, curve 2 may be more correct than curve 3, for collisions with the "last neutron" in Be^9.

It is important to note that the intensity transformations 1, 2 or 3 are about the same for laboratory angles $\phi = 0 \rightarrow 80^o$; beyond 80° the differences in the curves become large. The conclusion is that in the region of the best experimental data ($15 \rightarrow 75^o$) the transformations to center-of-mass will be fairly insensitive to the uncertainties in βCM and β'_π.

The π^- and π^+ from Be^9 and C^{12} were transformed by curve 3, and the results are shown in Table VII and Figures 55, 56, 57. The π^- yield from Be^9 - 2/3 C^{12} was transformed by curve 2 and 3 with results in Table VIII and Figures 58, 59.

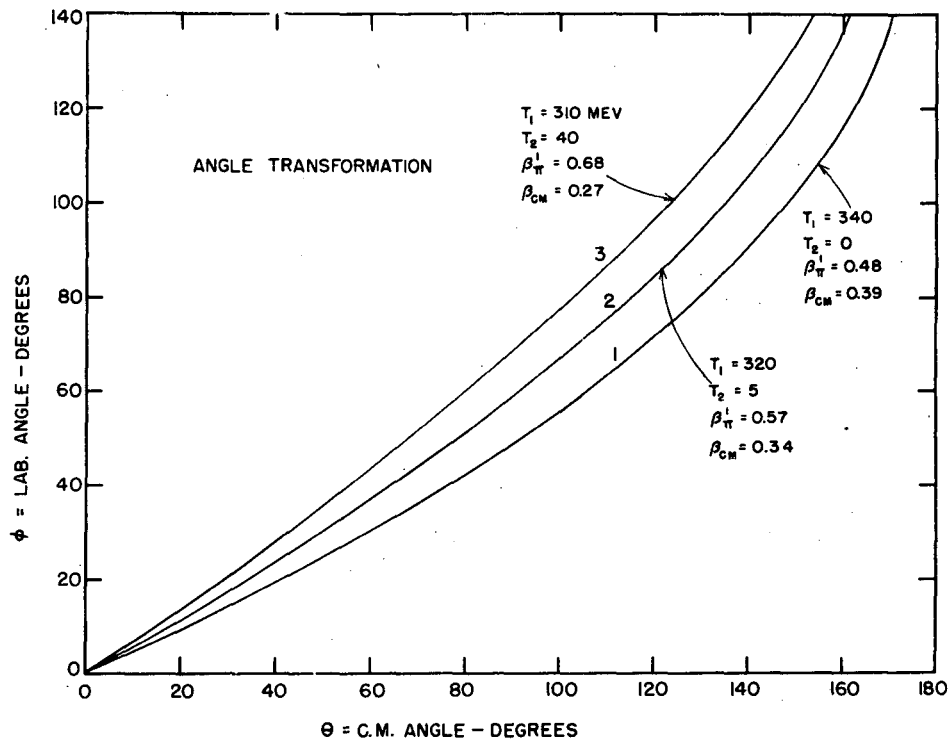

FIG. 53

MU-5417

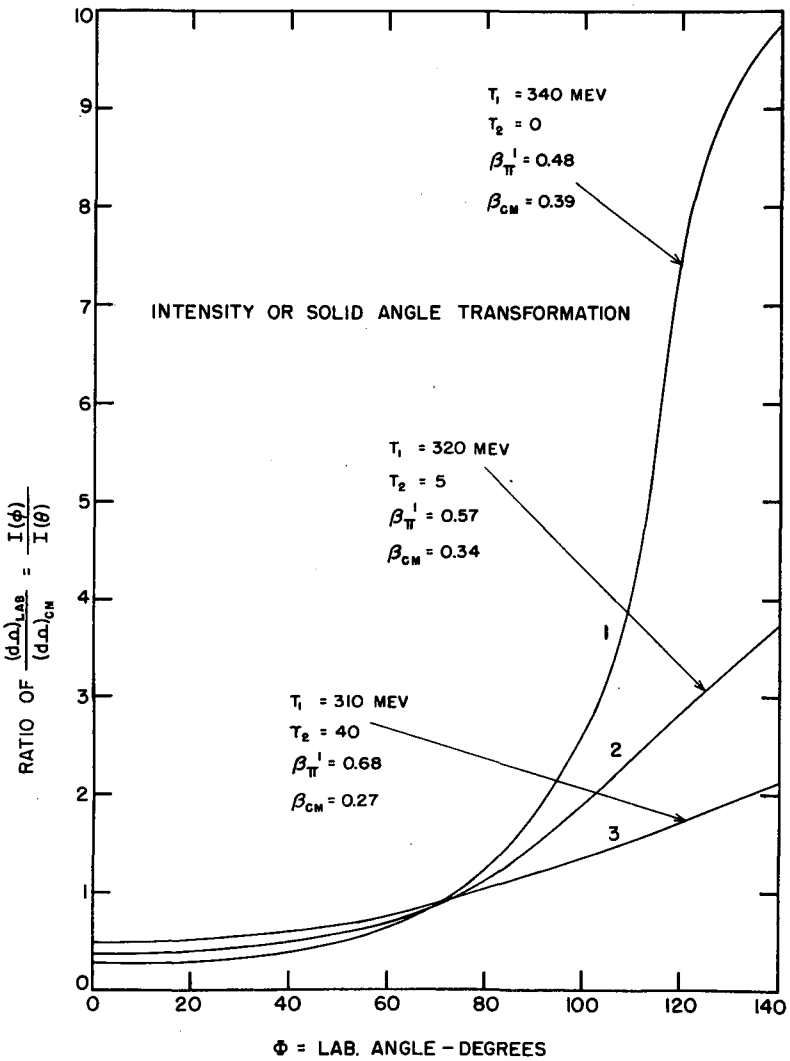

FIG. 54

MU-5487

TABLE VII

ANGULAR DISTRIBUTION OF CHARGED MESONS IN AVERAGE CENTER-OF-MASS SYSTEM*

$[d\sigma(\theta)/d\Omega]_{C.M.}$ sterad. $^{-1}$

θ (Degrees)	In 10^{-28} cm^2 nucleus^{-1}		In 10^{-30} cm^2 nucleus^{-1} (Weighted Average)
	π^- from Be^9	π^- from C^{12}	π^+ from Be^9 or 2/3 C^{12}
22	3.2 ± 0.1	3.1 ± 0.1	10 ± 2
42	2.7 ± 0.1	2.7 ± 0.1	------
62	1.6 ± 0.1	1.8 ± 0.1	2 ± 1
80	1.0 ± 0.1	1.4 ± 0.1	4 ± 1
98	0.9 ± 0.1	1.1 ± 0.1	4 ± 1
113	1.1 ± 0.1	1.3 - 0.1	2 ± 1
131	1.2 ± 0.2	1.9 - 0.1	3 ± 2
142	2.5 ± 0.4	2.9 - 0.4	23 ± 7

* transform. curve No. 3

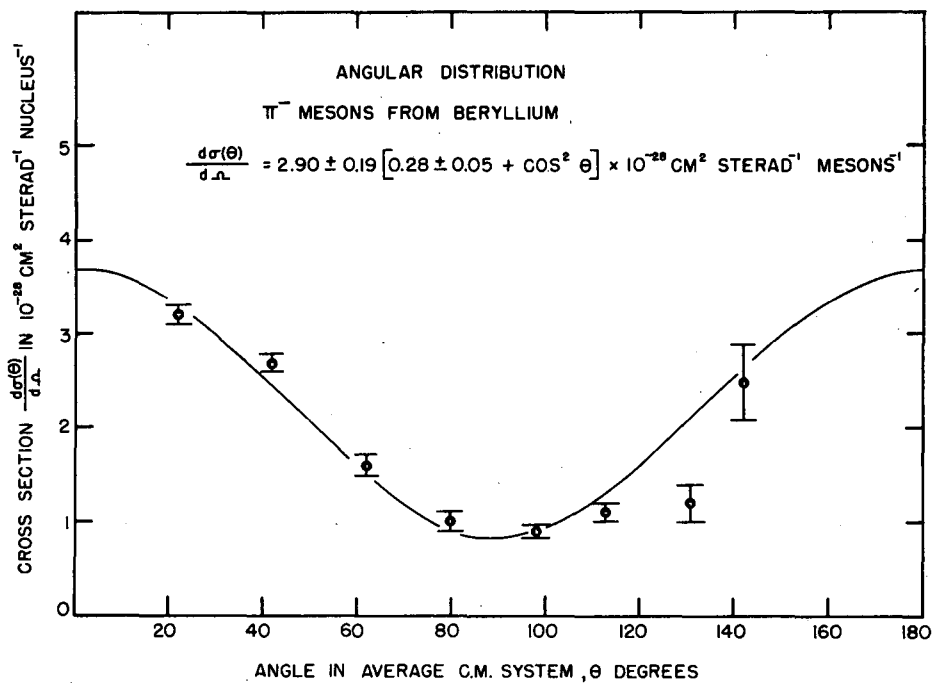

FIG. 55

MU-5418

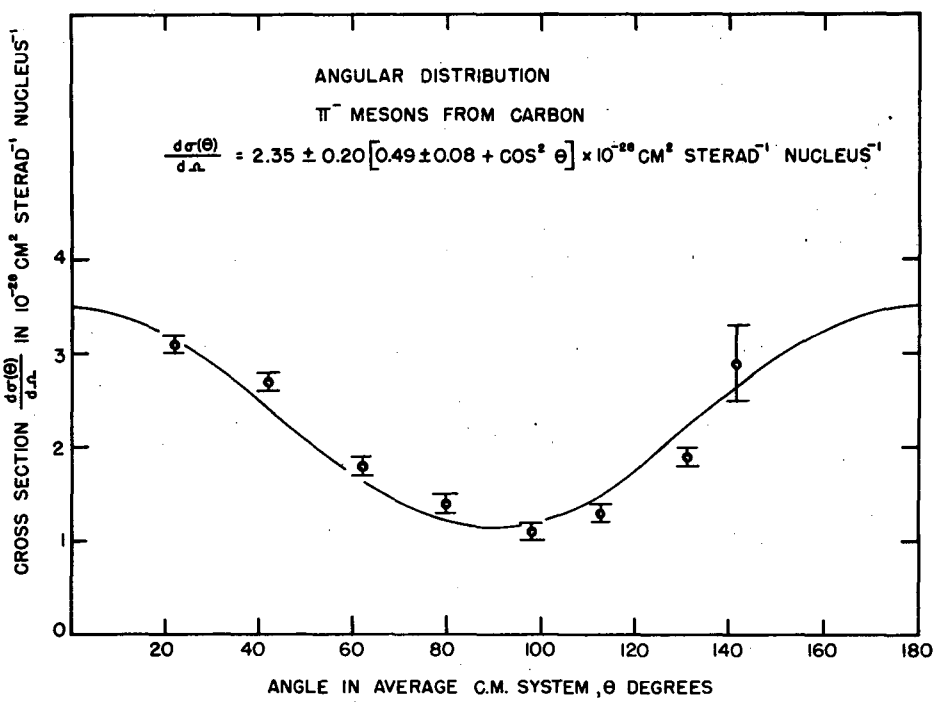

FIG. 56

MU-5419

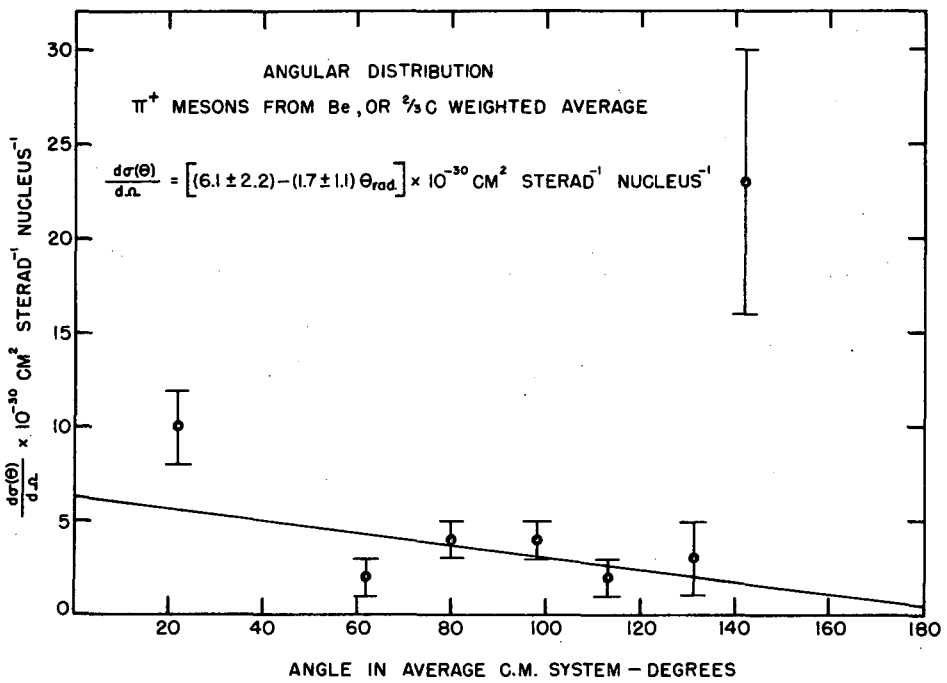

FIG. 57

MU-5405

TABLE VIII

ANGULAR DISTRIBUTION OF π^- MESONS
IN AVERAGE CENTER-OF-MASS SYSTEM

$n + n \rightarrow \pi^- + d$

$[d\sigma(\theta)/d\Omega]_{C.M.}$ in 10^{-29} cm^2 sterad.$^{-1}$ neutron^{-1}

Transform. Curve	θ C. M.	from (Be^9 - 2/3 C^{12})
No. 3	22	12 ± 1
	42	9 ± 2
	68	4 ± 1
	80	1 ± 1
	98	1 ± 1
	113	2 ± 1
	131	0 ± 2
	142	6 ± 4
No. 2	24	9 ± 1
	50	7 ± 1
	72	3 ± 1
	92	1 ± 1
	110	1 ± 1
	127	3 ± 1
	144	0 ± 3
	155	16 ± 11

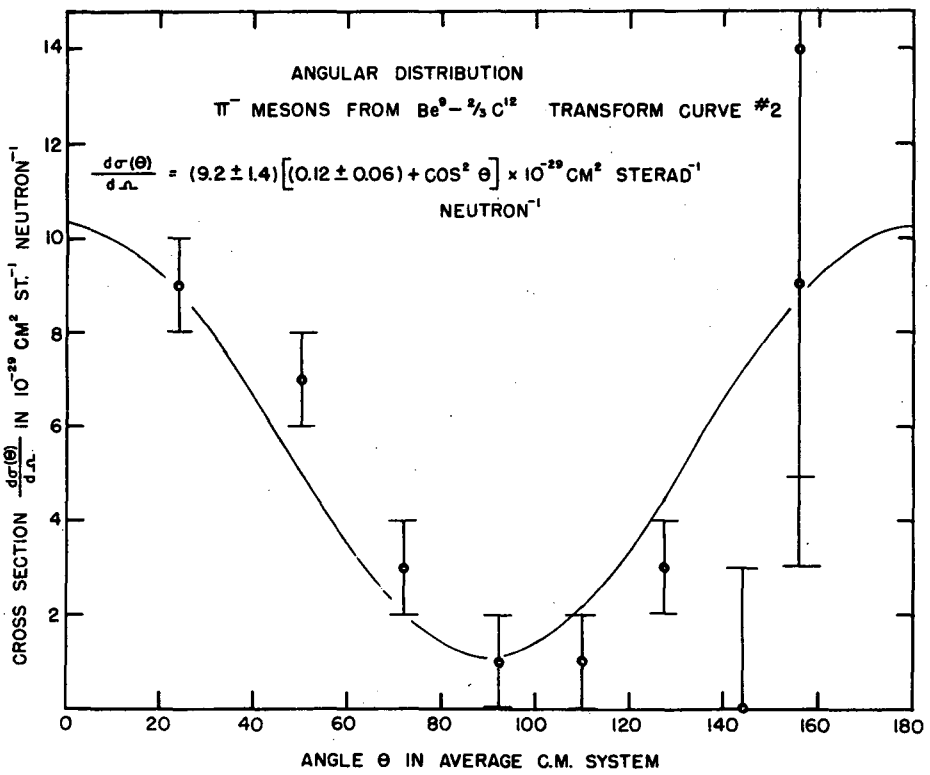

FIG. 58

MU-5420

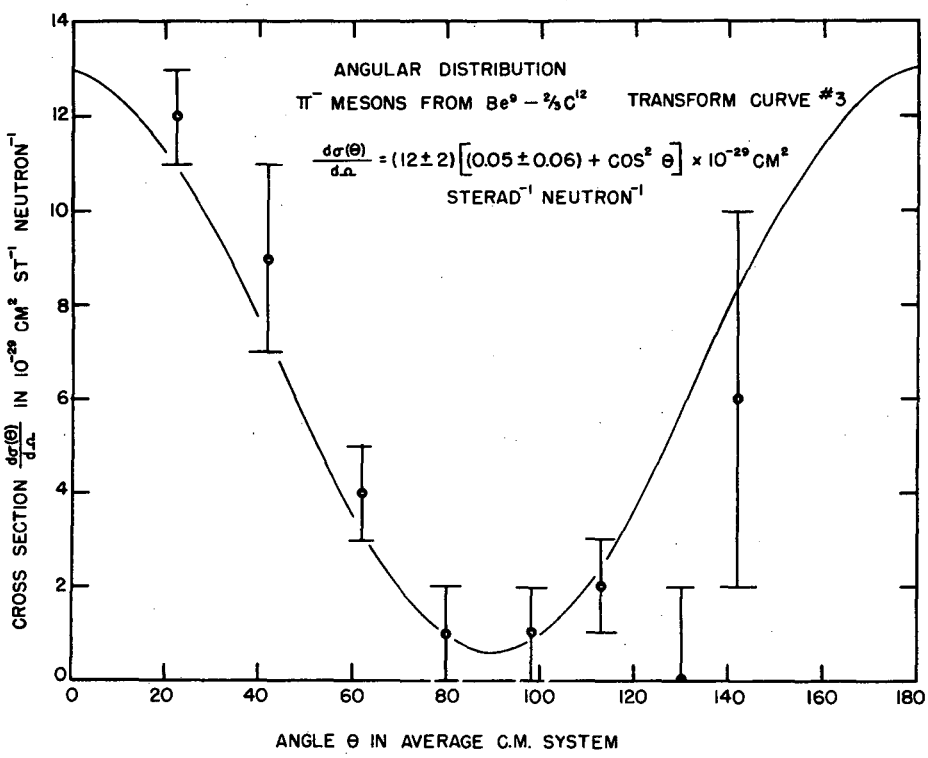

FIG. 59

MU-5421

C. Fitting of the Data in the C. M. System

1. π^- Yield

The angular distributions extend from $\theta = 22$ to 142°. The interesting features of the π^- data are the tendency for symmetry and a minimum at $\theta = 90^o$. Symmetry is a necessary property for a collision between identical particles. It is expected that π^- mesons are predominately made in n - n collisions because of the large π^-/π^+ ratio, and the equivalence of the $n + p \rightarrow \pi^\pm$ processes, as predicted from charge symmetry.

The simplest curve which fits the π^- angular distribution is

$$\left[\frac{d\sigma(\theta)}{d\Omega}\right]_{\pi^-} = B(A + \cos^2\theta)$$

The probable errors of the adjusted coefficients are determined by the method of least squares.[31] The differential cross is integrated over θ, for the total cross section.

$$\sigma_t(\pi^-) = 4\pi B(A + 1/3)$$

The results for π^- from Be, C and Be - 2/3 C are shown in Table IX.

2. π^+ Yield

The reaction $n + p \rightarrow \pi^+ + n + n$, has no àpriori requirement for symmetry. A straight line for the distribution was chosen; however, a weighted average value (zero degree equation) has about the same residuals for the fit.

$$\left[\frac{d\sigma(\theta)}{d\Omega}\right]_{\pi^+} = (C + D\,\theta)$$

$$\text{and } \sigma_t(\pi^+) = 2\pi[2C + \pi D]$$

The coefficients are given in Table X.

3. Total Yield Ratios

The ratio of total π^- to total π^+ yields are large:

From Table IX and X:

$$\left[\frac{\sigma_t(\pi^-)}{\sigma_t(\pi^+)}\right]_{carbon} = 40 \pm 20$$

$$\left[\frac{\sigma_t(\pi^-)}{\sigma_t(\pi^+)}\right]_{Be} = 55 \pm 26$$

TABLE IX

π^- DIFFERENTIAL AND TOTAL CROSS SECTIONS IN C. M. SYSTEM

Target	Interpretation	$[d\sigma(\theta)/d\Omega]_{\pi^-}$ in 10^{-28} cm^2 sterad^{-1}	$\sigma_t(\pi^-)$ in 10^{-27} cm^2
1. Be^9	$n + n \rightarrow \pi^- + d$	$(2.90 \pm 0.19)\,[(0.28 \pm 0.05) + \cos^2\theta]$ nucleus^{-1}	2.2 ± 0.3 nucleus^{-1}
2. C^{12}	$n + n \rightarrow \pi^- + d$	$(2.35 \pm 0.20)\,[(0.49 \pm 0.08) + \cos^2\theta]$ nucleus^{-1}	2.4 ± 0.3 nucleus^{-1}
3. Be^9 -2/3 C^{12}	$n + n \rightarrow \pi^- + d$	$(0.92 \pm 0.14)\,[(0.12 \pm 0.06) + \cos^2\theta]$ neutron^{-1}*	0.5 ± 0.1 neutron^{-1}
		$(1.2 \pm 0.2)\,[(0.05 \pm 0.06) + \cos^2\theta]$ neutron^{-1}**	0.5 ± 0.1 neutron^{-1}

* Transform. Curve 2
** Transform. Curve 3

TABLE X

π^+ DIFFERENTIAL AND TOTAL CROSS SECTIONS IN C. M. SYSTEM

Target	Interpretation	$[d\sigma(\theta)/d\Omega]_{\pi^+}$ in 10^{-30} cm^2 sterad^{-1}	$\sigma_t(\pi^+)$ in 10^{-29} cm^2
1. Be^9	$n + p \rightarrow \pi^+ + 2n$	$(6.1 \pm 2.2) - (1.7 \pm 1.1)\,\theta_{rad}$ nucleus^{-1}	4 ± 2 nucleus^{-1}
2. C^{12}	$n + p \rightarrow \pi^+ + 2n$	$(9.1 \pm 3.3) - (2.6 \pm 1.7)\,\theta_{rad}$ nucleus^{-1}	6 ± 3 nucleus^{-1}

D. Fitting of Data in the Laboratory System

1. Comparison with a Constant C.M. Distribution

A best fit for the angular distribution data in the laboratory system is automatically obtained by transforming the least squares fitted C.M. curves to the laboratory system. For comparison a constant distribution in the center-of-mass has also been transformed and presented with the laboratory data (indicated by dashed lines in Figures 46, 48, 50 and 52). None of the π^- data can be explained by a flat cross section in the C.M. system.

The π^+ angular distribution is in question because of the poor statistics. However, the data are consistent with constant C.M. distribution.

2. Construction of $\frac{d^2\sigma(\phi, T)}{d\Omega dT}$ for π^- mesons:

The ordinate of the computed energy spectra (Figure 37) may be adjusted at each ϕ so that

$$\frac{d\sigma(\phi)}{d\Omega} = \int_0^\infty \frac{d^2\sigma(\phi, T)}{d\Omega dT}\, dT$$

where T = meson kinetic energy.

The differential cross sections as a function of (ϕ, T) are not of particular value for this experiment; however, they may serve as a guide for future work on π^- energy spectra from carbon bombarded by neutrons or π^+ spectra from carbon bombarded by protons at 310 Mev. The cross sections are shown in Figures 60 and 61.

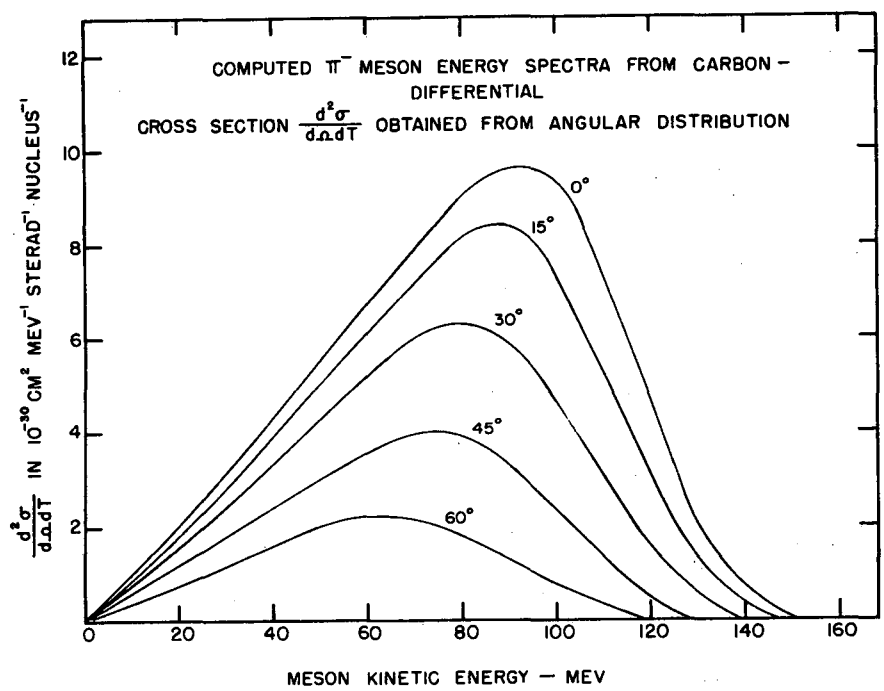

FIG. 60

MU-5422

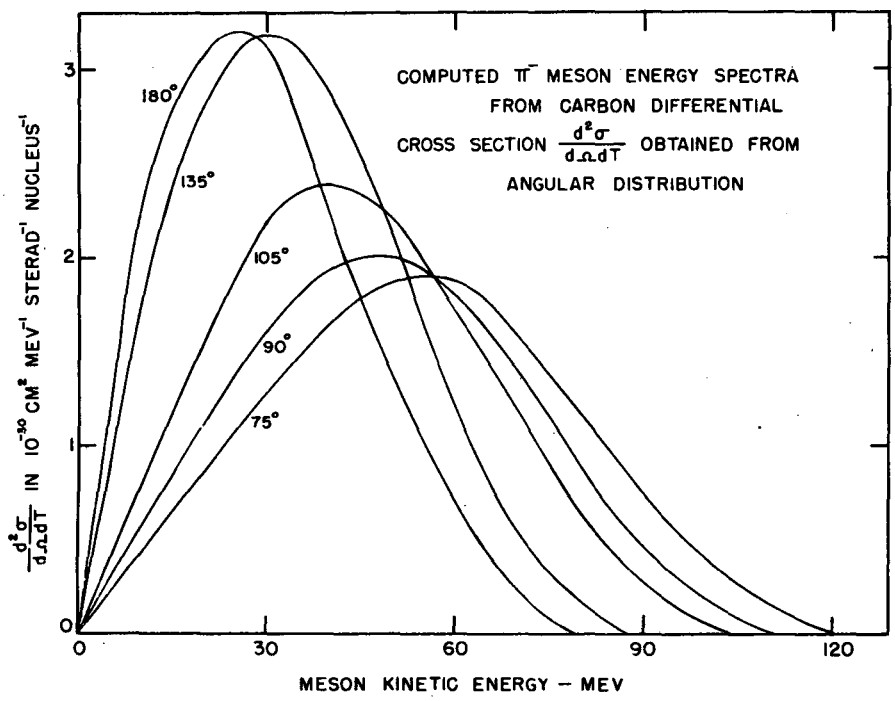

FIG. 61

MU-5423

VIII. DISCUSSION OF RESULTS

The angular distributions of charged π mesons from 300 ± 30 Mev neutron bombardment of C^{12} and Be^9 have been measured. These data may be used to infer the identity, within limits, of the $n + n \rightarrow \pi^-$ and $p + p \rightarrow \pi^+$ angular distribution and cross section. They thus not only imply charge symmetry of nuclear forces but also support the idea of charge independence and the suggestion that the virtual meson-nucleon state of isotopic spin 3/2 is one of strong interaction, leading to a $(1/3 + \cos^2\theta)$ angular distribution.[8a,b] The $n + p \rightarrow \pi^+$ process has an intermediate state of isotopic spin 1/2 for the π^+ and either neutron,[7b] and the reaction is observed to be forbidden in this experiment by a factor of 40 to 50 compared to the $n + n \rightarrow \pi^-$. The experimental facts are summarized below.

A. Results from Uncorrected Data

In the laboratory system:

1. π^- mesons are made in n - n collision; observed directly from Be^9 -2/3 C^{12} subtraction; observed indirectly from C^{12} or Be^9, because of the large π^-/π^+ ratio.
2. At 85 ± 8 Mev, π^-, π^+ production and π^-/π^+ ratio are largest at the forward angles.
3. π^+ angular distribution is probably peaked less forward than π^-.

B. Results from Corrected Data

In average C. M. system:

The data corrections and transformation involved the assumptions and calculations for the π^- energy spectra from carbon in the laboratory system and the energy resolution of the meson detector. The data corrections implied no assumptions for the meson angular distribution.

1. π^- Data

The π^- data is symmetric in the center-of-mass system and can be represented by $B(A + \cos^2\theta)$ for the differential cross section. The reaction is interpretated as $n + n \rightarrow \pi^- + d$.

(a) π^- from C^{12}, $(1/2 + \cos^2\theta)$

(b) π^- from Be^9, $(1/3 + \cos^2\theta)$

(c) π^- from Be^9 - 2/3 C^{12}, $(1/10 + \cos^2\theta)$

The total cross section $\sigma_t(\pi^-)$ per target neutron is the same, within statistics, for targets a, b, or c.

$$\sigma_t(\pi^-) = (4.5 \pm 0.5) \times 10^{-28}\ cm^2 \text{ per neutron.}$$

These facts are to be compared with the charge symmetric process $p + p \rightarrow \pi^+ + d$, where A ranges from 0.1 to 0.3 depending upon the experimenter,[3c, d, e] and $\sigma_t(\pi^+) = (1.6 \pm 0.5) \times 10^{-28}\ cm^2$ per proton. The factor of 3 in the total cross section is not an unreasonable increase (See π^+ excitation curve, Figure 23) since the meson energy for $\sigma_t(\pi^+)$ is 22 Mev and for $\sigma_t(\pi^-)$ ranges from 30 to 60 Mev due to the momentum distribution of the target neutron.

2. π^+ Data

The large errors due to the small number of events makes the angular distribution of π^+ mesons unreliable. The data is consistent with a flat distribution. The reaction is interpretated as $n + p \rightarrow \pi^+ + n + n$. The total cross section per proton in C^{12} or Be^9 is equal to

$$\sigma_t(\pi^+) = (1 \pm 0.3) \times 10^{-29}\ cm^2 \text{ per proton.}$$

There is no data for $\sigma_t(\pi^-)$ for the reaction $p + n \rightarrow \pi^- + p + p$; however, there is evidence that it is also small[7a] compared to $p + p \rightarrow \pi^+ + d$.

IX. ACKNOWLEDGMENTS

I wish to express my appreciation to Professor Burton J. Moyer, my graduate research advisor, for his encouragement during the development of the time-of-flight counter and for helpful suggestions and criticisms during the meson production experiment.

It is also a pleasure to thank Dr. James Carothers and Dr. Calvin Andre who grew most of the twenty-four trans-stilbene crystals and helped in many ways with the development of the meson detector, and to Mr. Dwight Dixon for his reliable neutron monitor and measurement of the neutron intensity, as well as his valuable assistance with the electronic equipment throughout the experiment.

I am also indebted to Dr. J. Lepore for aid in the theoretical interpretation of the data and for his advice on the computation of meson energy spectra, and to Dr. Sidney Bludman and Professor C. Richman for many interesting discussions of meson phenomena.

It was a pleasure to work with the members of the 184-inch cyclotron crew, under the able direction of Mr. James Vale, who kindly supplied a total of two weeks of neutron beam.

X. APPENDIX

A. Kinematics of Meson Production

1. Conservation of Energy and Momentum

In this section, we are concerned with the conservation of energy and momentum for meson production in a nucleon-nucleon collision according to the basic reaction,

$$n_1 + n_2 \rightarrow \pi^- + d.$$

The target nucleon, n_2, is a bound neutron in carbon for example, and is believed to have a distribution of momenta. Since the carbon target is at rest, we assume that any instant, the momentum $\vec{p}_2$ of n_2 is equal and opposite to the combined momentum, $\overrightarrow{P_{C^{11}}}$, of the remaining carbon nucleons. When n_2 is struck by a high energy, incoming neutron n_1 to form a meson, the momentum transfer from n_1 to n_2 is large compared to p_2, and from n_1 to the rest of the nucleons the momentum transfer will be considered as negligible. After collision, we would observe, in a cloud chamber for example, a meson with momentum $\vec{p}_\pi$, a deutron $\vec{p}_d$, and a recoil nucleus $\overrightarrow{P_{C^{11}}}$, where the recoil is opposite to the initial direction of n_2. The final momentum $\vec{P}_f$ is

$$\vec{P}_f = \vec{p}_\pi + \vec{p}_d + \overrightarrow{P_{C^{11}}}$$

and it must be equal to the initial momentum $\vec{p}_1$ of the bombarding neutron.

Since $\overrightarrow{P_{C^{11}}} = -\vec{p}_2$, the conservation of total momentum $\vec{p}_t$ is

$$\vec{P}_t = \vec{p}_1 = \vec{p}_\pi + \vec{p}_d - \vec{p}_2 \qquad (1)$$

or

$$\boxed{\vec{p}_1 + \vec{p}_2 = \vec{p}_\pi + \vec{p}_d} \qquad (2)$$

The total energy E_t before collision is

$$E_t = E_1 + M_o C^2$$

where $M_o C^2$ = rest energy of carbon nucleus

E_1 = total energy of bombarding neutron

$= m_n C^2 + T_1$

After collision, we have

E_π = total energy of meson

E_d = total energy of deuteron

$M'C^2$ = total energy of recoil nucleus

$= (M'_o C^2) + T_{C^{11}}$ + excitation energy of C^{11}.

$M'_o C^2$ = rest energy of C^{11}.

Therefore, the conservation of total energy E_t is

$$E_t = E_1 + M_o C^2 = E_\pi + E_d + M' C^2 \qquad (3)$$

If we consider $C^{12} = C^{11}$ + free neutron - b

where b = binding energy of struck nucleon in C^{12}

then $E_1 + (m_n C^2 - b) = E_\pi + E_d + T_{C^{11}}$

if we assume zero excitation energy of C^{11}.

Now $T_{C^{11}} \approx 1/11\ (p_2{}^2/\ 2\ m_n) \approx 10$ Mev max for p_2 (max)

and $b \approx 8$ Mev

Let $\delta = b + T_{C^{11}} = 20$ Mev.

Then $\boxed{E_1 + (m_n C^2 - \delta) = E_\pi + E_d}$ (4)

Equations (1) and (3) are the conservation equations for the neutron beam and carbon-nucleus system. Equations (2) and (4) are derived from (1) and (3) and are conservation equations for the beam and carbon-nucleon system.

The interesting feature of the energy equation (4) or (3) is that T_2, the kinetic energy of the struck nucleon, $(T_2 = p_2{}^2/2\ m_n)$, does not contribute to the energy of the final products. In this way, the large values for p_2, permitted by a gaussian momentum density for example, can never produce total energies for the meson and deuteron which would violate the conservation of total energy.

2. Meson Kinetic Energy in the C.M. System

The two neutrons collide at an angle α to form a meson. The center-of-mass of n_1 and n_2, moves along the direction of $\vec{p_t} = \vec{p_1} + \vec{p_2}$ with a velocity β_f

$$\text{where } \beta_f = \frac{c\, p_t}{E_1 - E_2} \tag{5}$$

$$E_1 = \sqrt{(p_1\, c)^2 - (m_n\, c^2)^2} = m_n\, c^2 + T_1$$

$$E_2 = \sqrt{(p_2\, c)^2 - (m_n\, c^2)^2} = m_n\, c^2 + T_2$$

In the C.M. system, the total energy of the colliding neutrons ϵ_t'

$$\text{is } \epsilon_t' = \sqrt{\epsilon_t^2 - (p_t\, c)^2}$$

$$\text{where } \epsilon_t = E_1 + (m_n\, C^2 - \delta) \tag{4}$$

$$(p_t c)^2 = (p_1\, c)^2 + (p_2\, c)^2 + (2\, p_1 c\, p_2 c)(\cos \alpha) \tag{2}'$$

The energy available E_a in the collision is

$$E_a = \epsilon_t' - 2\, m_n\, c^2 = 2\, m_n\, c^2\, (\gamma_n' - 1) \tag{6}$$

It is easy to show from the relation $c\, p_\pi' = c\, p_d'$

$$\text{that } \gamma_\pi' = \gamma_n' \frac{m_n}{m} - \frac{(m_d^2 - m_\pi^2)}{4\, \gamma_n'\, m_\pi\, m_n}$$

Therefore, $T_\pi' = (\gamma_n' - 1)\, m_\pi\, c^2$ = kinetic energy of meson in C.M. system. (7)

Equation (7) was plotted for various values of T_1, T_2 and α in Figures 24, 25 and 26.

3. Meson Energy in the Laboratory System

We are interested in the solution of equations (2) and (4) for the meson kinetic energy in the laboratory system, and with arbitrary parameters for the collision of n_1 with n_2. (See Figure 62.)

Let x axis be the beam axis defined by n_2

α = angle n_2 makes with x axis.

= collision angle between n_1 and n_2

ϕ = angle of emission of meson

ϕ_1 = angle between n_2 and π.

The deuteron can be eliminated from equations (2) and (4) and with some algebraic labor the total energy E_π of the meson is obtained,

$$E_\pi = \frac{a\,d + b\sqrt{a^2 - m_\pi c^2 [d^2 - b^2]}}{d^2 - b^2} \qquad (8)$$

where $a = E_1 E_2 (1 - \beta_1 \beta_2 \cos \alpha) + Q$

$$Q = \left[\frac{2(m_n c^2)^2 + (m_\pi c^2)^2 - (m_d c^2)^2}{2}\right] - \left[(T_2 + \delta)(T_1 + 2 m_n c^2 + \frac{T_2 - \delta}{2})\right]$$

$b = \beta_1 E_1 \cos \phi + \beta_2 E_2 \cos \phi_1$

$d = E_1 + (m_n c^2 - \delta)$

and $p c = \beta E$.

When $\phi = 90^\circ$ and the collision plane is restricted so that $\phi_1 = 90^\circ$, then equation (8) reduces to a simpler form,

$$\boxed{E_\pi = a/d \quad \text{For } 90^\circ \text{ meson energy spectra}} \qquad (9)$$

COLLISION DIAGRAM FOR REACTION

$n + n \rightarrow \pi^- + d$ IN LAB. SYSTEM

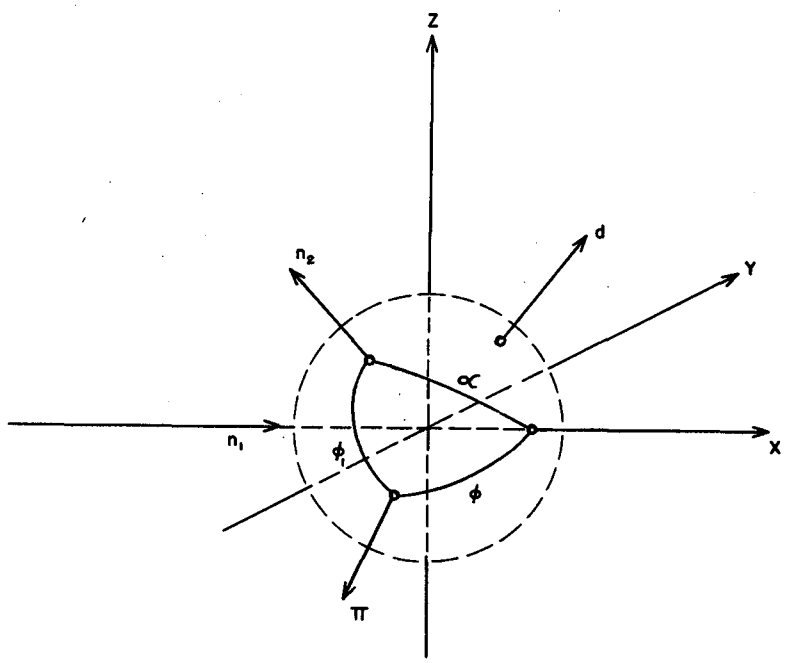

FIG. 62

MU-5488

B. Transformation Equations

The transformation of angle $\phi \rightarrow \theta$, and solid angle $d\Omega \rightarrow d\Omega'$, from the laboratory to the center-of-mass system is simplest when the x' axis of the C.M. frame is moving parallel to the x axis of the laboratory system, defined by the direction of the beam. We have considered, therefore, the projection of the weighted average values of β_f (Equation 5), along the laboratory axis. (See Section VI.)

Let $\overline{\beta}_f$ = projected value β_f

β'_π = velocity of meson in C.M. system,

then it is easy to show from the Einstein theorem for transformation of velocities, that

$$\tan \phi = \frac{1}{\gamma_f} \left[\frac{\sin \theta}{\cos \theta + \overline{\beta}_f / \beta'_\pi} \right] \tag{10}$$

$$\gamma_f^2 = 1/\ 1 - \overline{\beta}_f^2$$

From (10), the relation for the solid angles is easily derived,

$$\frac{d\Omega}{d\Omega'} = \frac{\sin \phi \, d\phi}{\sin \theta \, d\theta} = \frac{\gamma_f \left[1 + \frac{\overline{\beta}_f}{\beta'_\pi} (\cos \theta) \right]}{\left[\sin^2 \theta + \gamma_f^2 \left(\cos \theta + \frac{\overline{\beta}_f}{\beta'_\pi} \right)^2 \right]^{3/2}} . \tag{11}$$

XI. REFERENCES

1. E. Gardner and C. M. G. Lattes. Science 107, 270 (1948).

2. Neutron Beam Energy Measurement. Unpublished results by J. Cladis, W. Ball, and W. Hess. Radiation Laboratory.

3. a. W. Cartwright, C. Richman, M. Whitehead, and H. A. Wilcox. Phys. Rev. 78, 823 (1950).
   b. V. Peterson, E. Iloff, and D. Sherman. Phys. Rev. 84, 855 (1951).
   c. M. N. Whitehead and C. Richman. Phys. Rev. 83, 855 (1951).
   d. R. Durbin, H. Loar, and J. Steinberger. Phys. Rev. 84, 581 (1951).
   e. F. Crawford and L. Stevenson. UCRL-1098, unpublished results on reaction $p + p \rightarrow \pi^+ + d$.

4. C. Richman, M. Weissbluth, and H. A. Wilcox. Phys. Rev. 85, 161 (1952).

5. H. Bradner, D. J. O'Connel, and B. Rankin. Phys. Rev. 79, 720 (1950).

6. K. M. Watson and K. A. Breuckner. Phys. Rev. 83, 1 (1951).

7. a. J. Carothers and C. G. Andre. Phys. Rev. 88, 1426, (1952).
   b. M. A. Ruderman. Phys. Rev. 88, 1427 (1952).

8. a. S. Matsuyama and H. Meazawa. Prog. of Theor. Phys. 8, 140 (1952).
   b. K. A. Breuckner and K. M. Watson. Phys. Rev. 86, 927 (1952).

9. L. R. Hafstad and E. Teller. Phys. Rev. 54, 681 (1938).

10. J. B. Cladis, W. N. Hess and B. J. Moyer. Phys. Rev. 87, 425 (1952).

11. G. F. Chew and B. J. Moyer. American Journal Phys. 19, 17 (1951).

12. E. Kelly, C. Leith, E. Segrè, and C. Wiegand. Phys. Rev. 79, 96 (1950).

13. Z. Bay. Nature, 141, 1011 (1938).

14. H. Kallman. Natur and Tecknik (July 1947).

15. a. Z. Bay and G. Papp, Rev. Sci. Instr. 19, 565 (1948).
    b. K. P. Meyer, E. Baldinger and P. Huber. Helv. Phys. Acta 23, 121 (1950).
    c. R. E. Bell and H. E. Petch. Phys. Rev. 76, 1409 (1949).

16. Z. Bay. Phys. Rev. 79, 233 (1950).

17. Z. Bay. Rev. Sci. Inst. 22, 397 (1951).

18. S. De Benedetti and H. J. Richings. Rev. Sci. Inst. 23, 37 (1952).

19. R. F. Post. Nucleonics 10, 56, June 1952.

20. The magnet was suggested and designed by Dr. John S. Foster.

21. R. Bjorklund, W. E. Crandall, B. J. Moyer, and H. F. York. Phys. Rev. 77, 213 (1950).

22. a. J. de Juren, and B. J. Moyer. Phys. Rev. 81, 919 (1951).
    b. R. Fox, C. Leith, L. Wouters, and K. R. MacKenzie. Phys. Rev. 80, 23 (1950).

23. W. H. Barkas. American Journal Phys. 20, 5 (1952).

24. R. P. Durbin, H. H. Loar, and W. W. Havens, Jr. Phys. Rev. 88, 179 (1952).

25. E. M. Henley, Phys. Rev. 85, 204 (1952).

26. M. M. Block, S. Passman, and W. W. Havens, Jr. Phys. Rev. 88, 1239 (1952), and Phys. Rev. 88, 1247 (1952).

27. A. G. Schulz, Jr. Thesis, University of California, UCRL-1756.

28. W. Dudziak and S. Leonard have kindly made available their unpublished spectra for 0° and 180° from carbon bombarded by 340 Mev protons.

29. W. A. Aron, B. G. Hoffman and F. C. Williams. UCRL-121, AECU-663.

30. B. Rossi and K. Greisen. Rev. Mod. Phys. 13, 240 (1941).

31. Raymond T. Birge and J. W. Weinberg, Rev. Mod. Phys. 19, 298-360, (1947), also, lectures on Reduction of Observations, by R. T. Birge, Physics Department, University of California.